CHALMERS
UNIVERSITY OF TECHNOLOGY

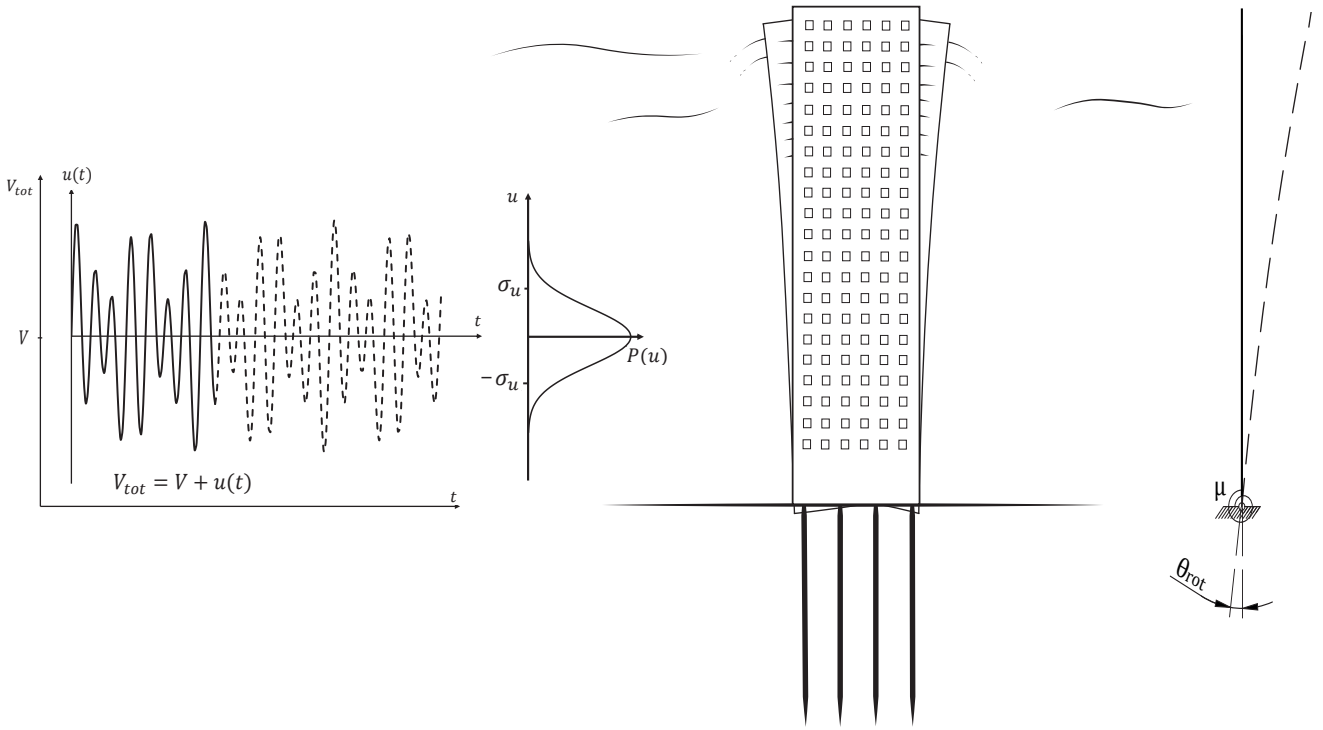

Wind-Induced Acceleration in High-Rise Buildings

An investigation on the dynamic effects due to a deep foundation

Master's Thesis in the Master's Programme Structural Engineering and Building Technology

ALEXANDER NYBERG
GUSTAV SÖDERLUND

Department of Civil and Environmental Engineering
Division of Structural Engineering
CHALMERS UNIVERSITY OF TECHNOLOGY
Master's Thesis BOMX02-17-32

Master's Thesis BOMX02-17-32

Wind-Induced Acceleration in High-Rise Buildings

An investigation on the dynamic effects due to a deep foundation

Master's Thesis in the Master's Programme Structural Engineering and Building Technology

ALEXANDER NYBERG & GUSTAV SÖDERLUND

Department of Civil and Environmental Engineering
Division of Structural Engineering
CHALMERS UNIVERSITY OF TECHNOLOGY
Göteborg, Sweden 2017

Wind-Induced Acceleration in High-Rise Buildings

An investigation on the dynamic effects due to a deep foundation

Master's Thesis in the Master's Programme Structural Engineering and Building Technology

ALEXANDER NYBERG
GUSTAV SÖDERLUND

Examensarbete BOMX02-17-32/ Institutionen för bygg- och miljöteknik,
Chalmers tekniska högskola 2017

Department of Civil and Environmental Engineering
Division of Structural Engineering
Chalmers University of Technology
SE-412 96 Göteborg
Sweden
Telephone: + 46 (0)31-772 1000

Cover:
Stochastic process for fluctuating wind and illustration of idealization of a high-rise building on deep foundation. Illustrations created by Isabelle Nyberg.
Department of Civil and Environmental Engineering Göteborg, Sweden, 2017

Wind-Induced Acceleration in High-Rise Buildings

An investigation on the dynamic effects due to a deep foundation

Master's thesis in the Master's Programme Structural Engineering and Building Technology

ALEXANDER NYBERG & GUSTAV SÖDERLUND
Department of Civil and Environmental Engineering
Division of Structural Engineering
Chalmers University of Technology

ABSTRACT

As Gothenburg expands, several new high-rise buildings are being planned in the area. Ideally, tall buildings are constructed on a foundation close to the bedrock, but for the city of Gothenburg, where the ground conditions commonly consist of clay, a deep pile foundation is often necessary. When designing tall buildings, it is important to consider the wind-induced horizontal acceleration in serviceability limit state. The available design codes such as, Eurocode 1 Part 1-4 and Swedish national annex EKS 10, are based on an idealization of a cantilever beam with fixed support. However, this assumption is reasonable when the foundation lies directly on bedrock, but becomes more questionable when a deep pile foundation is used.

The aim of this Thesis was to investigate how wind-induced horizontal acceleration in the along-wind direction was affected when the rotational stiffness of the support decreases. An objective was also to study the validity of current design norms for decreasing rotational stiffness of the support.

To be able to determine a representable mode shape and fundamental frequency for a structure with changeable support conditions, an analytical model was developed where the foundation was idealized as a rotational spring and the core as a cantilever beam.

To study the effect of support conditions on the horizontal acceleration and the validity of current design norms, two theoretical approaches with response spectrum analysis were studied, and all four approaches were evaluated in a parameter study. The analytical model was implemented in a MATLAB-program with the possibility to change rotational stiffness of the support, and the effects on mode shape, fundamental frequency and horizontal acceleration were studied.

The study showed that horizontal acceleration increases for decreasing rotational stiffness of the support. Further, the results proved that the Swedish national annex, EKS 10, was conservative for all studied cases and that the estimated wind-induced acceleration can be reduced by up to 33 % by using the approach suggested in Eurocode 1 Part 1-4 Annex B.

Key words: High-rise buildings, tall buildings, deep foundation, pile foundation, wind-induced acceleration, response spectrum analysis, dynamics of structures, Eurocode 1 Part 1-4, EKS 10, Einar Strømmen, Kamal Handa

Contents

Preface

This Master's Thesis investigates the consequences of a deep foundation for the wind-induced horizontal acceleration, in the along-wind direction, for high-rise buildings. The work was carried out between January and June of 2017, at Integra Engineering, as a final part of the master's programme *Structural Engineering and Building Technology* at *Chalmers University of Technology,* Sweden.

We would like to show our gratitude to Integra Engineering for giving us access to their office and to necessary software, and especially our supervisor, Björn Walhelm, Integra Engineering, for the opportunity to write this Thesis and for his support during the work. We would also like to thank out examiner, Adjunct Professor Morgan Johansson, Chalmers, for his support and important guidance throughout the work of the Thesis. Last but not least, we would truly like to show our gratitude to wind expert, Kamal Handa, for his inspiring passion about the subject and for his contribution with valuable information on his spare time.

Alexander Nyberg & Gustav Söderlund
Göteborg, June, 2017

Notations

Roman upper case letters

A	Area, Constant
B	Constant
B^2	Factor for background response
C	Constant
$\tilde{C}_{ae_i}$	Aerodynamic damping derivative
C_D, C_L, C_M	Force coefficient for along-wind, crosswind and torsional component respectively
$\tilde{C}_i$	Generalized damping
C_{mn}	Decay coefficient for turbulence component m in direction n
$\hat{C}o_{mn}$	Co-spectrum for m turbulence component and n-direction
D	Constant
EI	Flexural rigidity
H	Height of structure
H_c	Correlation factor in horizontal direction
H_{exp}	Part of the structure exposed to flow
H_{ref}	Reference height
$\widehat{H}_i$, $\widehat{H}_x$	Frequency response function for direction i and x respectively
F	Inertia force
I_u	Turbulence intensity for turbulence component u
J_x	Joint acceptance function
$\widetilde{K}_{ae_i}$	Aerodynamic stiffness derivative
$\widetilde{K}_i$, $\widetilde{K}_x$	Generalized stiffness for direction i and x respectively
K_x	Dimensionless coefficient
$K_{z'}$	Line support stiffness in z-direction
L_1	Width of building, perpendicular to wind flow
L_2	Depth of building, parallel to wind flow
L_u^x	Integral length scale for turbulent component in wind direction
M	Bending moment
$\widetilde{M}_{ae_i}$	Aerodynamic mass derivative
$\widetilde{M}_i$, $\widetilde{M}_x$	Generalized mass for direction i and x respectively
N	Number of degrees of freedom
P	External force
$\tilde{Q}_{ae_i}$	Generalized motion-induced loading for direction i
$\tilde{Q}_i$, $\tilde{Q}_x$	Generalized flow-induced loading for direction i and x respectively
$\tilde{Q}_{x,tot}$	Total generalized loading for direction x
R_{EKS}^2, R_{EC}^2	Resonance response coefficient according to EKS 10 and EN 1991-1-4
R_h, R_b	Correlation factors in horizontal and vertical direction respectively
R_N	Wind-spectral density
St	Strouhal number
S_{nn}	Cross spectral density for component n, n
S_{uu}	Cross spectral density for component u, u
$S_{\tilde{Q}_i}$, $S_{\tilde{Q}_x}$	Spectral density of loading
S_{r_i}	Spectral density of displacement for direction i
$S_{\ddot{u}_i}$	Spectral density of acceleration for direction i

T	Time of re-occurance for reference wind velocity
T_n	Natural period of vibration
V	Mean wind velocity
V_c	Correlation factor in vertical direction
V_{crit}	Critical wind velocity
$V_{b,T}$	Reference wind velocity with T years of re-occurrence
V_{rel}	Wind velocity in flow direction
W	Generlised wind load

Roman lower case letters

$a_{\ddot{u}_i}$	Fourier amplitude for acceleration
a_{η_i}	Fourier amplitude for generalized displacements
$a_{\tilde{Q}_i}$, $a_{\tilde{Q}_x}$	Fourier amplitude for flow-induced loading for direction i and x respectively
$a_{\tilde{Q}_{ae_i}}$	Fourier amplitude for motion-induced loading
a_{r_i}	Fourier amplitude for structural displacement
a_u	Fourier amplitude for turbulent component u
c	Viscous damping coefficient
$\boldsymbol{c}$	Damping matrix
c_{ae}	Aerodynamic cross-sectional damping property
c_f	Force coefficient
f_x	Fundamental frequency
f_L	Non-dimensional frequency
f_n	Eigenfrequency
f_s	Frequency of vortex shedding
i	Arbitrary direction
k	Elastic spring stiffness
$\boldsymbol{k}$	Stiffness matrix
$\tilde{k}$	Generalised stiffness
k_{ae}	Aerodynamic cross-sectional stiffness property
k_p	Peak coefficient
k_r	Terrain factor
m	Mass, Number of horizontal degrees of freedom
$\boldsymbol{m}$	Mass matrix
$\widetilde{m}$	Generalised mass
m_{ae}	Aerodynamic cross-sectional mass property
m_e	Equivalent mass per meter
m_i, m_x	Mass per meter for direction i and x respectively
n	Number of storeys
p	External force
$\tilde{p}$	Generalised force
p_0	Amplitude of force
q_n	Modal coordinates
q_D, q_L, q_M	Velocity pressure for along-wind, crosswind and torsional direction respectively
q_i, q_x, q_y, q_θ	Velocity pressure for direction i, x, y and θ respectively
q_m	Mean velocity pressure
q_{tot}	Total velocity pressure

r_i	Structural displacement in direction i
$\dot{r}_x$	Structural velocity in x-direction
t	Time
u	Displacement, fluctuating component in along-wind
u_0	Amplitude of displacement
u_c	Complementary solution
u_{max}	Maximum displacement
u_{min}	Minimum displacement
u_p	Particular solution
$\dot{u}$	Velocity
$\ddot{u}$	Acceleration
$\ddot{u}_{max}$	Peak acceleration
v	Mean value of upcrossing frequency, fluctuating component in crosswind direction
w	Fluctuating component in vertical direction
x	Coordinate of wind direction
y	Coordinate perpendicular to wind direction
y_1, y_2	Integration variables
z	Axial coordinate of the structure
z_{min}	Terrain parameter
z_{ref}	Reference height
z_s	Reference height used in design codes
z_{top}	Coordinate in top of the building
z_0	Rawness length
z_1, z_2	Integration variables

Greek upper case letters

$\mathbf{\Phi}$	Matrix containing mode shapes

Greek lower case letters

α	Power law exponent
β	Angle for flow inclination
δ	Damping given as logarithmic decrement
δ_a	Aerodynamical damping given as logarithmic decrement
δ_s	Mechanical damping given as logarithmic decrement
ζ, ζ_i	Damping ratio
ζ_{ae_i}	Aerodynamic damping ratio
η	Generalized coordinates
$\dot{\eta}_i$	Generalized velocity
$\ddot{\eta}_i$	Generalized acceleration
θ_1, θ_2	Integration variables
θ_{rot}	Rotational displacement
μ	Rotational spring stiffness
ξ	Exponent for mode shape
ρ	Density of air
$\sigma_{r_i}, \sigma_{r_x}$	Standard deviation of displacement for direction i and x respectively
σ_B^2	Background response
σ_R^2	Resonance response
σ_u	Standard deviation of the turbulent component

$\sigma_{\ddot{u}_i}$, $\sigma_{\ddot{u}_x}$	Standard deviation of acceleration for direction i and x respectively
τ_1, τ_2	Integration variables
ω	Excitation frequency
$\boldsymbol{\omega}$	Vector containing eigenfrequencies
ω_n	Natural circular frequency
ω_D	Damped natural circular frequency
ϕ	Phase angle
ϕ_n	Mode shape
ϕ_i, ϕ_x	Mode shape direction i and along-wind direction respectively
ϕ_b	Size coefficient, based on width of the structure
ϕ_h	Size coefficient, based on height of the structure
ψ	Shape function

1 Introduction

1.1 Background

The region of Gothenburg is growing and the population is expected to increase with 20 % up to 1 200 000 inhabitants over the next 15 years (Västra Götalandsregionen, 2016). Densification of cities combined with the ambition to keep green areas and develop sustainable, put great demands on city planning and area efficiency. As a result of this development, buildings are getting taller and several new buildings in the range of 100-240 meters are being planned in the region.

Tall buildings increase the urban density, which comes with several sustainable advantages that can reduce the total carbon footprint of the building. Compact cities promote the possibility to take advantage of shared energy systems and simplify the use of sustainable transportations, e.g. walking, cycling and public transportation.

The carbon emissions associated with the construction of a building is typically in the range of 10-30 % compared to the operational carbon emissions (Skidmore, Owings & Merrill, LLP, 2013). When constructing high-rise buildings, construction emissions is generally higher per square meter, than for normal height buildings. This is mainly due to an additional need for structural material to sustain stiffness and strength when constructing high-rise buildings. However, tall buildings have the ability to be more energy efficient since the amount of weather exposed surfaces compared to building volume is less for a given base area, and through the use of central services. In this way, operational carbon emissions can be reduced per square meter.

When designing tall buildings, the dynamic effects from wind loads will cause horizontal oscillation and acceleration of greater significance than for normal height buildings. These oscillations may cause discomfort, e.g. motion sickness, for people visiting the building (Kwok, Burton, & Abdelrazaq, 2015). Design with regard to acceleration is done for the serviceability limit state, SLS, and is usually determined either for peak value or a standard deviation, root-mean-square, value. Recommendations for acceptable values are given in ISO 10137 (SIS, 2008) and ISO 6897 (International Organisation for Standardization, 1984). However, estimating the acceleration of large structures is complex and the structure is often idealized as a cantilever.

Ideally, high-rises are constructed on a foundation close to the bedrock. However, for the city of Gothenburg, the ground conditions commonly consist of clay and the bedrock lies at a depth of up to 100 m (Geological Survey of Sweden, 2017). With such conditions, deep foundation on piles is often necessary to carry the loads of the building and associated actions.

1.2 Problem description

The methods presented in EKS 10 (Boverket, 2015) and Eurocode 1 Part 1-4 (CEN, 2005), when designing a tall building with regard to acceleration in SLS, are based on a building constructed on rigid foundation. The governing assumption is an idealization and proposed mode shape corresponding to a cantilever beam with fixed support. However, this idealization is reasonable when the foundation lies directly on bedrock, but becomes more questionable when a pile foundation is used.

When constructing on deep layers of clay, a pile foundation will contribute differently to the restraint conditions and rigidity of the building, therefore questioning the legitimacy of the model based on a fixed support.

1.3 Aim and objectives

The overall aim of this project was to investigate how wind-induced horizontal acceleration, in along-wind direction, is affected when rotational stiffness of the support decreases. To reach this principle aim, one objective was to set up an analytical model by idealizing both the foundation and the lateral bearing system of a high-rise building. Another objective was to investigate if current design norms are valid for decreasing rotational stiffness of the support.

1.4 Methodology

Literature studies were performed to increase the understanding within the field of wind-induced motions, wind turbulence and dynamics of structures. Further, it was necessary to study todays workflow and theoretical methods regarding wind-induced accelerations to understand the origin of the expressions stated in EKS 10 and Eurocode 1 Part 1-4. Supplementary specialization was gained through consultation with engineers from Integra Engineering AB and experts within the field of wind-induced acceleration.

The ground conditions were idealized, and an analytical model was created for a general case. The analytical model was developed to be able to determine a representable mode shape and fundamental frequency for a structure with changeable support condition. To validate the analytical model, fundamental frequencies from the analytical model were compared with results from a commercial finite element software, FEM-design 16 (StruSoft, 2016), for various support conditions.

To study the effect of support conditions on horizontal acceleration, and the validity of current design norms, four different expressions for determining the acceleration were evaluated in a parameter study. Two of the approaches are based on design codes, EKS 10 (Boverket, 2015) and Eurocode 1 Part 1-4 Annex B (CEN, 2005), and two theoretical approaches based on response spectrum analysis developed by (Strømmen, 2010) and (Handa, 1982).

1.5 Limitations

To focus this Master's Thesis with regard to horizontal acceleration, several factors have been disregarded. No regard to shear or axial deformation, or the effect axial force may have on the stiffness of columns have been taken. Further, the problem has been regarded as linear elastic with the assumption of uncracked concrete cross sections, which is reasonable to assume when designing in SLS.

To further simplify calculations, the lateral bearing system of the building has been regarded as a cantilever, and a homogeneous core was used in the parameter study.

The true deformations and bearing capacity of piles in clay have not been investigated. When idealizing the sub-structure, an expected behaviour of a pile foundation was assumed and simplified as a line support with linear elastic stiffness in vertical direction. Any horizontal movements in the foundation are disregarded.

1.6 Outline of the report

Initially, in Chapter 2, the basic theory within the field of dynamics of structures are presented. The governing differential equation and methods to find the solution are presented both for single- and for multi degree of freedom systems.

In Chapter 3, the theory of wind, wind turbulence and basic statistical expressions to describe wind loads are explained. Finally, it is described how humans perceive motion and how this is considered in design.

Chapter 4, gives an explanation of the basic concepts of response spectrum analysis for wind-induced acceleration on structures. The Chapter also presents two expressions for determining the standard deviation of acceleration according to the theoretical approach.

Two approaches to determine standard deviation of acceleration according to design norms, EKS 10 and Eurocode 1 Part 1-4 Annex B, is presented in Chapter 5. Further, a method to estimate peak acceleration is presented followed by comfort recommendations according to ISO-standards.

Chapter 6, describes the development and verification of the analytical model and how the mode shape and fundamental frequency is estimated in the model.

Chapter 7, contains the parameter study, where the effect of support conditions on important parameters is investigated.

A final discussion of the results and important choices regarding input in the methods and analytical model, is handled in Chapter 8.

Finally, in Chapter 9 conclusions of the Thesis are presented, followed by proposed aspects for further investigation.

2 Dynamics of Structures

This chapter aims to increase the basic knowledge in dynamics of structures and to understand the connection between dynamic properties, loading and acceleration for structures. Initially, basic concepts are introduced for a single degree of freedom, *SDOF*. This is done for three general cases: single degree of freedom, generalized single degree of freedom and multi degree of freedom.

2.1 Equation of motion

Dynamic response, or structural motion, is characterized by its time-dependence, and is thus more complex than static response. To derive expressions for structural motion, it is convenient to start by observing a rigid body with mass, m, on roller support, attached to an elastic spring with stiffness, k, and a viscous damper with viscous damping coefficient, c, as shown in Figure 2-1 *(a)*.

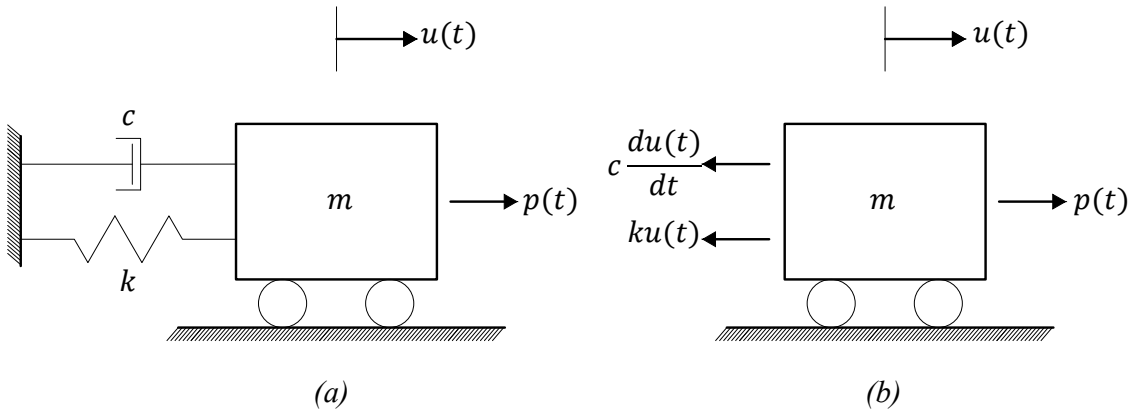

Figure 2-1 (a) Mass on roller support. (b) Free-body diagram.

As Newton states in his second law: a mass that is exposed to forces will result in an acceleration, $\ddot{u}(t)$. The product of mass and acceleration is called *inertia force, F*, and Newton's second law of motion states:

$$\sum F = m\ddot{u}(t) \tag{2-1}$$

The free-body diagram of the system in Figure 2-1 *(a)* is shown in Figure 2-1 *(b)*. The displacement, $u(t)$, and velocity, $\dot{u}(t)$, caused by the time dependent force $p(t)$, are resisted by internal, elastic and damping, forces caused by the elastic spring and the viscous damper respectively. From the free-body diagram, Newton's second law of motion gives:

$$p(t) - c\dot{u}(t) - ku(t) = m\ddot{u}(t) \tag{2-2}$$

Equation (2-2) is the governing differential equation describing the response of the system, also known as *equation of motion*. The equation of motion is fundamental in dynamics of structures and will from here on be referred to as EoM. It is usually re-written to the form:

$$m\ddot{u}(t) + c\dot{u}(t) + ku(t) = p(t) \tag{2-3}$$

2.2 Single degree of freedom

The system in Figure 2-1, is prevented from torsion and vertical displacement and the response of the system is determined by a single independent coordinate. The system is referred to as a *Single degree of freedom,* SDOF, system. To find a solution, $u(t)$, to the EoM for a SDOF system, it is convenient to start by examine the system in free vibration.

2.2.1 Free vibration

2.2.1.1 Undamped systems in free vibration

If a system without damping or dynamic excitation, is disturbed from its statically equilibrium position, it is said to be in free vibration, i.e. the motion is infinite. If a system vibrates freely, the solution to the EoM is characterized by the frequency of the vibrations.

The solution may be derived by introducing a cantilever, without damping and external forces, with a lumped mass in the top according to Figure 2-2.

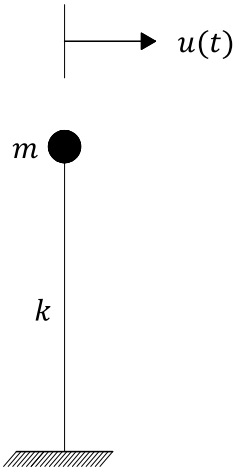

Figure 2-2 Cantilever with a lumped mass.

With the same way of reasoning as in Section 2.1, the EoM for the cantilever is expressed as:

$$m\ddot{u}(t) + ku(t) = 0 \tag{2-4}$$

The expression may be rewritten by dividing by mass:

$$\ddot{u}(t) + \omega_n^2 u(t) = 0 \tag{2-5}$$

Where ω_n is the undamped natural circular frequency, expressed as cycles per radians:

$$\omega_n = \sqrt{\frac{k}{m}} \tag{2-6}$$

The circular frequency can be expressed as cycles per seconds or (Hz) by:

$$f_n = \frac{\omega_n}{2\pi} \tag{2-7}$$

It may be shown that the solution to the linear homogenous second order differential equation (2-5) with constant coefficient, is:

$$u(t) = A\cos\omega_n t + B\sin\omega_n t \tag{2-8}$$

Since there are no external forces acting on the system, it is necessary for the free vibrating system to have initial conditions that does not correspond with the statically equilibrium, otherwise there would be no motion. If these initial conditions are expressed as $u(0)$ and $\dot{u}(0)$, the constants *A* and *B* in equation (2-8) can be determined. The final solution for a system in free vibration, may then be written as:

$$u(t) = u(0)\cos\omega_n t + \frac{\dot{u}(0)}{\omega_n}\sin\omega_n t \tag{2-9}$$

2.2.1.2 Damped systems in free vibration

By introducing linear viscous damping to the system in Figure 2-2, the EoM is written as:

$$m\ddot{u}(t) + c\dot{u}(t) + ku(t) = 0 \tag{2-10}$$

By defining the damping ratio, ζ, and dividing by the mass, the EoM can be rewritten.

$$\zeta = \frac{c}{2m\omega_n} \tag{2-11}$$

$$\ddot{u}(t) + 2\zeta\omega_n\dot{u}(t) + {\omega_n}^2 u(t) = 0 \tag{2-12}$$

By using initial conditions, $u(0)$ and $\dot{u}(0)$, in expression (2-12), the exact solution to the EoM for a damped system is expressed as:

$$u(t) = e^{-\zeta\omega_n t}\left(u(0)\cos\omega_D t + \frac{\dot{u}(0) + \zeta\omega_n u(0)}{\omega_D}\sin\omega_D t\right) \tag{2-13}$$

Where the damped natural circular frequency, ω_D, is defined as:

$$\omega_D = \omega_n\sqrt{1-\zeta^2} \tag{2-14}$$

By observing expression (2-14), it can be noticed that damping decreases the natural frequency of the system. For linear viscous damping, systems can be classified as: underdamped for $\zeta < 1$, critically damped for $\zeta = 1$ and overdamped for $\zeta > 1$. However, structures in civil engineering are most often underdamped, and the effect on natural frequency is negligible for damping ratios less than 20 %, a range that includes most structures (Chopra, 2012).

To examine the damping ratios further, it is useful to rewrite Equation (2-13). This is done by the use of trigonometric identities, and the result is as follows:

$$u(t) = e^{-\zeta\omega_n t} u_{max} \cos(\omega_D\, t - \theta) \tag{2-15}$$

Where:

$$u_{max} = \sqrt{u(0)^2 + \left(\frac{\dot{u}(0) + \zeta\omega_n u(0)}{\omega_D}\right)^2} \tag{2-16}$$

$$\theta = \tan^{-1} \frac{\dot{u}(0) + \zeta\omega_n u(0)}{\omega_D u(0)} \tag{2-17}$$

Investigating Equation (2-15) and (2-16) further, it is clear that neither, $\cos(\omega_D t - \theta)$, or u_{max}, will decay with time, t. However, $e^{-\zeta\omega t}$, do decay with time when $\zeta > 0$ and the total behaviour is schematically shown for $0 < \zeta < 1$ in Figure 2-3.

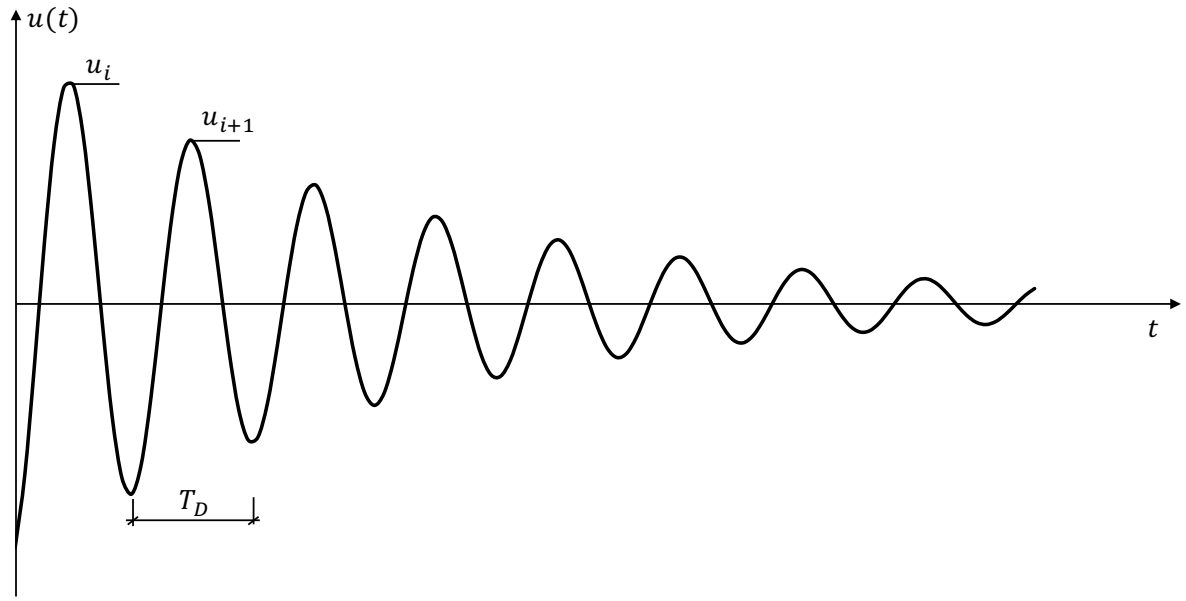

Figure 2-3 Peak values decreases due to damping.

The difference between two amplitudes, u_i and u_{i+1}, separated by period T_D, will depend on $e^{-\zeta\omega t}$. The ratio between the two amplitudes can be written as:

$$\frac{u_i}{u_{i+1}} = \frac{e^{-\zeta\omega_n t}}{e^{-\zeta\omega_n (t+T_D)}} = e^{\zeta\omega_n T_D} = e^{\zeta\omega_n \frac{2\pi}{\omega_D}} = e^{\frac{2\pi\zeta}{\sqrt{1-\zeta^2}}} \tag{2-18}$$

This means that the damping ratio can be determined from two peak displacement values and be determined by:

$$\delta = \ln\left(\frac{u_i}{u_{i+1}}\right) = \frac{2\pi\zeta}{\sqrt{1-\zeta^2}} \tag{2-19}$$

Where δ is called the logarithmic decrement. According to (Chopra, 2012), for small damping ratios, $\zeta < 0.2$, which includes most structures, the equation can be simplified to:

$$\delta \approx 2\pi\zeta \tag{2-20}$$

2.2.2 Response to excitation

So far only systems in free vibration have been examined. In this Section, the behaviour of a simple cantilever with a lumped mass that is influenced by an arbitrary external force $p(t)$ will be examined, see Figure 2-4.

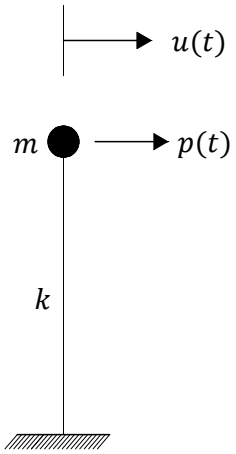

Figure 2-4 Cantilever with a lumped mass, exposed to an external force.

For a system exposed to an external load, the complete solution, $u(t)$, consists of a complementary solution, $u_c(t)$, and a particular solution, $u_p(t)$.

$$u(t) = u_c(t) + u_p(t) \tag{2-21}$$

2.2.2.1 Undamped systems with excitation

If the force $p(t)$ is a harmonic excitation where $p(t) = p_0 \sin \omega t$, where p_0 is the amplitude of the force and ω is the excitation frequency, the EoM is expressed as:

$$m\ddot{u}(t) + ku(t) = p_0 \sin \omega t \tag{2-22}$$

The complementary solution to this differential equation, when disregarding damping, will be the same as the solution for a system in free vibration according to Equation (2-5):

$$u_c(t) = A \cos \omega_n t + B \sin \omega_n t \tag{2-23}$$

This will always be the complementary solution for a single degree of freedom system without damping. However, the particular solution depends on the nature of the force. In the case of a harmonic excitation $p(t) = p_0 \sin \omega t$, the particular solution is:

$$u_p(t) = \frac{p_0}{k}\frac{1}{1-\left(\omega/\omega_n\right)^2} \tag{2-24}$$

The complete solution is obtained by combining the complementary solution and particular solution, according to Equation (2-21), such as:

$$u(t) = A\cos\omega_n t + B\sin\omega_n t + \frac{p_0}{k}\frac{1}{1-\left(\omega/\omega_n\right)^2} \tag{2-25}$$

Where the constants *A* and *B* is determined by the initial condition of the system.

Regard the same system as in Figure 2-4, but with $p(t) = p_0$. The complementary solution would be the same, but the particular solution, which is related to the force, different.

$$u(t) = A\cos\omega_n t + B\sin\omega_n t + \frac{p_0}{k} \tag{2-26}$$

With $u(0) = \dot{u}(0) = 0$ as initial condition the constant A and B can be determined and the response becomes:

$$u(t) = \frac{p_o}{k}(1-\cos\omega_n t) \tag{2-27}$$

What can be noticed from equation above is that undamped SDOF system exposed to step force, will oscillate between $u_{min} = 0$ and $u_{max} = 2\frac{p_0}{k}$, reaching a maximum displacement twice that of the static displacement.

2.2.2.2 Damped systems with excitation

Taking damping into consideration complicates the solution somewhat. If the external force is expressed as $p(t) = p_0\sin\omega t$, the EoM can be expressed as:

$$m\ddot{u}(t) + c\dot{u}(t) + ku(t) = p_0\sin\omega t \tag{2-28}$$

The complementary solution for a damped system looks as follows, and note the resemblance for the solution for equation (2-12):

$$u_c(t) = e^{-\zeta\omega_n t}(A\cos\omega_D t + B\sin\omega_D t) \tag{2-29}$$

While the particular solution takes the form of:

$$u_p(t) = C\sin\omega t + D\ \cos\omega t \tag{2-30}$$

Where *C* and *D* is defined as:

$$C = \frac{p_0}{k} \frac{1 - \left(\frac{\omega}{\omega_n}\right)^2}{\left[1 - \left(\frac{\omega}{\omega_n}\right)^2\right]^2 + \left[2\zeta\left(\frac{\omega}{\omega_n}\right)\right]^2} \tag{2-31}$$

$$D = \frac{p_0}{k} \frac{-\frac{2\zeta\omega}{\omega_n}}{\left[1 - \left(\frac{\omega}{\omega_n}\right)^2\right]^2 + \left[2\zeta\left(\frac{\omega}{\omega_n}\right)\right]^2} \tag{2-32}$$

According to (Chopra, 2012) the complementary solution, $u_c(t)$, can be seen as transient and that after a certain time regarded as negligible. That means that the response only depends on the particular solution, $u_p(t)$, which Chopra refers to as steady-state response. It should however be noticed that the peak deformation can occur before the system reaches a steady state. The behaviour is shown in Figure 2-5, where the total response approaches the steady-state solution.

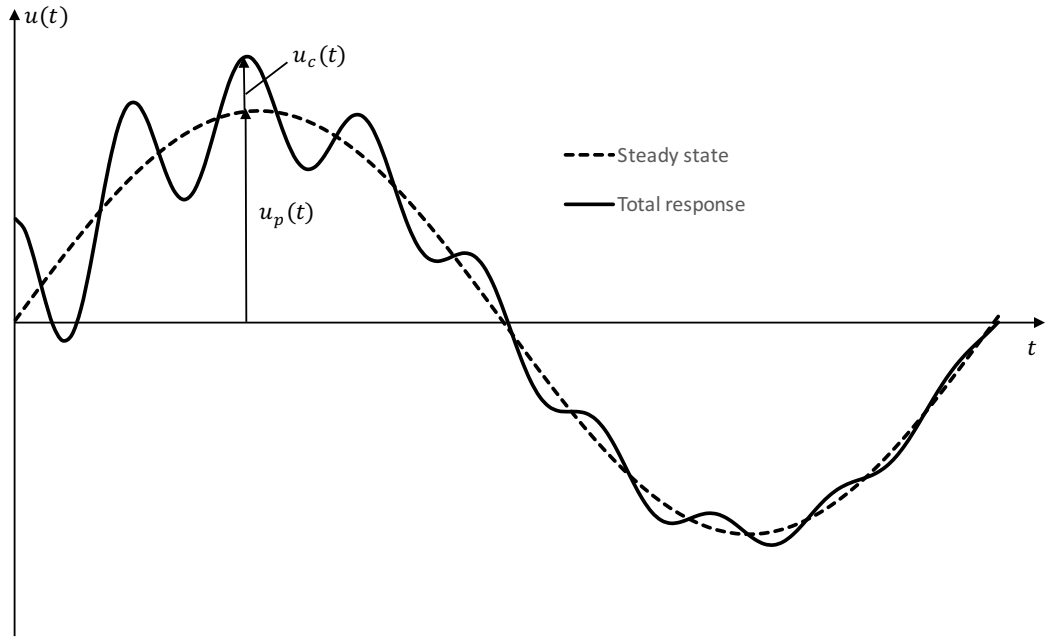

Figure 2-5 Illustration of total response and steady state response.

2.2.3 Deformation response function

A convenient method to determine the maximum response for a system subjected to harmonic excitation, is to use a response spectrum for the structure. It will be shown that the response of the structure will depend on the excitation frequency, natural frequency, and damping of the system.

Equation (2-30) can together with equations (2-31) and (2-32), with the help of trigonometric rules, be written as:

$$u(t) = u_0 \sin(\omega t - \phi) \tag{2-33}$$

Where:

$$\phi = \tan^{-1}\frac{-D}{C} = \tan^{-1}\frac{2\zeta\left(\frac{\omega}{\omega_n}\right)}{1-\left(\frac{\omega}{\omega_n}\right)^2} \tag{2-34}$$

$$u_0 = \frac{p_0}{k}\frac{1}{\sqrt{\left[1-\left(\frac{\omega}{\omega_n}\right)^2\right]^2 + \left[2\zeta\left(\frac{\omega}{\omega_n}\right)\right]^2}} \tag{2-35}$$

By examine Equation (2-33) when investigating the maximum response, it is clear that $\sin(\omega t - \phi)$ will reach a maximum value equal to 1. Therefore, the maximum response is determined from the amplitude u_0, which consist of the static displacement due to the amplitude of the excitation multiplied with a term referred to as the deformation response factor, R_d, in (Chopra, 2012).

$$R_d = \frac{1}{\sqrt{\left[1-\left(\frac{\omega}{\omega_n}\right)^2\right]^2 + \left[2\zeta\left(\frac{\omega}{\omega_n}\right)\right]^2}} \tag{2-36}$$

This means that the maximum displacement is found by:

$$u_{max} = \frac{p_0}{k}R_d \tag{2-37}$$

What can be noticed is that, if the system is in resonance with the excitation frequency, i.e. $\omega = \omega_n$, the maximum response is obtained and the deformation response factor becomes:

$$R_d = \frac{1}{2\zeta} \tag{2-38}$$

Figure 2-6 illustrates how the deformation response factor, R_d, varies with excitation frequency and different damping ratios.

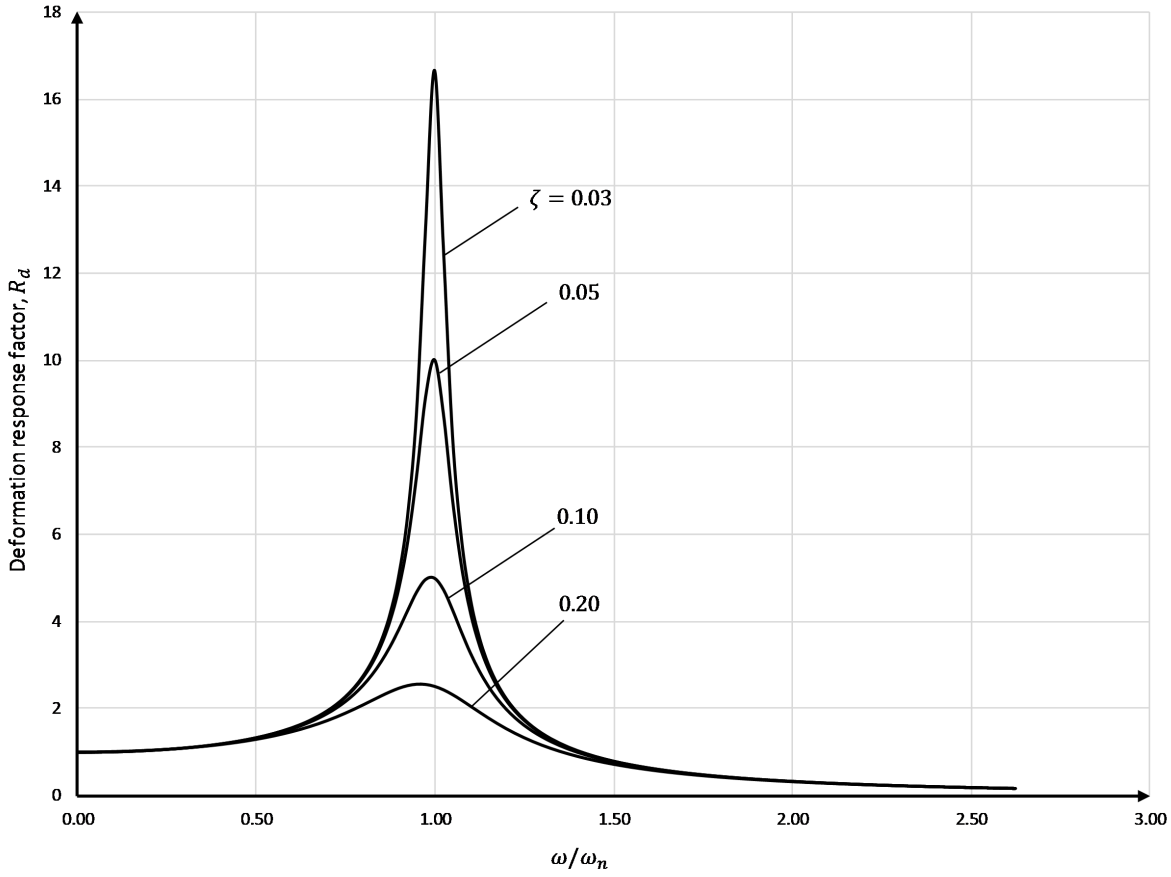

Figure 2-6 Four different deformation response functions with corresponding damping ratio.

2.2.4 Systems with distributed mass and stiffness

So far only systems that have a point mass and constant stiffness have been regarded. However, it is not uncommon for structures in civil engineering that mass and stiffness vary along the coordinate, z. An illustration is shown in Figure 2-7.

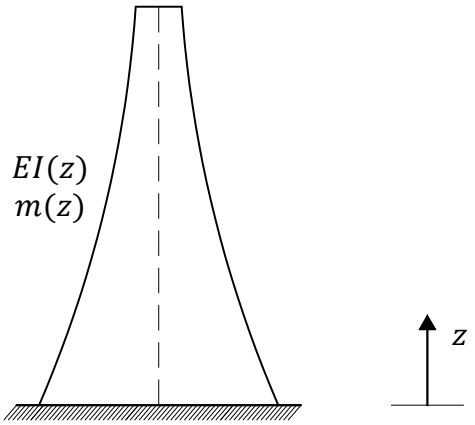

Figure 2-7 Cantilever with varying mass and stiffness.

To solve the EoM for such a case, it is convenient to introduce a generalized coordinate, $\eta(t)$, and describe the motion of the system through a chosen shape function, $\psi(z)$, as:

$$u(z,t) = \psi(z)\eta(t) \tag{2-39}$$

The shape function is chosen with regard to boundary condition and the behaviour of the beam. This implies that every position of the beam is constrained to move according to the shape function, $\psi(z)$, and by doing this an infinite DOF system can be regarded as an SDOF system, with $\eta(t)$ as only unknown.

By regarding the system in Figure 2-7 and assuming no damping, the inertia force, F, acting on a small section, dz, of the cantilever can be expressed using generalized coordinates, as:

$$F = m(z)\, dz\, \ddot{u}(z,t) = m(z)\, dz\, \ddot{\eta}(t)\psi\,(z) \tag{2-40}$$

By using principle of virtual work, it can be proven that the EoM can be written as:

$$\begin{aligned} &\ddot{\eta}(t)\int_0^H m(z)\psi(z)^2 dz + \eta(t)\int_0^H EI(z)\{\,\psi''(z)\}^2 dz \\ &\quad = \int_0^H P(z,t)\psi(z)dz \end{aligned} \tag{2-41}$$

Where the generalized mass, stiffness and force are introduced as:

$$\tilde{m} = \int_0^H m(z)\psi(z)^2 dz \tag{2-42}$$

$$\tilde{k} = \int_0^H EI(z)\{\,\psi''(z)\}^2 dz \tag{2-43}$$

$$\tilde{p} = \int_0^H P(z,t)\psi(z)dz \tag{2-44}$$

If Equations (2-42), (2-43) and (2-44) are substituted into Equation (2-41), an expression can be formulated, that is similar to the EoM for a system with lumped mass and constant stiffness:

$$\ddot{\eta}(t)\tilde{m} + \eta(t)\tilde{k} = \tilde{p} \tag{2-45}$$

Where the generalized coordinate $\eta(t)$ is determined by solving differential Equation (2-45), and then the behaviour of the beam can be determined by equation (2-39).

The natural frequency of the system can be determined according to:

$$\omega_n = \sqrt{\frac{\tilde{k}}{\tilde{m}}} \tag{2-46}$$

2.3 Multi degree of freedom

2.3.1 Equation of motion for multi degree of freedom systems

There are several methods to determine the response of a *multi degree of freedom*, MDOF, system, but this Thesis focuses on modal analysis which is described in this Section.

An example of a MDOF system is a cantilever with two lumped masses, as shown in Figure 2-8. Lumping the mass means that the elements between the nodes are massless and replaced by equivalent masses in the nodes. This is an alternative approach to the method with generalized coordinates, described in Section 2.2.4, and is convenient when formulating the mass matrix.

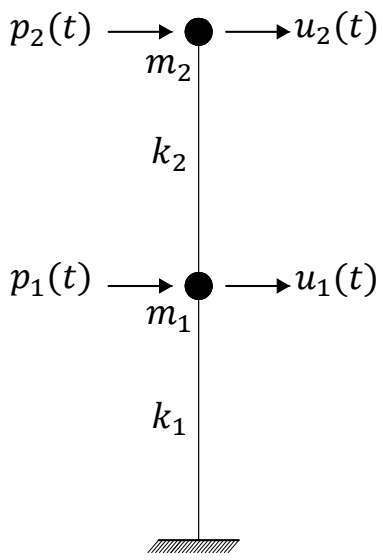

Figure 2-8 Cantilever with two degrees of freedom.

The main difference compared to a SDOF system, is that the EoM is formulated on matrix form, as:

$$\begin{bmatrix} m_1 & 0 \\ 0 & m_2 \end{bmatrix}\begin{bmatrix} \ddot{u}_1(t) \\ \ddot{u}_2(t) \end{bmatrix} + \begin{bmatrix} c_1 + c_2 & -c_2 \\ -c_2 & c_2 \end{bmatrix}\begin{bmatrix} \dot{u}_1(t) \\ \dot{u}_2(t) \end{bmatrix} + \begin{bmatrix} k_1 + k_2 & -k_2 \\ -k_2 & k_2 \end{bmatrix}\begin{bmatrix} u_1(t) \\ u_2(t) \end{bmatrix} = \begin{bmatrix} p_1(t) \\ p_2(t) \end{bmatrix} \tag{2-47}$$

Which is equivalent of writing it on the form of:

$$\boldsymbol{m\ddot{u} + c\dot{u} + ku = p} \tag{2-48}$$

If both the acceleration and velocity would be zero, the expression will turn to a static problem, $\boldsymbol{ku = p}$, which is familiar from structural mechanics.

2.3.2 Free vibration & eigenvalue statement

The expression of free vibration for a MDOF system can be seen below:

$$\boldsymbol{m\ddot{u} + ku = 0} \tag{2-49}$$

A SDOF system moves with a single harmonic motion with the same natural frequency regardless of the initial condition. This is something that cannot be said about a MDOF system. It is however, possible to choose initial conditions, $\boldsymbol{u} = \boldsymbol{u}(0)$ and $\dot{\boldsymbol{u}} = \dot{\boldsymbol{u}}(0)$, such that the system vibrate with a constant natural frequency and maintains its deflected shape through one cycle. Which means that both DOFs reaches its maximum deflection at the same time and pass through equilibrium simultaneously. The system is said to move in a simple harmonic motion and it is then possible to determine the natural frequencies. Let's regard the cantilever in Figure 2-8, its simple harmonic motion can be seen in Figure 2-9. The deflected shape is referred to as the natural mode of vibration for a MDOF system.

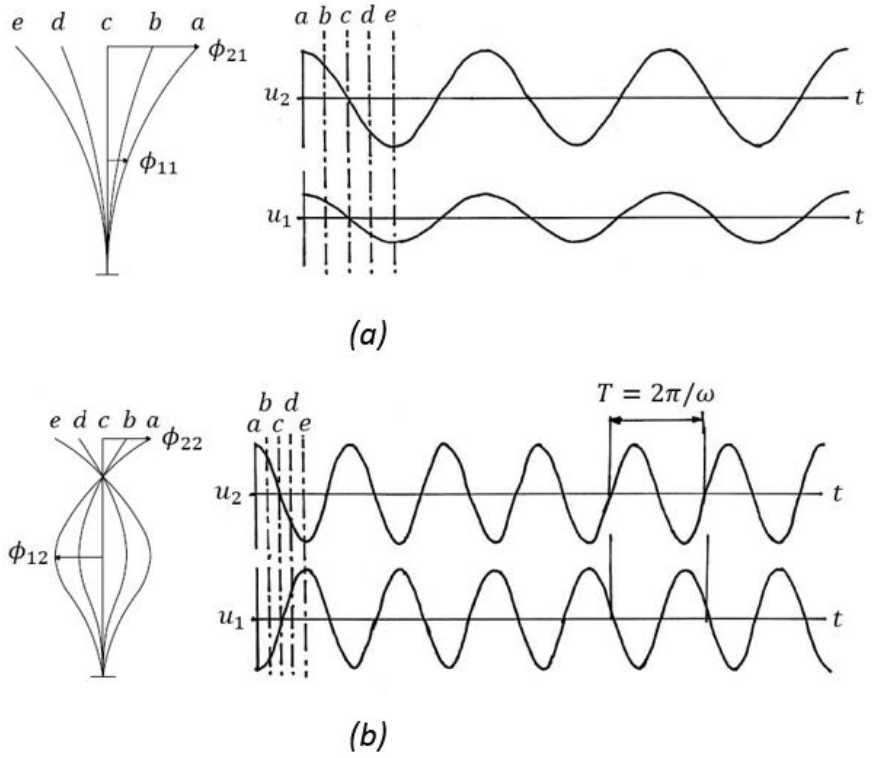

Figure 2-9 Free vibration of two degree of freedom system according to (a) First mode (b) Second mode. Figure inspired by (Chopra, 2012).

The two vibration modes in Figure 2-9, will have two different eigenfrequencies, the smaller of the two eigenfrequencies is expressed as ω_1, also known as the fundamental frequency, and the larger ω_2. Where the natural period of vibration for one of the mode is:

$$T_n = \frac{2\pi}{\omega_n} \tag{2-50}$$

The free vibration of an undamped system in one of its natural modes can mathematically be described as:

$$\boldsymbol{u}(t) = q_n(t)\phi_n \tag{2-51}$$

Where the deflected shape ϕ_n is constant over time. The time dependent part, $q_n(t)$, of the displacement can be described by a simple harmonic function:

$$q_n(t) = A_n \cos \omega_n t + B_n \sin \omega_n t \tag{2-52}$$

Where A_n and B_n can be determined by initial conditions. Substituting Equation (2-52) in Equation (2-51) yields:

$$\boldsymbol{u}(t) = \phi_n(A_n \cos \omega_n t + B_n \sin \omega_n t) \tag{2-53}$$

Combining equations (2-49) and (2-53), where ϕ_n and ω_n are unknown, yields:

$$[-\omega_n^2 \boldsymbol{m}\phi_n + \boldsymbol{k}\phi_n]q_n(t) = \boldsymbol{0} \tag{2-54}$$

This equation can satisfy its condition in two ways, either $q_n(t)$=0 which implies no motion of the system and the system is said to have a trivial solution. Else the natural mode and the eigenfrequencies must satisfy following equation:

$$[\boldsymbol{k} - \omega_n^2 \boldsymbol{m}]\phi_n = \boldsymbol{0} \tag{2-55}$$

This equation is referred to as matrix eigenvalue problem, with a set of N homogenous equation, where $\phi_{jn}(j = 1, 2, \ldots, N)$. This set of equation always has the trivial solution $\phi_n = \boldsymbol{0}$, but that also implies no motion to the system. For the system to have a non-trivial solution it must satisfy this equation:

$$det[\boldsymbol{k} - \omega_n^2 \boldsymbol{m}] = 0 \tag{2-56}$$

When the determinant is expanded, it yields a polynomial of order N, where the unknown variable is ω_n^2. This polynomial has N real and positive roots for ω_n^2, due to the fact that $\boldsymbol{m}$ and $\boldsymbol{k}$ (mass and stiffness matrix) are symmetric and positive definite. This means that it is possible to obtain the eigenfrequencies of the system by solving this polynomial. When the eigenfrequencies for the system is solved, then the mode shapes ϕ_n for respectively eigenfrequency ω_n can be solved using equation (2-55).

3 Wind Load

Wind is omnipresent in our environment and inevitable an important element to consider when designing buildings in general, but high-rise buildings in particular. When designing for wind-induced motion, the structure is generally assumed to have a linear elastic behaviour and that any non-linear effects may be disregarded (Strømmen, 2010).

The theory of wind fields, stochastic processes and its role in civil engineering, will be handled in this Chapter.

3.1 High-rise buildings

If a structure is exposed to an airflow, the interaction between the flow and the body will result in forces acting on the body, i.e. the kinetic energy from the airflow is converted to potential energy in the structure. Unless the structure is very streamlined and the velocity of the flow is low, these forces will fluctuate (Strømmen, 2010). Fluctuation of forces are caused by three main mechanisms: Buffeting, wind induced motion and vortex shedding.

3.1.1 Buffeting response and wind induced motion

Firstly, the wind itself contains turbulence, i.e. it fluctuates in time and space. This phenomenon is known as *Buffeting* (Strømmen, 2010). Secondly, the body might start to oscillate itself, and when it interacts with the fluctuating forces, additional forces may be created. This is known as *Motion induced forces*.

Both of these mechanisms will contribute to along-wind vibrations.

3.1.2 Vortex shedding

Finally, if a body is placed in a steady flow, forces may fluctuate due to friction between air and the surfaces which causes vortices. These vortices alternate on each side of the cross-section which result in fluctuating load perpendicular to the flow direction, causing vibrations in cross-wind direction, see Figure 3-1. This phenomenon is referred to as *Vortex shedding* and could results in great structural response if the frequency of vortex shedding, f_s, equals the eigenfrequency, f_n, corresponding to a mode perpendicular to the flow direction.

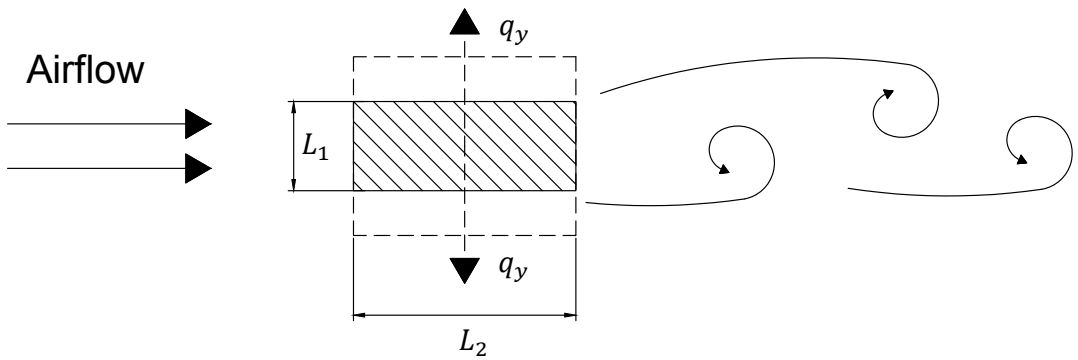

Figure 3-1 Illustration of vortex shedding.

The critical wind velocity can be determined by Eurocode 1 Part 1-4 (CEN, 2005) to:

$$V_{crit} = \frac{1}{St} L_1 f_n \tag{3-1}$$

Where the Strouhal number, St, is defined by the dimensions of the cross-section according to Figure 3-2. For a rectangular cross-section, St varies between 0,05-0,15 dependent on the ratio, L_2/L_1.

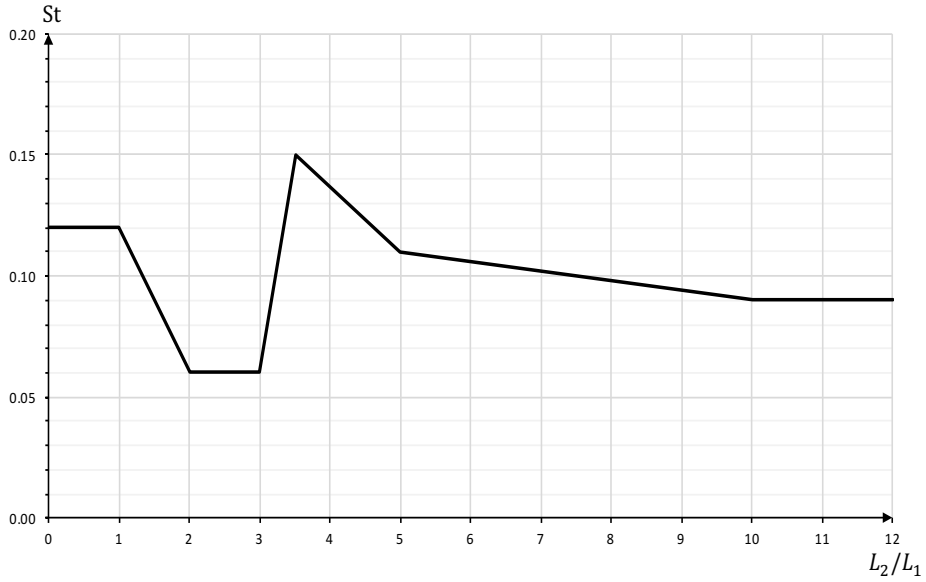

Figure 3-2 Strouhal number for a rectangular cross-section, reproduced from Figure E.1 in Eurocode 1 Part 1-4.

This means that vortex shedding may be governing for very slender structures, where the fundamental frequency is low and ratio L_2/L_1 is great.

Further, the risk of vortex shedding increases if several slender structures are placed in line with distance less than approximately 10-15 times the width of the structures (Dyrbye & Hansen, 1997).

Vortex shedding results in cross-wind vibrations, which is beyond the scope of this Thesis, and is therefore not further treated.

3.2 Wind field

The wind field can be divided into three orthogonal fluctuating components, in along-wind, crosswind and vertical direction.

In the along-wind direction	$V(z) + u(x, y, z, t)$	(3-2)
In the crosswind direction	$v(x, y, z, t)$	(3-3)
In the vertical direction	$w(x, y, z, t)$	(3-4)

Where V is in the mean velocity varying with height above ground and u, v and w are fluctuating part of the wind field. (Strømmen, 2010). These three fluctuating components can be treated mathematically as stationary, stochastic processes with zero mean value (Dyrbye & Hansen, 1997). The wind field at a given time, t, can be described by applying a Cartesian coordinate system, where x is in the direction of mean velocity, y in lateral horizontal direction and z in vertical direction with positive value upwards.

The wind flow acting on the building will cause motions composed by three vibrational components, along-wind, crosswind and torsional vibrations (Kwok, Burton, & Abdelrazaq, 2015). However, this Thesis focuses on the along-wind response caused by buffeting and motion induced forces and thus only on the components $V(z)$ and $u(x, y, z, t)$ as shown in Figure 3-3.

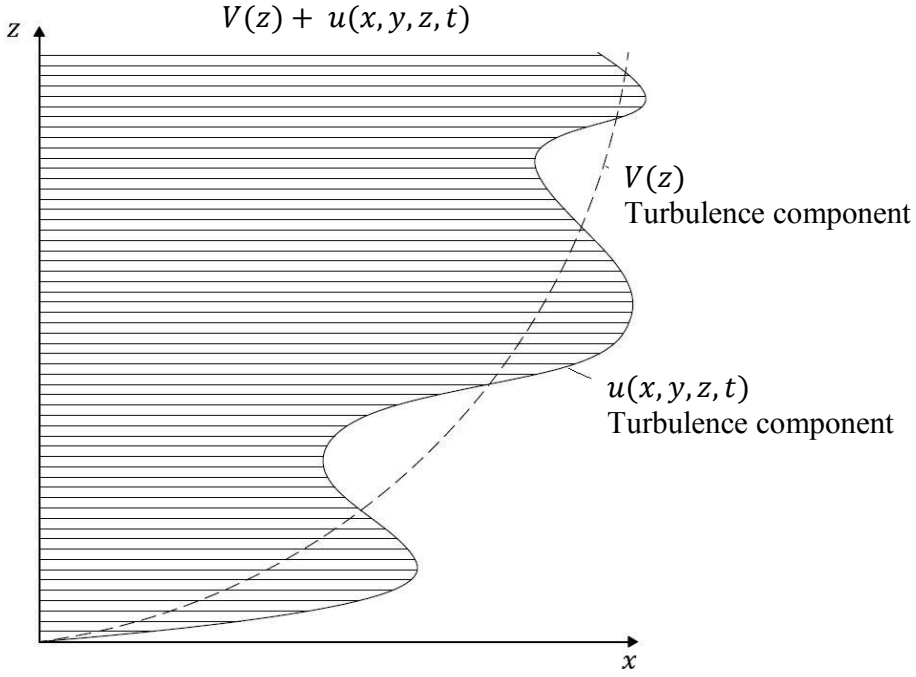

Figure 3-3 Wind field in along-wind direction.

3.3 Statistical parameters

A turbulent wind flow is complex and varies in both time and space in a random way. It is rather difficult to determine its exact value and it is therefore necessary to describe it by statistical terms (Dyrbye & Hansen, 1997). Since wind is omnipresent in our environment, it is important to distinguish between short and long term conditions. Short term events represent a time domain for conditions during a certain weather situation, while long term conditions represent a large set of short term events.

When designing structures, it is required that the time window for the short-term events are sufficiently stationary with zero mean value, to result in homogeneous statistical properties. Thus, it is a general assumption to set a period of $T = 10$ minutes (Strømmen, 2010).

Figure 3-4 *(a)* illustrates a variation of along-wind velocity, V_{tot}. As can be seen in the figure, the magnitude consists of a constant mean value, V, and a fluctuating time-dependent part, $u(t)$.

$$V_{tot} = V + u(t) \tag{3-5}$$

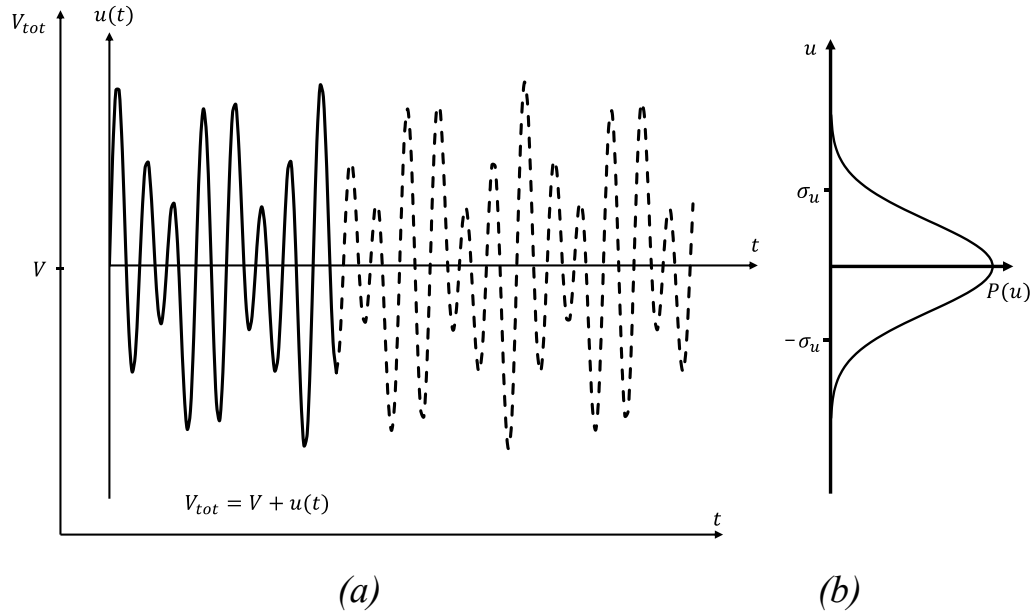

(a) *(b)*

Figure 3-4 Short-term variations, and Gaussian distribution. Figure inspired by (Strømmen, 2010).

The mean value, V, is a typical stochastic variable for which, long-term statistics are used, while statistics in the short-term time window is more interesting for the fluctuating component, $u(t)$. The stochastic process will generate a Gaussian distribution, as illustrated in Figure 3-4 *(b)*.

3.4 Structural response related to wind

Likewise, the acceleration and structural displacement may be regarded as stochastic processes as well. The mean component is time invariant (static) and are typically based on predetermined values taken from design standards (Strømmen, 2010). These characteristic values have been established to represent short-term weather conditions for a specific purpose and location. Thus, only the fluctuating (dynamic) part requires treatment as stochastic processes according to (Strømmen, 2010). It may be shown that, if a stochastic process with zero mean value is stationary and Gaussian distributed, its extreme values is proportional to its standard deviation. As an example, the horizontal peak acceleration, $\ddot{u}_{max}$, is proportional to the standard deviation of acceleration, $\sigma_{\ddot{u}}$, according to:

$$\ddot{u}_{max} = k_p \sigma_{\ddot{u}} \tag{3-6}$$

where k_p is the time invariant peak factor. This means that the focus, when designing for wind load and acceleration, is mainly on the standard deviation, $\sigma_{\ddot{u}}$, of the fluctuating part.

The standard deviation of acceleration can be obtained in two ways. Either by a *Time History Analysis* of the dynamic load effect, which is computationally demanding (Strømmen, 2010). The other alternative, called *Response Spectrum Analysis*, is to use modal approach in the frequency domain. It essentially involves conversion from a power spectrum, representing the loading, to the sought response spectrum (Strømmen, 2010).

This Thesis covers four approaches with response spectrum analysis for estimating the standard deviation of acceleration. These are further investigated and explained in Chapter 4 and 5.

3.5 Mean wind velocity

As described in Section 3.2, the along-wind velocity is described by a mean value, $V(z)$, and a turbulent component, $u(x, y, z, t)$. The mean wind velocity is not only dependent on weather conditions, but also on the terrain, since the friction between air flow and the roughness of terrain cause turbulence, which reduces the mean velocity (Dyrbye & Hansen, 1997). The mean velocity, $V(z)$, can therefore be described by a reference wind velocity based on location and long term weather statistics, and by roughness parameters based on the surroundings of the building.

3.5.1 Reference wind velocity

As described in Section 3.3, wind events can be seen as statistical parameters. When designing structures for wind loads, these statistical processes are based on a reference wind velocity.

Reference wind velocity, V_b, is defined in national annex EKS 10 (Boverket, 2015) for various locations in Sweden. It represents a characteristic mean value of wind velocity during 10 minutes at a height of 10 meters in terrain category II, see Table 3-1, and 50 years of re-occurrence. The interval of re-occurrence represents the probability of exceeding this wind velocity during one year, e.g. 2 % for 50 years of re-occurrence. Magnitudes of reference wind velocity can be found in Figure 3-5 and value for Gothenburg is, $V_{b,50} = 25\ m/s$.

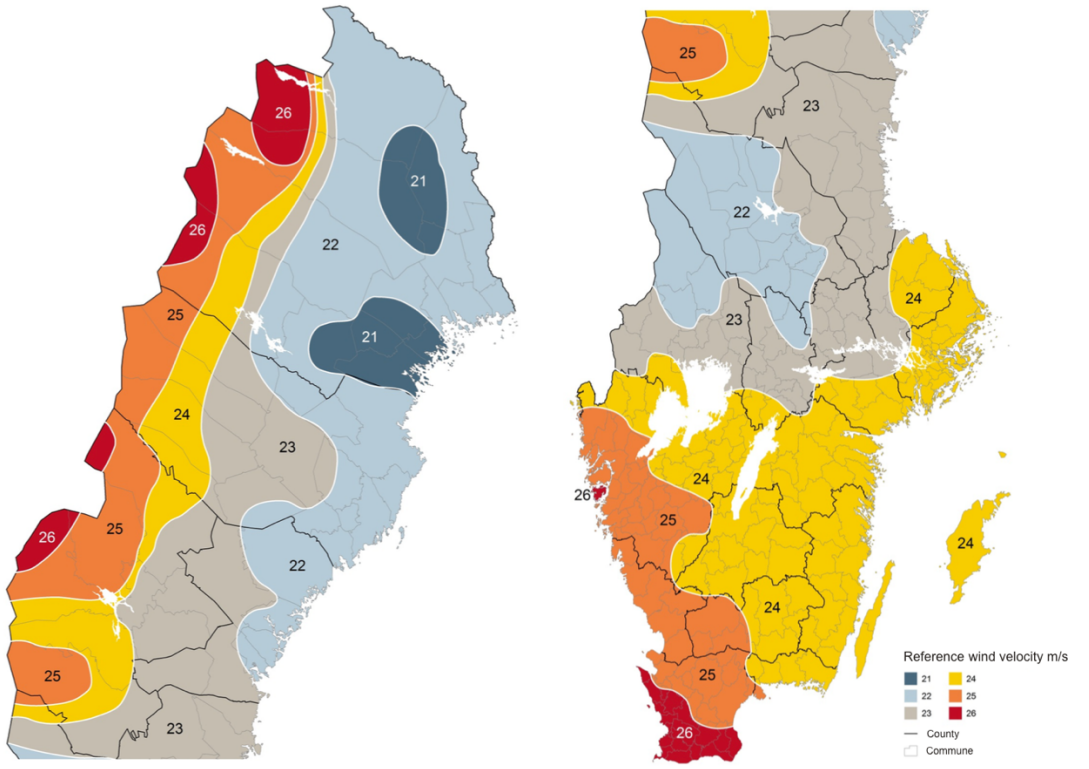

Figure 3-5 Reference wind velocity for different locations in Sweden, from Figure C-4 in EKS 10 (Boverket, 2015).

The reference wind velocity, $V_{b,T}$ at T years of re-occurrence, is then determined according to EKS 10 (Boverket, 2015) as:

$$V_{b,T} = 0{,}75V_{b,50}\sqrt{\left\{1 - 0{,}2\ln\left(-\ln\left(1-\frac{1}{T}\right)\right)\right\}} \qquad (3\text{-}7)$$

When designing for SLS, the acceleration can be determined either as a peak value or standard deviation value. Recommended thresholds for the standard deviation value, stated in ISO 6897 (International Organisation for Standardization, 1984), are based on reference wind velocity with 5-year of re-occurrence, while the limits for peak acceleration are regulated for a 1-year return interval according to ISO 10137 (SIS, 2008).

3.5.2 Terrain categories

In Eurocode 1 Part 1-4 (CEN, 2005), five different terrain categories dependent on location, are introduced. These categories and corresponding characteristics are presented in Table 3-1.

Table 3-1 Terrain categories and terrain parameters, from Table 4.1 in Eurocode 1 Part 1-4 (CEN, 2005) and Table 3.2 in (Dyrbye & Hansen, 1997).

Terrain category		z_o[m]	z_{min}[m]	k_r [-]	α
0	Sea or coastal area exposed to the open sea	0.003	1	0.16	-
I	Lakes or flat and horizontal area with negligible vegetation and without obstacles	0.01	1	0.17	0.12
II	Area with low vegetation such as grass and isolated obstacles (trees, buildings) with separations of at least 20 obstacle heights	0.05	2	0.19	0.16
III	Area with regular cover of vegetation or buildings or with isolated obstacles with separations of maximum 20 obstacle heights (such as villages, suburban terrain, permanent forest)	0.3	5	0.22	0.22
IV	Area in which at least 15 % of the surface is covered with buildings and their average height exceeds 15 m	1.0	10	0.24	0.3

The roughness length, z_0, can be explained as the size of a characteristic vortex which may be created by friction between air flow and inhomogeneous terrain (Dyrbye & Hansen, 1997). The parameter k_r is a terrain factor proportional to the friction velocity. z_{min} is a height, below which the velocity is assumed constant (Dyrbye & Hansen, 1997) and α is the power law exponent used for power law profile in Section 3.5.3.2.

3.5.3 Wind velocity profile

The mean wind velocity, $V(z)$, will decrease with decreasing height since turbulence is caused by roughness of the terrain. The influence of surface roughness decreases with increasing height and the wind velocity is assumed constant at heights around 300-1000m (Handa, 1982). It is called *Geostrophic wind.* It is therefore convenient to describe the mean velocity between the surface and the geostrophic wind by a wind velocity profile.

There are different ways to describe the velocity profile, but a logarithmic profile is used in Eurocode 1 Part 1-4, which is presented in Section 3.5.3.1. However, Kamal Handa (Handa, 1982) uses the power law profile in his method presented in Section 4.2.2.2, and therefore this profile is described in Section 3.5.3.2.

3.5.3.1 Logarithmic profile

The variation of wind velocity along the height, $V(z)$, according to logarithmic velocity profile is determined, in Eurocode 1 Part 1-4 (CEN, 2005), as:

$$V(z) = V_{b,T}\sqrt{C_{exp}(z)} \tag{3-8}$$

$$C_{exp}(z) = \left[k_r \ln\left(\frac{z}{z_0}\right)\right]^2 \quad for\ z \geq z_{min}$$
$$C_{exp}(z) = C_{exp}(z_{min}) \quad for\ z < z_{min} \tag{3-9}$$

With terrain properties, k_r, z_0 and z_{min}, in Table 3-1 and $V_{b,T}$ determined according to Equation (3-7).

For each terrain category, the wind velocity can be plotted along the axial coordinate, z, which gives the logarithmic velocity profile, shown in Figure 3-6.

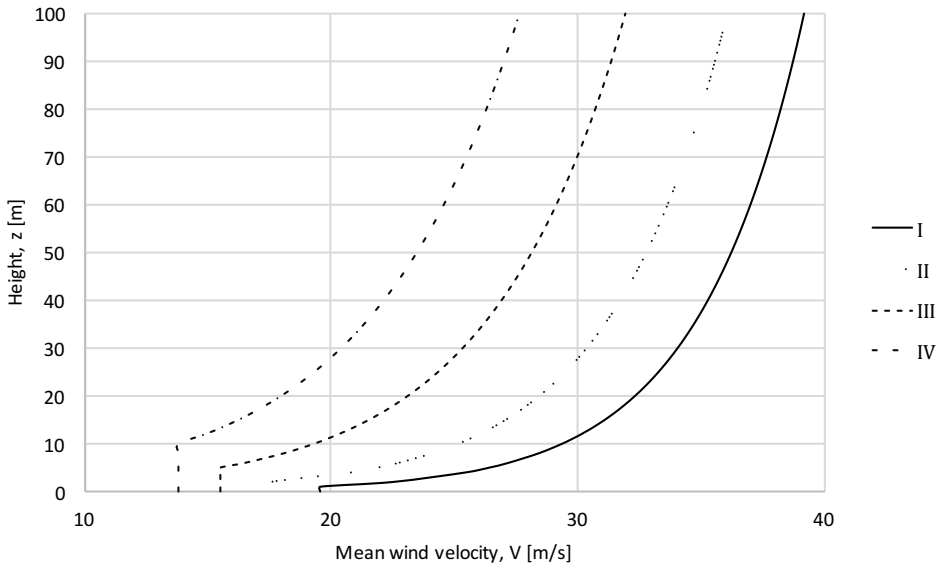

Figure 3-6 Logarithmic velocity profile for different terrain categories as defined in Table 3-1 for Gothenburg climate.

3.5.3.2 Power law profile

The wind profile can also be described by an empirical power law profile (Dyrbye & Hansen, 1997) as:

$$V(z) = V(z_{ref})\left(\frac{z}{z_{ref}}\right)^{\alpha} \tag{3-10}$$

where α is the power law exponent in Table 3-1, and z_{ref} is a reference height which is chosen dependent on the purpose.

As a comparison, the logarithmic profile and power law profile are plotted for terrain category II in Figure 3-7. As shown in the figure, the difference between the two profiles is rather small.

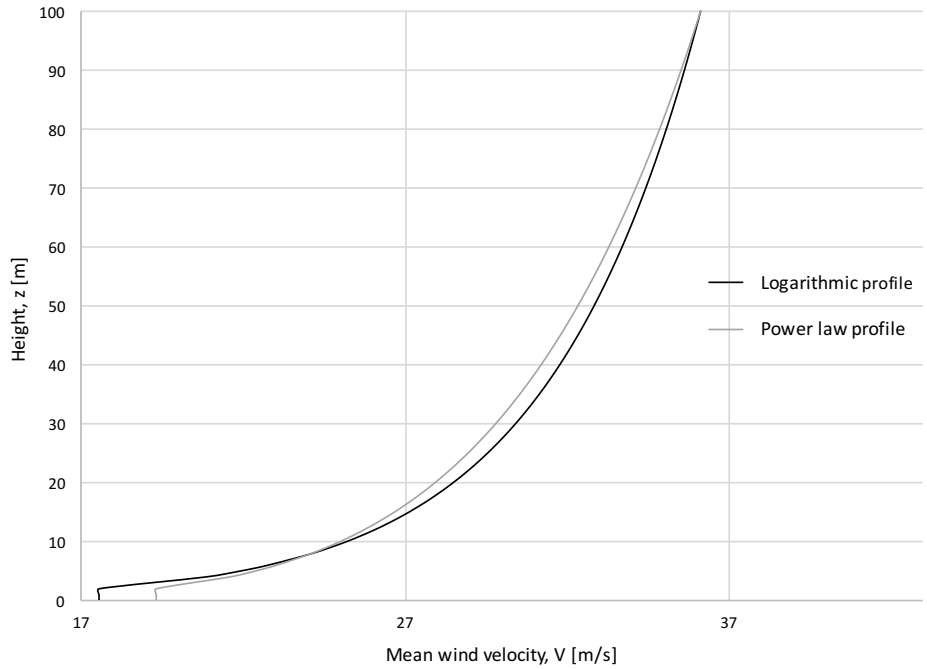

Figure 3-7 Comparison between logarithmic and power law profile for terrain category II, with reference height $z_{ref} = 100m$.

3.5.4 Wind velocity pressure

Mean velocity pressure, $q_m(z)$, can generally be determined as the dynamic pressure as:

$$q_m(z) = \frac{\rho V(z)^2}{2} \tag{3-11}$$

where $\rho = 1.25\ kg/m^3$ is the density of air.

3.6 Wind turbulence

As previously mentioned in Section 3.2, the along-wind field also consist of a turbulence component, $u(x, y, z, t)$, which is more complex than the mean wind velocity, $V(z)$. The turbulence fluctuates in time and space and is therefore described by a stationary stochastic process with a Gaussian distribution, as described in Section 3.3.

3.6.1 Wind-spectral density

Structural response from the turbulence component can be determined with response spectrum analysis, by a power spectrum defined by the wind. This power spectrum is referred to as *Wind-spectral density* and there are several proposed wind-spectral densities based on experiments (Handa, 1982). The wind-spectral density is a probabilistic measure that describes how common turbulence fluctuations are at a given frequency. Figure 3-8 shows an example of Von Kármán's wind-spectral density.

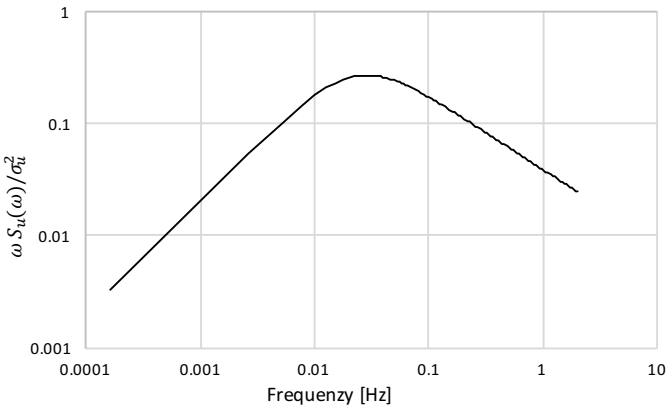

Figure 3-8 Von Kármán's wind-spectral density.

Response spectrum analysis with wind-spectral density is derived and further explained in Chapter 4.

3.6.2 Turbulence intensity

The turbulence is also described by a turbulence intensity, which is defined as the ratio between standard deviation of the turbulence component, $\sigma_u(z)$, and the mean wind velocity, $V(z)$. For flat terrain, and by using logarithmic velocity profile, this can be simplified to:

$$I_u(z) = \frac{\sigma_u(z)}{V(z)} = \frac{1}{\ln(z/z_0)} \tag{3-12}$$

As previously mentioned, influence of turbulence decrease with the height. The intensity of turbulence for terrain category II is shown in Figure 3-9.

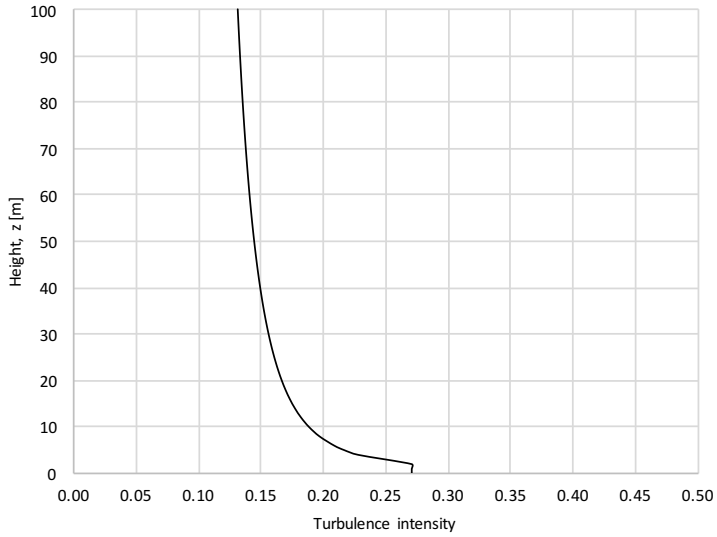

Figure 3-9 Turbulence intensity, $I_u(z)$, for terrain category II.

3.7 Wind tunnel test

An alternative approach to estimate the wind load on structures is to perform a wind tunnel test. The objective of wind tunnel analysis is to fully replicate the real physics of wind loading and the surroundings at model scale, including along-wind, cross-wind and torsional wind loading (Irwin, Denoon, & Scott, 2013). Further, the tests aim to include load combinations, building motion, topography and terrain effects. Wind tunnel tests are however relatively costly.

According to the report by Irwin, Denoon and Scott, a wind tunnel test may be advisable if either: height of the building exceeds 120 m, height of the building is greater than four times its average width, or if the lowest eigenfrequency is less than 0.25 Hz.

The advantages with wind tunnel test compared to a code based approach is that the surroundings and interaction between adjacent buildings can be accounted for, as well as unique design of the building. Further, as described in Chapter 3, only response in along-wind direction can be handled with the approach described in EKS 10 (Boverket, 2015), while other wind phenomena such as cross-wind response can be taken into account with wind tunnel analysis (Irwin, Denoon, & Scott, 2013). Measurements that have been made on finished buildings indicate that wind tunnel predictions of motion correlate fairly well (Kwok, Burton, & Abdelrazaq, 2015).

Even if wind tunnel test has clear advantages, it comes with some uncertainties, such as the validity of wind climate and the assumed structural properties of the building model (Irwin, Denoon, & Scott, 2013).

3.8 Human perception of motion

Human body consists of several subsystems, which are all connected and controlled by our brain. One of these systems that are relevant for perceiving motion is the vestibular system, which control our balance and are located in our inner ear.

Humans ability of localizing in space and controlling its limbs in relation to movement, comes from the receptors that are inside the muscles and tendons (Kwok, Burton, & Abdelrazaq, 2015). These sensors are integrated with the vestibular system, and gives humans the ability to detect acceleration, and distinguish between actively and passive generated head movements (The University of Texas, 2017).

When buildings are exposed to wind, lateral forces will cause certain vibrations in the structure. Human perception of this wind-induced motion is individual and very subjective (Kwok, Burton, & Abdelrazaq, 2015). Some occupants sense this motion and may experience symptoms as nausea, headache and dizziness, while others may be oblivious to the motion. The situation reminds a bit about sickness at sea.

To ensure a good living environment and well-being for visitors in the building, horizontal acceleration is determined for SLS and regulated by comfort requirements based on occupants' tolerance thresholds.

3.9 Regulation and norms

Design for building motion due to wind loads is often governed by tolerance limits for human perception rather than for ultimate structural capacity (Kwok, Burton, & Abdelrazaq, 2015). Norms for estimating wind effects on buildings in the along-wind direction are stated in Eurocode 1 Part 1-4 (CEN, 2005) and Swedish national annex EKS 10 (Boverket, 2015), and these approaches are further explained in Chapter 5.

Also, two alternative approaches, based on theoretical derivations presented by (Strømmen, 2010) and (Handa, 1982), are investigated and explained in Chapter 4.

Recommended limits for horizontal acceleration in SLS are based on occupants' tolerance thresholds. There are separate limits, dependent on the purpose of the building. A typical office building is mainly occupied for eight hours a day, and in case of extreme weather events, people will generally seek refuge in their residence. To ensure that people seeking refuge to their homes, do not fear for their safety nor are discomforted by the vibrations, the requirements are more stringent for residential buildings.

Recommendations on threshold values that are based on standard deviation of acceleration are stated in ISO 6897 (International Organisation for Standardization, 1984) and for the peak acceleration in ISO 10137 (SIS, 2008). These are further described in Section 5.3.

4 Theoretical Approaches to Estimate Wind-Induced Acceleration

Standard deviation and peak value for acceleration for the buffeting response, can be determined on the basis of theoretical derivations for response spectrum analysis. This chapter will derive the expressions for accelerations based on the theory proposed by Einar Strømmen in (Strømmen, 2010) and Kamal Handa in (Handa, 1982).

Strømmen formulates the equations for horizontal, line-like, bridges, which differs from tall buildings in the sense that the height above ground for a bridge is constants, and therefore the wind velocity is constant. However, for a tall building, the wind profile varies with the height above ground, as described in Section 3.5.3. To make the theory applicable for vertical structures, variations in wind velocity along the main coordinate are included.

Determination of structural response for vertical structures with response spectrum analysis have been presented by Kamal Handa (Handa, 1982). The fundamental concepts and derivations are similar with Strømmen's and therefore are the concepts only presented on the basis of (Strømmen, 2010). However, the final expression for standard deviation of acceleration differ between the two approaches and both will be handled in Section 4.2.2.

4.1 Displacement response

The variance of the displacement, $\sigma_{r_i}{}^2$, is defined as the integral of the spectral density of displacement, S_{r_i}, over the entire frequency domain. Hence, the standard deviation of displacement, $\sigma_{r_i}(z)$, can be obtained from:

$$\sigma_{r_i}(z) = \sqrt{\int_0^\infty S_{r_i}(z,\omega)d\omega} \tag{4-1}$$

The spectral density of displacement, $S_{r_i}(\omega)$, describes the response spectrum for the structure, and it is obtained by using a load spectrum described by spectral density of loading, $S_{\tilde{Q}_i}(\omega)$, and the frequency response function, $\widehat{H}_i(\omega)$, describing the the deformation response of the structure. A schematic illustration of the relationship between loading and structural response is shown in Figure 4-1.

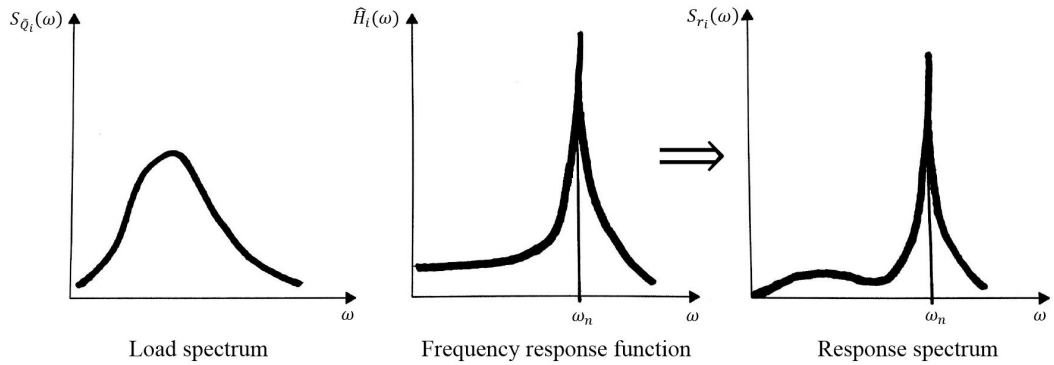

Figure 4-1 Connection between loading and structural response. Figure inspired by (Handa, 1982).

The expression for spectral density of displacement, $S_{r_i}(\omega)$, also contain generalized stiffness, $\widetilde{K}_i$, and mode shape, $\phi_i(z)$, and will be derived in Section 4.1.1.

4.1.1 Spectral density of displacement

The spectral density of displacement, S_r, describes how the modal displacement is distributed over the frequency domain.

It is convenient to start by examine the equation of motion on generalized form.

$$\widetilde{M}_i\ddot{\eta}_i(t) + \tilde{C}_i\dot{\eta}_i(t) + \widetilde{K}_i\eta(t) = \tilde{Q}_i(t) + \tilde{Q}_{ae_i}(t,\eta,\dot{\eta},\ddot{\eta}) \tag{4-2}$$

$$\left.\begin{aligned} \begin{bmatrix}\widetilde{M}_i \\ \tilde{C}_i \\ \widetilde{K}_i\end{bmatrix} &= \begin{bmatrix}\int_0^H {\phi_i}^2(z)m_i(z)dz \\ 2\widetilde{M}_i\omega_n\zeta_i \\ {\omega_n}^2\widetilde{M}_i\end{bmatrix} \\ \begin{bmatrix}\tilde{Q}_i(t) \\ \tilde{Q}_{ae_i}(t,\eta,\dot{\eta},\ddot{\eta})\end{bmatrix} &= \int_{H_{exp_1}}^{H_{exp_2}} \phi_i(z)\begin{bmatrix}q \\ q_{ae}\end{bmatrix}dz \end{aligned}\right\} \tag{4-3}$$

where $\widetilde{M}_i$ is the generalized modal mass, $\tilde{C}_i$ is the generalized modal damping and $\widetilde{K}_i$ is the generalized modal stiffness for mode i. The generalized coordinates and its derivatives are denoted as $\eta, \dot{\eta}, \ddot{\eta}$. The flow-induced loading on the building is denoted as $\tilde{Q}_i(t)$ and $\tilde{Q}_{ae_i}(t,\eta,\dot{\eta},\ddot{\eta})$ is the loading caused by interaction between wind flow and structural motion and H_{exp} is the part of the structure exposed to flow. In the following, it is assumed that the total height of the building is exposed to flow and thus $H_{\exp_1} = 0$ and $H_{exp_2} = H$.

By using Fourier Transform and going from time domain to frequency domain, equation (4-2) can be written as:

$$(-\widetilde{M}_i\omega^2 + \tilde{C}_i i\omega + \widetilde{K}_i)a_{\eta_i} = a_{\tilde{Q}_i}(\omega) + a_{\tilde{Q}_{ae_i}}(\omega,\eta,\dot{\eta},\ddot{\eta}) \tag{4-4}$$

The a-factors are the Fourier amplitudes of the generalized displacements and loadings. According to (Strømmen, 2010) it is assumed that the Fourier amplitude of motion-induced part of the motion induced part, $a_{\tilde{Q}_{ae_i}}$ contains the three known cross-sectional properties, k_{ae}, c_{ae}, m_{ae} and it is further assumed that:

$$a_{\tilde{Q}_{ae_i}} = (-\widetilde{M}_{ae_i}\omega^2 + \tilde{C}_{ae_i}i\omega + \widetilde{K}_{ae_i})a_{\eta_i} \tag{4-5}$$

Where:

$$\begin{bmatrix}\widetilde{M}_{ae_i} \\ \tilde{C}_{ae_i} \\ \widetilde{K}_{ae_i}\end{bmatrix} = \int_0^H \phi_i^2(z)\begin{bmatrix}m_{ae} \\ c_{ae} \\ k_{ae}\end{bmatrix}dz \tag{4-6}$$

By combining expressions (4-3), (4-4) and (4-5), it is obtained that:

$$\left(1-\frac{\widetilde{K}_{ae_i}}{\omega_n^2\widetilde{M}_i}-\left(1-\frac{\widetilde{M}_{ae_i}}{\widetilde{M}_i}\right)\left(\frac{\omega}{\omega_n}\right)^2+2i\left(\zeta_i-\frac{\tilde{C}_{ae_i}}{2\omega_n\widetilde{M}_i}\right)\frac{\omega}{\omega_n}\right)a_{\eta_i}(\omega)=\frac{a_{\tilde{Q}_i}(\omega)}{\widetilde{K}_i} \quad (4\text{-}7)$$

In wind engineering the aerodynamic derivative, $\widetilde{M}_{ae_i}$, is most often negligible (Strømmen, 2010). Further, Strømmen states that $\widetilde{K}_{ae_i}$, will generally only have a significant impact on total stiffness in the velocity region at instability limits. This is not the case for characteristic mean wind velocity and thus $\tilde{C}_{ae_i}$ is the only aerodynamic derivative of interest.

Equation (4-5) can be formulated with the non-dimensional modal frequency response function, $\widehat{H}_i(\omega)$ and by introducing $\zeta_{ae_i}=\tilde{C}_{ae_i}/2\omega_n\widetilde{M}_i$ the following expressions holds:

$$a_{\eta_i}(\omega)=\frac{\widehat{H}_i(\omega)}{\widetilde{K}_i}a_{\tilde{Q}_i}(\omega) \quad (4\text{-}8)$$

$$\widehat{H}_i(\omega)=\left[1-\left(\frac{\omega}{\omega_n}\right)^2+2i\left(\zeta_i-\zeta_{ae_i}\right)\frac{\omega}{\omega_n}\right]^{-1} \quad (4\text{-}9)$$

Where the frequency response function, $\widehat{H}_i(\omega)$, describes the structural response to various frequencies. An illustration of the frequency response function is shown in Figure 4-1.

The spectral density of the generalized coordinates, $S_{\eta_i}(\omega)$, are found by using Equation (4-10). The index * represents complex conjugate.

$$S_{\eta_i}(\omega)=\lim_{T\to\infty}\frac{1}{\pi T}\left(a^*{}_{\eta_i}a_{\eta_i}\right)=\frac{\left|\widehat{H}_i(\omega)\right|^2}{\widetilde{K}_i{}^2}\lim_{T\to\infty}\frac{1}{\pi T}\left(a^*{}_{\tilde{Q}_i}a_{\tilde{Q}_i}\right) \quad (4\text{-}10)$$

$$\Rightarrow S_{\eta_i}(\omega)=\frac{\left|\widehat{H}_i(\omega)\right|^2}{\widetilde{K}_i{}^2}S_{\tilde{Q}_i}(\omega) \quad (4\text{-}11)$$

$S_{\tilde{Q}_i}(\omega)$ in Equation (4-11) represents the spectral density of loading which is derived in Section 4.1.3. The definition of generalized coordinates $r_i(z,t)=\phi_i(z)\eta_i(t)$ implies that:

$$a_{r_i}(\omega)=\phi_i(z)a_{\eta_i}(\omega) \quad (4\text{-}12)$$

By combining equation (4-8) and (4-10), the spectral density of displacement $S_{r_i}(z,\omega)$ can be expressed as:

$$S_{r_i}(z,\omega)=\frac{\phi_i{}^2(z)}{\widetilde{K}_i{}^2}\left|\widehat{H}_i(\omega)\right|^2S_{\tilde{Q}_i}(\omega) \quad (4\text{-}13)$$

Equation (4-13) describes the connection between structural response and loading, which was illustrated in Figure 4-1. To calculate the spectral density of displacement, $S_{r_i}(z,\omega)$, and thus the standard deviation of displacement, $\sigma_{r_i}(z)$, the spectral density of loading, $S_{\tilde{Q}_i}(\omega)$, has to be determined. This is explained in Section 4.1.3.

4.1.2 Damping

The term $(\zeta_i - \zeta_{ae_i})$ in Equation (4-9) contains the structural damping ratio ζ_i and the aerodynamic damping ratio ζ_{ae_i}. The aerodynamical damping is defined positive in the opposite direction of the mechanical damping ratio, and the total damping ratio is therefore the sum of these two. These ratios can be measured by wind tunnel tests or calculated, but since the objective is to compare this method with the ones proposed in Eurocode 1 Part 1-4 (CEN, 2005), logarithmic decrement, δ, are determined according to standards and recalculated to damping ratios using Equation (2-20).

4.1.3 Spectral density of loading

To derive an expression for the spectral density of displacement, the load itself has to be formulated. As explained in Section 3.2, the wind velocity is divided into a time invariant mean value and a fluctuating part with configuration: $V(z) + u(z,t)$ in the along-wind direction and $v(z,t)$ in the direction perpendicular to the flow and $w(z,t)$ in the vertical direction.

By examine an illustration of a general case, in Figure 4-2 , the wind field can be expressed in terms of geometries and displacements. Displacement quantities r_i and velocity pressure q_i for direction i are dependent on flow inclination.

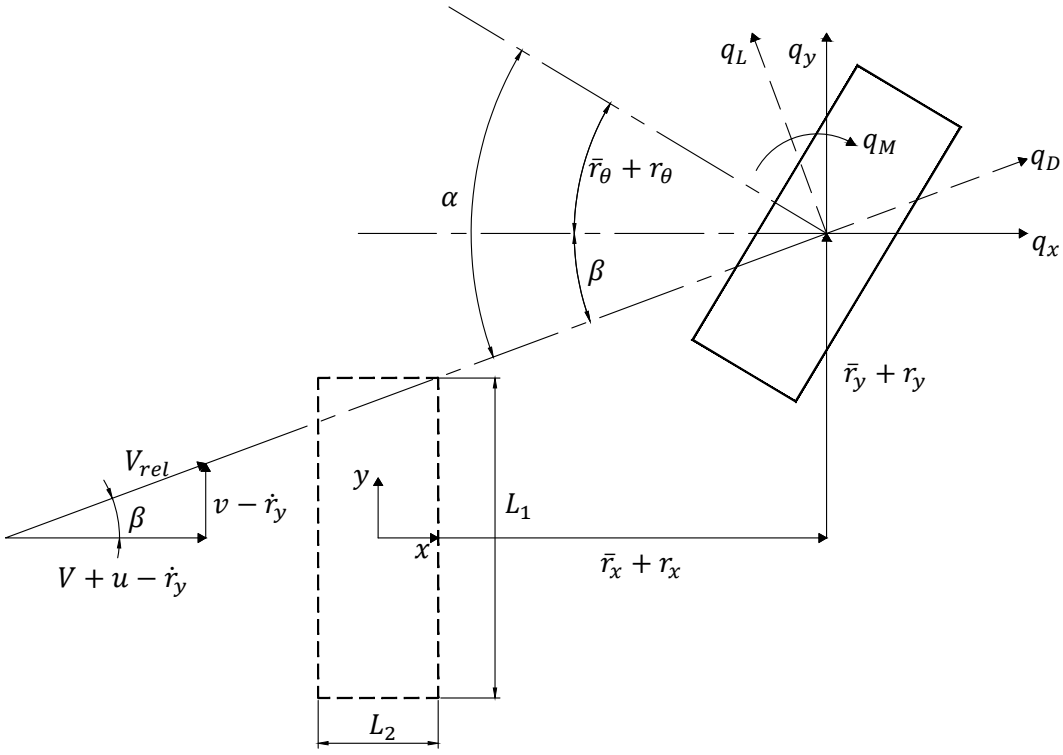

Figure 4-2 Velocity pressure and displacement quantities. Figure inspired by (Strømmen, 2010).

The corresponding wind load can be expressed as:

$$q_{tot}(z,t) = \begin{bmatrix} q_x \\ q_y \\ q_\theta \end{bmatrix}_{tot} = \begin{bmatrix} \cos\beta & -\sin\beta & 0 \\ \sin\beta & \cos\beta & 0 \\ 0 & 0 & 1 \end{bmatrix} \begin{bmatrix} q_D \\ q_L \\ q_M \end{bmatrix} \tag{4-14}$$

$$\begin{bmatrix} q_D(z,t) \\ q_L(z,t) \\ q_M(z,t) \end{bmatrix} = \frac{1}{2}\rho V_{rel}^2 \begin{bmatrix} L_1 C_D \\ L_2 C_L \\ L_2^2 C_M \end{bmatrix} \tag{4-15}$$

Since this Thesis only focuses on the along-wind response with wind flow perpendicular to side L_1, angle $\beta = 0$ and $q_L = q_M = 0$. Thus, the velocity pressure can be expressed:

$$q_{tot}\,(z,t) = q_{x,tot} = \frac{\rho V_{rel}^2 L_1 C_D}{2} \tag{4-16}$$

where C_D is the force coefficient in along-wind direction. It is introduced in Section 3.5.4 as c_f, and this notation is therefore used from here on too.

By assuming that the fluctuating component, $u(z,t)$, is small compared to mean value, $V(z)$, and that the cross-sectional displacement r_x is small, the following linearization could be proven:

$$V_{rel}^2 = (V + u - \dot{r}_x)^2 \approx V^2 + 2Vu - 2V\dot{r}_x \tag{4-17}$$

By combining equation (4-16) and (4-17), the following expression is obtained:

$$q_{x,tot}(z,t) = \frac{\rho V(z)^2 L_1 c_f}{2} + \rho V(z) L_1 c_f u(z,t) - \rho V(z) L_1 c_f \dot{r}_x \tag{4-18}$$

The total load $q_{x,tot}(z,t)$ could be separated into a flow induced part and an aerodynamic part, in the same way as shown in Equation (4-2). The latter term in Equation (4-18) is an aerodynamic property related to damping and for a general case, this should be moved to the left-hand side and included in the frequency response function. However, in this Thesis the damping ratio is estimated from Eurocode 1 Part 1-4 (CEN, 2005) and consequently this term is not further used. Thus, the load term is obtained:

$$q_{x,tot}(z,t) = \frac{\rho V(z)^2 L_1 c_f}{2} + \rho V(z) L_1 c_f u(z,t) \tag{4-19}$$

With the definition in Equation (4-3), the modal load is expressed as:

$$\tilde{Q}_{x,tot}(t) = \int_0^H \phi_x(z) q_{x,tot}(z,t)\, dz \tag{4-20}$$

The first term in Equation (4-19) represents the static loading, $\bar{q}_x$, and the second term is the flow-induced dynamic part. In the following, only the dynamic part will be considered. Combining Equation (4-19) and (4-20), modal loading induced by the fluctuating part of the wind is obtained as:

$$\tilde{Q}_x(t) = \rho L_1 c_f \int_0^H \phi_x(z) V(z) u(z,t) dz \tag{4-21}$$

With corresponding Fourier transform:

$$a_{\tilde{Q}_x}(\omega) = \rho L_1 c_f \int_0^H \phi_x(z) V(z) a_u(z,\omega) dz \tag{4-22}$$

The spectral density of loading is given by:

$$\begin{aligned} S_{\tilde{Q}_x}(\omega) =& \left(\rho L_1 c_f\right)^2 \lim_{T\to\infty} \frac{1}{\pi T} \left[\int_0^H \phi_x(z) V(z) a^*{}_u(z,\omega) dz\right] \cdot \\ &\cdot \left[\int_0^H \phi_x(z) V(z) a_u(z,\omega) dz\right] \end{aligned} \tag{4-23}$$

Rewriting Equation (4-23) and introducing integration variables z_1 and z_2 to transform the product into a double integral, gives:

$$\begin{aligned} S_{\tilde{Q}_x}(\omega) =& \left(\rho L_1 c_f\right)^2 \iint_0^H \phi_x(z_1)\phi_x(z_2) V(z_1) V(z_2) \cdot \\ &\cdot \left(\lim_{T\to\infty} \frac{1}{\pi T} a^*{}_u(z,\omega) a_u(z,\omega)\right) dz_1 dz_2 \end{aligned} \tag{4-24}$$

4.1.3.1 Joint acceptance function

By recognizing the definition of cross spectral density, $S_{nn}(\Delta z, \omega)$ and turbulence intensity, I_u:

$$S_{nn}(\Delta z, \omega) = \lim_{T\to\infty} \frac{1}{\pi T} a^*{}_n(z_1,\omega) a_n(z_2,\omega) \tag{4-25}$$

$$I_u(z) = \frac{\sigma_u(z)}{V(z)} \tag{4-26}$$

By using Equations (4-25) and (4-26) and multiplying Equation (4-24) by $\frac{V(z)^2}{V(z)^2}$, following expression is obtained:

$$S_{\tilde{Q}_x}(\omega) = \left[\rho L_1 c_f J_x(\omega)\right]^2 \tag{4-27}$$

Where the joint acceptance function $J_x(\omega)$ is given by:

$$\begin{aligned} J_x^2(\omega) =& \iint_0^H (\phi_x(z_1)\phi_x(z_2) V(z_1)^2 V(z_2)^2) \cdot \\ &\cdot \left(I_u(z_1) I_u(z_2) \frac{S_{uu}(\Delta z, \omega)}{\sigma_u^2}\right) dz_1 dz_2 \end{aligned} \tag{4-28}$$

The joint acceptance function describes the interaction between the mode shape of the structure and the fluctuating wind load. It should be mentioned that the joint acceptance function in

Equation (4-28) is not equal to the one presented by Strømmen. The differences are that Strømmen does not include mean velocity, V, but does include properties, L_1, L_2 and c_f in the joint acceptance function. However, this is not an issue since the joint acceptance function itself is not of interest, and the differences will not affect the standard deviation of displacement nor the standard deviation of acceleration.

4.1.3.2 Wind-spectral density and Co-spectrums

The cross spectral density, S_{nn}, describes the statistical correlation of fluctuations, at a given frequency, in n-direction between two arbitrary points, (y_1, z_1) and (y_2, z_2). For a horizontal line-like structure such as a bridge, when the width perpendicular to wind flow is very small compared to its length, only the coherence along the main axis is of interest. This is why the theory described in (Strømmen, 2010), only accounts for coherence along the main axis.

However, in the case of a tall building, when the width perpendicular to the flow is significant, also coherence in y-direction may be interesting. This is why, the cross spectral density, in this Thesis, includes both directions, $S_{nn}(\Delta y, \Delta z, \omega)$, between two arbitrary points according to Figure 4-3.

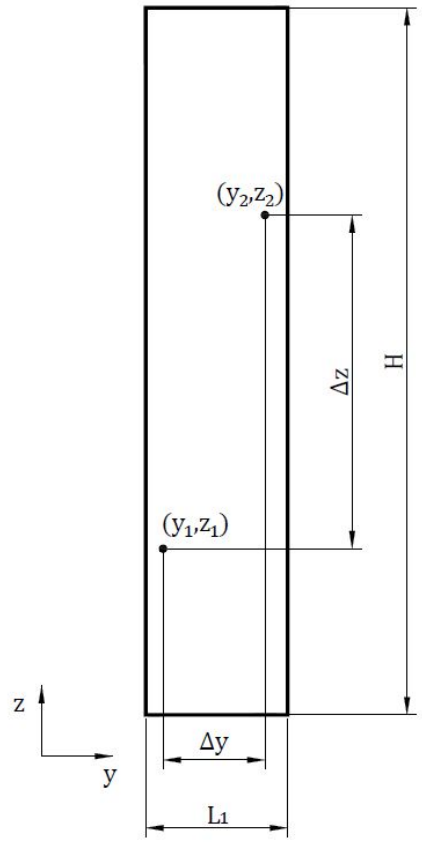

Figure 4-3 Coherence between two arbitrary points.

By using Co-spectrums, $\hat{C}o_{mn}(\Delta i, \omega)$, the cross spectral density can be written in terms of spectral density of a given turbulence component, as:

$$\frac{S_{nn}(\Delta y, \Delta z, \omega)}{\sigma_n^2} = \frac{S_n(\omega)}{\sigma_n^2} \hat{C}o_{mn}(\Delta y, \omega)\hat{C}o_{mn}(\Delta z, \omega) \tag{4-29}$$

The spectral density, $\frac{S_n(\omega)}{\sigma_n^2}$, describes the amount of wind turbulence over the frequency domain. It is a probabilistic measure that describes how common turbulence fluctuations are at a given frequency.

To find expressions for the spectral density of turbulence, the non-dimensional wind-spectral density, $R_N(z, f)$, is introduced. Several empirical wind-spectral densities have been proposed, but the method presented in national annex, EKS 10 (Boverket, 2015), uses the expression presented by (von Kármán, 1948).

$$\begin{aligned} R_N(z,f) &= \frac{fS_u(f)}{\sigma_u^2(z)} = \frac{2\pi f S_u(\omega)}{\sigma_u^2(z)} = \frac{\omega S_u(\omega)}{\sigma_u^2(z)} = \frac{4f_L}{(1+70{,}8f_L^2)^{5/6}} \\ \Rightarrow \frac{S_u(\omega)}{\sigma_u^2(z)} &= \frac{4f_L}{\omega(1+70{,}8f_L^2)^{5/6}} \end{aligned} \tag{4-30}$$

Where the non-dimensional frequency, f_L, is determined according to (Strømmen, 2010):

$$f_L = \frac{fL_u^x(z)}{V(z)} = \frac{\omega L_u^x(z)}{2\pi V(z)} \tag{4-31}$$

The integral length scale, L_u^x, represents the average size of vortices in the wind direction (Dyrbye & Hansen, 1997) and may be expressed as a function of the height, z. However, according to K. Handa (Personal communication, April 26, 2017) it is unnecessary to include height-dependence for the integral length scale, and a reasonable assumption is $L_u^x = 150\ m$.

The two last terms of Equation (4-29), $\hat{C}o_{mn}(\Delta y, \omega)$ and $\hat{C}o_{mn}(\Delta z, \omega)$, are the normalized Co-spectrum, which represents the coherence of spatial properties of the wind turbulence between two points, see Figure 4-3. According to Strømmen, there are several expressions for $\hat{C}o_{mn}$ but for homogeneous conditions, it is suitable to use the one developed by (Davenport, 1962):

$$\hat{C}o_{ui}(\Delta i, \omega) = e^{-C_{ui}\frac{\Delta i \omega}{2\pi V(z)}} \tag{4-32}$$

C_{ui} is the decay coefficient, and according to K. Handa (Personal communication, April 26, 2017) this can be chosen as $C_{uz} = C_{uy} = 8$.

As can be seen from the expression, the normalized Co-spectrum depends on the distance between two points, Δi in i-direction. If the points are located far from each other, the wind field at these locations could not be assumed equal, and thus the cross spectral density is reduced by $\hat{C}o_{ui}$.

By combining expressions (4-29), (4-30), (4-31) and (4-32), the following is obtained:

$$\frac{S_{uu}(\Delta y, \Delta z, \omega)}{\sigma_u^2} = \frac{4\left(\frac{\omega L_u^x}{V(z)}\right)}{\omega\left(1 + 70{,}8\left(\frac{\omega L_u^x}{V(z)}\right)^2\right)^{5/6}} e^{-C_{uy}\frac{|y_1 - y_2|\omega}{2\pi V(z)}} e^{-C_{uz}\frac{|z_1 - z_2|\omega}{2\pi V(z)}} \tag{4-33}$$

Note that expression (4-33) depends on the mean wind velocity $V(z)$ and since it is not squared, it is not possible to include both z_1 and z_2 in $V(z)$ in the double integral in Equation (4-28). However, since the main interest is to determine the acceleration in the top of the building, it is assumed that $V(z)$ is constant for $z = z_{top}$ in Equation (4-33).

Note also that the normalized Co-spectrum in y- direction requires its own double integral over the width, L_1, which are multiplied with the joint acceptance function, $J_x^2(\omega)$, stated in Equation (4-28). This gives the joint acceptance function as:

$$\begin{aligned} J_x^2(\omega) = \iint_0^H (\phi_x(z_1)\phi_x(z_2)V(z_1)^2V(z_2)^2) \cdot \\ \cdot \left(I_u(z_1)I_u(z_2)\frac{S_u(\omega)}{\sigma_u^2}\hat{C}o_{uz}(\Delta z, \omega)\right) dz_1 dz_2 \cdot \\ \cdot \iint_{-\frac{L_1}{2}}^{\frac{L_1}{2}} \hat{C}o_{uy}(\Delta y, \omega)\, dy_1 dy_2 \end{aligned} \tag{4-34}$$

4.1.4 Standard deviation of displacement

By recognizing that $\widetilde{K}_x = {\omega_n}^2 \widetilde{M}_x$ from (4-3) and using expressions (4-13) and (4-27) into Equation (4-1), the standard deviation of displacement for along-wind response can be expressed as:

$$\sigma_{r_x}(z) = |\phi_x(z)| \frac{\rho L_1 c_f}{{\omega_n}^2 \widetilde{M}_x} \left[\int_0^\infty \left|\widehat{H}_x(\omega)\right|^2 J_x^2(\omega) d\omega\right]^{1/2} \tag{4-35}$$

4.1.5 Resonance and background response

It is in structural engineering convenient to separate the deformation response into a background, σ_B^2, and resonance response, σ_R^2, see Figure 4-4.

$$\sigma_{r_x}(z) = \sqrt{\sigma_B^2(z) + \sigma_R^2(z)} \tag{4-36}$$

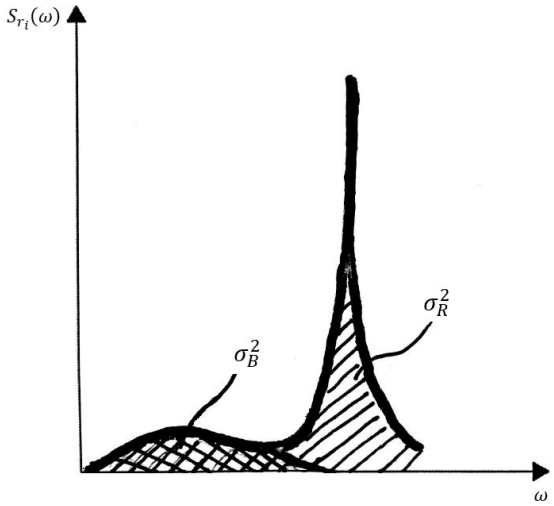

Figure 4-4 Illustration of background and resonant part of total response. Figure inspired by (Handa, 1982).

The background part corresponds to lower frequencies and can be seen as quasi-static and its contribution to inertia forces may be disregarded (Strømmen, 2010). Therefore, the acceleration should be determined by the fluctuating, resonant, part of the response, σ_R^2. This is illustrated in Figure 4-5.

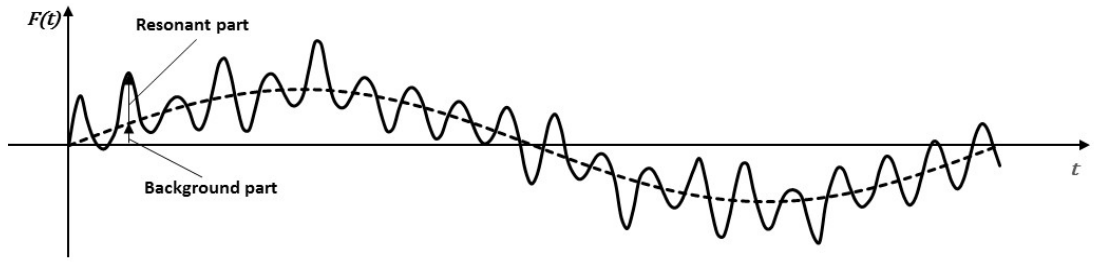

Figure 4-5 Background and resonant part in time domain.

4.2 Acceleration

By definition, the variance of acceleration, $\sigma_{\ddot{u}_i}^2$, is determined by integrating the spectral density of acceleration, $S_{\ddot{u}\,i}$, over the frequency domain.

4.2.1 Spectral density of acceleration

By assuming that the structure oscillates like a cosine function, the following can be obtained:

$$\begin{aligned} u_i(t) &= A\cos(\omega t) \\ \dot{u}_i(t) &= -\omega A\sin(\omega t) \\ \ddot{u}_i(t) &= -\omega^2 A\cos(\omega t) \end{aligned} \tag{4-37}$$

From the expression, it can be seen that the acceleration is given as:

$$\ddot{u}_i(t) = -\omega^2 u_i(t) \tag{4-38}$$

With the Fourier transform, it is obtained that:

$$a_{\ddot{u}_i}(\omega) = -\omega^4 a_{r_i}(\omega) \tag{4-39}$$

With the same way of reasoning as in Section 4.1.1, the spectral density of acceleration can be determined as:

$$\begin{aligned} S_{\ddot{u}_i}(\omega) &= \lim_{T\to\infty} \frac{1}{\pi T}\left(a^*{}_{\ddot{u}_i} a_{\ddot{u}_i}\right) = \omega^4 \lim_{T\to\infty} \frac{1}{\pi T}\left(a^*{}_{r_i} a_{r_i}\right) \\ \Rightarrow S_{\ddot{u}_i}(\omega) &= \omega^4 S_{r_i}(\omega) \end{aligned} \tag{4-40}$$

The spectral density of acceleration, $S_{\ddot{u}_i}(\omega)$, can be expressed as a function of the displacement response. Since it is multiplied with ω^4, the acceleration response tends to zero for lower frequencies. The behaviour is illustrated in Figure 4-6.

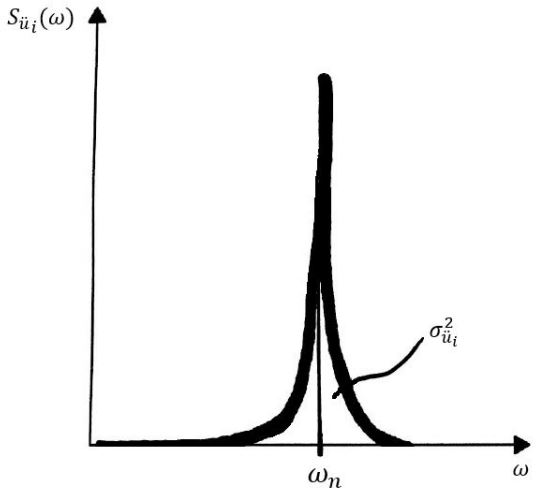

Figure 4-6 Illustration of variation of spectral density of acceleration.

As can be seen, the acceleration response is mainly occurring at frequencies in the region of resonance. This supports the reasoning in Section 4.1.5, that the acceleration can be determined for the resonant part of the response, σ_R^2.

4.2.2 Standard deviation of acceleration

Using the same way of reasoning as for the standard deviation of displacement in Equation (4-1), the standard deviation of acceleration can be determined as the square root of the integral of spectral density of acceleration over the frequency domain, and expressed as:

$$\sigma_{\ddot{u}_i}(z) = \sqrt{\int_0^\infty S_{\ddot{u}_i}(z,\omega)d\omega} \tag{4-41}$$

Using Equations (4-13), (4-27) and (4-40), and substituting $\widetilde{K}_x = {\omega_n}^2 \widetilde{M}_x$, in (4-41), the standard deviation of acceleration in the along-wind direction can be determined as:

$$\sigma_{\ddot{u}_x}(z) = |\phi_x(z)| \frac{\rho L_1 c_f}{{\omega_n}^2 \widetilde{M}_x} \left[\int_0^\infty \omega^4 \left| \widehat{H}_x(\omega) \right|^2 J_x^2(\omega) d\omega \right]^{1/2} \quad (4\text{-}42)$$

As described in Section 4.1.5, the acceleration is determined from the resonant part of the response. This could be found by integrating the spectral density of acceleration solely over the resonant part. But for systems with low damping, the width (frequency domain) of the resonant part is quite narrow and thus it could be approximately determined for the fundamental frequency $\omega = \omega_n$ (Handa, 1982).

4.2.2.1 According to Strømmen

On the basis of the reasoning in Section 4.1.5 and final expression (4-42), (Strømmen, 2010) suggests that the resonance part can be approximately determined as:

$$\sigma_{\ddot{u}_x}(z) = \sqrt{\omega_n^4 \sigma_{R_x}^2(z)} = \sqrt{\omega_n^4 \left[\frac{\phi_x(z)}{{\omega_n}^2 \widetilde{M}_x} \right]^2 \left[\frac{\pi \omega_n S_{\tilde{Q}_x}(\omega_n)}{4(\zeta_i - \zeta_{aei})} \right]} \quad (4\text{-}43)$$

4.2.2.2 According to Handa

An alternative way of determining the acceleration from the response spectrum is given in (Handa, 1982). Handa's final expression for standard deviation of acceleration is:

$$\begin{aligned} \sigma_{\ddot{u}_x}(z) &= \sqrt{\omega_n^4 \sigma_{R_x}^2(z)} \\ &= \sqrt{\omega_n^4 4 \left[W \frac{\phi_x(z)}{{\omega_n}^2 \widetilde{M}_x} \right]^2 I_u^2(z_{top}) \frac{H_c V_c}{(\zeta_i - \zeta_{aei})} \frac{\omega_n S_u(\omega_n)}{\sigma_u^2(z)}} \end{aligned} \quad (4\text{-}44)$$

By examining expression (4-44), one can notice some similarities with the expression according to Strømmen in Equation (4-43). However, the main difference between the two approaches is that the loading in Equation (4-44) is partly expressed by the generalized wind load, W, as:

$$W = H L_1 \frac{1}{2} \rho c_f V\left(z_{top}\right)^2 \int_0^1 \phi_x(\tau) (\tau)^{2\alpha} d\tau \quad (4\text{-}45)$$

where the integrated variables that Strømmen used, z_1, z_2, y_1 and y_2, are substituted to: $\tau_i = \frac{z_i}{H}$ and $\theta_i = \frac{y_i}{L_1}$.

Equation (4-45) can be explained by observing the expression for generalized force in Equation (2-44):

$$\tilde{p} = W = \int_0^H P(z,t) \phi_x(z) dz \quad (4\text{-}46)$$

With the expression for the wind load, P, velocity pressure, q_m, and mean wind velocity, $V(z)$, according to power law profile, all described in Section 3.5.

$$P(z,t) = c_f q_m(z) A \tag{4-47}$$

$$q_m(z) = \frac{\rho[V(z)]^2}{2} \tag{4-48}$$

$$V(z) = V(z_{top}) \left(\frac{z}{H}\right)^{\alpha} \tag{4-49}$$

$$A = HL_1 \tag{4-50}$$

H_c and V_c, are correlation factors in horizontal and vertical direction respectively. They are similar to what Strømmen introduced as Co-spectrum in Section 4.1.3.2, but in (Handa, 1982) expressed as:

$$H_c = \iint_0^1 e^{-|\theta_1 - \theta_2| \frac{C_{uy} L_1 \omega_n}{2\pi V(z_{top})}} d\theta_1 d\theta_2 \tag{4-51}$$

$$V_c = \frac{\iint_0^1 \phi_x(\tau_1)\phi_x(\tau_2)(\tau_1\tau_2)^{\alpha} e^{-|\tau_1 - \tau_2| \frac{C_{uz} H \omega_n}{2\pi V(z_{top})}} d\tau_1 d\tau_2}{\left[\int_0^1 \phi_x(\tau)(\tau)^{2\alpha} d\tau\right]^2} \tag{4-52}$$

The last term in Equation (4-44), $\frac{\omega_n S_u(\omega_n)}{\sigma_u^2(z)}$, is the non-dimensional wind-spectral density explained in Section 4.1.3.2 and can be determined from Equation (4-30).

5 Approach Suggested in Design Codes

In this chapter follows an explanation in how to design buildings for acceleration in serviceability limit state according to methods presented in two common codes used in the industry. Acceleration according to methods proposed in the Swedish national annex EKS 10 (Boverket, 2015) and Eurocode 1 Part 1-4 Annex B (CEN, 2005) will be explained.

The methods consider response in the first mode, for turbulence in along-wind direction, x, when the wind load are in resonance with the structure (CEN, 2005).

5.1 Idealization

According to the design approach described in Eurocode 1 Part 1-4 (CEN, 2005), structures exposed to lateral forces, such as wind loads, can be idealized as a cantilever with fixed support. For this idealization, Eurocode 1 Part 1-4 suggests that the acceleration should be determined for the first mode in the wind direction, where the mode shape $\phi_x(z)$, along the axial coordinate, z, is described as:

$$\phi_x(z) = \left(\frac{z}{H}\right)^{\xi} \tag{5-1}$$

where $\xi = 1.5$ is the recommended value for tall buildings according to Eurocode 1 Part 1-4 (CEN, 2005). The resulting mode shape are shown in Figure 5-1.

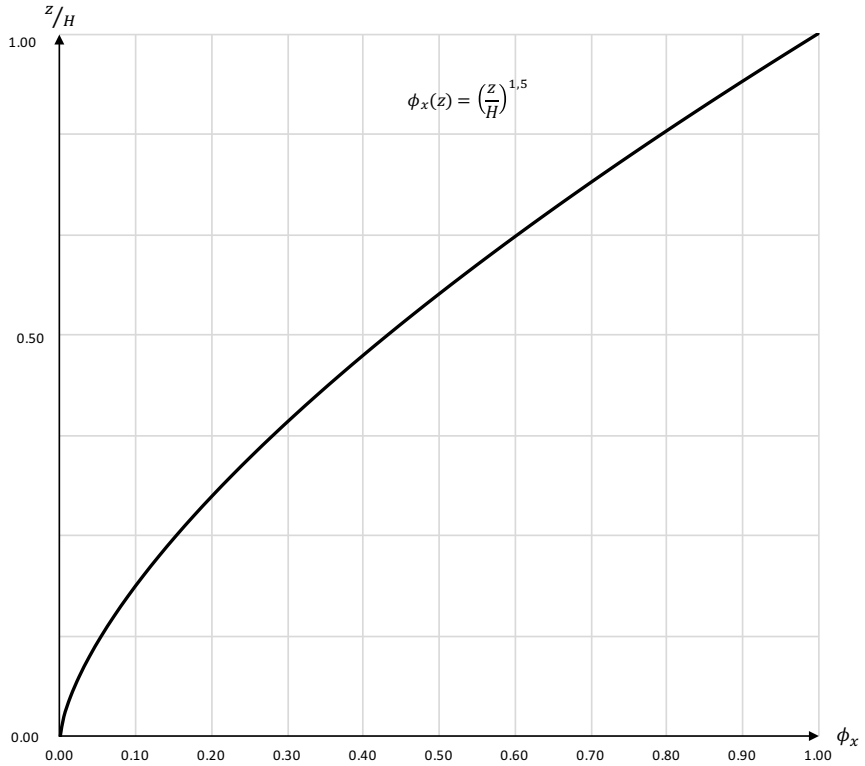

Figure 5-1 Suggested mode shape for tall buildings according to Eurocode 1 Part 1-4 (CEN, 2005).

5.2 Acceleration

As described previously, acceleration is regulated by comfort requirements in serviceability limit state. These recommended values are given both for the peak value of acceleration, $\ddot{u}_{max}$, and its standard deviation, $\sigma_{\ddot{u}_x}$.

5.2.1 Standard deviation of acceleration according to EKS 10

The method presented in Swedish national annex EKS 10 (Boverket, 2015), is based on the old design code for snow- and wind loads on structures (Boverket, 1997). The wind-induced acceleration part in the codes, is written by Kamal Handa, and is a simplified version to the method he developed in (Handa, 1982), described in Section 4.2.2.2.

EKS 10 suggests that the standard deviation of acceleration, $\sigma_{\ddot{u}_x}(z)$, should be determined by:

$$\sigma_{\ddot{u}_x}(z) = \frac{3I_u(z_{top})R_{EKS}q_m(z_{top})L_1 c_f \phi_x(z)}{m_e} \tag{5-2}$$

where:

$$R_{EKS} = \sqrt{\frac{2\pi R_N(f_x)\phi_b\phi_h}{\delta_s + \delta_a}} \tag{5-3}$$

$$R_N(f_x) = \frac{f_x S_u(f_x)}{\sigma_u^2} = \frac{4f_L(f_x)}{(1 + 70{,}8f_L(f_x)^2)^{\frac{5}{6}}} \tag{5-4}$$

$$f_L(f_x) = \frac{150 f_x}{V(z_{top})} \tag{5-5}$$

$$\phi_h = \frac{1}{1 + \frac{2f_x H}{V(z_{top})}} \tag{5-6}$$

$$\phi_b = \frac{1}{1 + \frac{3{,}2f_x L_1}{V(z_{top})}} \tag{5-7}$$

$$\delta_a = \frac{c_f \rho L_1 V(z_s)}{2 f_x m_e} \tag{5-8}$$

$$m_e = \frac{\widetilde{M}_x}{\int_0^H {\phi_x}^2(z)dz} \tag{5-9}$$

$$z_s = 0{,}6H \tag{5-10}$$

Where $V(z_{top})$ are determined according logarithmic velocity profile in Equation (3-8) in Section 3.5.3 and $q_m(z_{top})$ according to Equation (3-11) in Section 3.5.4.

As can be observed from Equation (4-5), the integral length scale introduced in Section 4.1.3.2, is chosen to be $L_u^x = 150\ m$. This is a reasonable assumption according to K. Handa (Personal communication, April 26, 2017).

Handa explained that these expressions are simplified from the equations presented in (Handa, 1982), described in Section 4.2.2.2. The mode shape, ϕ_x, was assumed according to Equation (5-1), when simplifying expressions containing integrals over the mode shape. He explained that ϕ_h and ϕ_b are simplified expressions representing, what was introduced in Section 4.2.2.2 as, H_c and V_c, respectively. These factors accounts for coherence in vertical and horizontal direction and are simplified with the assumption of $\alpha = 0{,}21$ and with decay constants $C_{uz} = C_{uy} = 8$.

5.2.2 Standard deviation of acceleration according to EN 1991-1-4

Eurocode 1 Part 1-4 Annex B (CEN, 2005) proposes following method for estimating the standard deviation of acceleration in SLS.

$$\sigma_{\ddot{u}_x}(z) = \frac{c_f \rho L_1 I_u(z_s) V^2(z_s)}{m_e} R_{EC} K_x \phi_x(z) \tag{5-11}$$

Where:

$$R_{EC} = \sqrt{\frac{\pi^2}{2(\delta_s + \delta_a)} R_N(z_s, f_x) R_h(\eta_h) R_b(\eta_b)} \tag{5-12}$$

$$R_N(z_s, f_x) = \frac{f_x S_u(z_s, f_x)}{\sigma_u^2} = \frac{6.8 f_L(z_s, f_x)}{\left(1 + 10.2 f_L(z_s, f_x)\right)^{5/3}} \tag{5-13}$$

$$f_L(z_s, f_x) = \frac{f_x L_u^x(z_s)}{V(z_s)} \tag{5-14}$$

$$L_u^x(z_s) = 300 \left(\frac{z_s}{200}\right)^{0.67 + 0.05 \ln(z_o)} \quad \text{for } z \geq z_{min}$$
$$L_u^x(z_s) = L_u^x(z_{min}) \quad \text{for } z < z_{min} \tag{5-15}$$

$$R_h = \frac{1}{\eta_h} - \frac{1}{2\eta_h^2}(1 - e^{-2\eta_h}) \tag{5-16}$$

$$R_b = \frac{1}{\eta_b} - \frac{1}{2\eta_b^2}(1 - e^{-2\eta_b}) \tag{5-17}$$

$$\eta_h = \frac{4.6H}{L_u^x(z_{top})} f_L(z_s, f_x) \tag{5-18}$$

$$\eta_b = \frac{4.6L_1}{L_u^x(z_{top})} f_L(z_s, f_x) \tag{5-19}$$

$$K_x = \frac{\int_0^H V^2(z) \phi_x(z) dz}{V^2(z_s) \int_0^H \phi_x^2(z) dz} \tag{5-20}$$

According to (Dyrbye & Hansen, 1997), the expressions related to wind turbulence in Eurocode 1 Part 1-4 are simplified from theoretical derivations. Dyrbye and Hansen states that the normalized Co-spectrums, $\hat{C}o_{ui}$, described in Section 4.1.3.2, are simplified with decay constants, $C_{uz} = C_{uy} = 11.5$.

By observing Equation (5-13), it can be noticed that the wind-spectral density, R_N, is not the same as introduced in previous methods. This expression is referred to as Kaimal's wind-

spectral density and is an empirical expression describing the same phenomenon as von Kármán's expression, in Section 4.1.3.2.

Further, it can be noticed that the integral length scale, L_u^x, not only affects the wind-spectral density, R_N, but also other variables, and is defined as a function of height instead of Handa's approximation of $L_u^x = 150\ m$.

5.2.3 Peak acceleration

As described in Section 3.4, the peak acceleration, $\ddot{u}_{max}(z)$ is calculated according to Equation (3-6) as a function of standard deviation of acceleration, $\sigma_{\ddot{u}_x}(z)$:

$$\ddot{u}_{max}(z) = k_p \sigma_{\ddot{u}_x}(z) \tag{5-21}$$

$$k_p = \sqrt{2\ln(\nu T)} + \frac{0{,}6}{\sqrt{2\ln(\nu T)}} \tag{5-22}$$

$$\nu = f_x \frac{R}{\sqrt{B^2 + R^2}} \tag{5-23}$$

$$B^2 = \exp\left[-0{,}05\left(\frac{H}{H_{ref}}\right) + \left(1 - \frac{L_1}{H}\right)\left(0{,}04 + 0{,}01\left(\frac{H}{H_{ref}}\right)\right)\right] \tag{5-24}$$

Where $R = R_{EKS}$ or $R = R_{EC}$ dependent on approach and $H_{ref} = 10\ m$ and $T = 600\ s$ (10 min) as described in Section 3.5.1 and stated in EKS 10 (Boverket, 2015).

5.3 Comfort recommendations

As described in Section 3.9, recommended limits for wind-induced motion are based on tolerance thresholds for acceleration in serviceability limit state. These are stated in ISO 6897 (International Organisation for Standardization, 1984) and ISO 10137 (SIS, 2008). The tolerance limits are different dependent on the purpose of the building and depends on what frequency the acceleration occurs at.

5.3.1.1 Peak acceleration

The peak acceleration should be evaluated in relation to corresponding fundamental frequency, f_x, according to ISO 10137 (SIS, 2008). The recommended values are shown in Figure 5-2. Important to note is that the evaluation curves shown in the figure is related to a reference wind velocity for one-year return period, which has to be taken into consideration when defining the reference wind velocity according to (3-7) in Section 3.5.1.

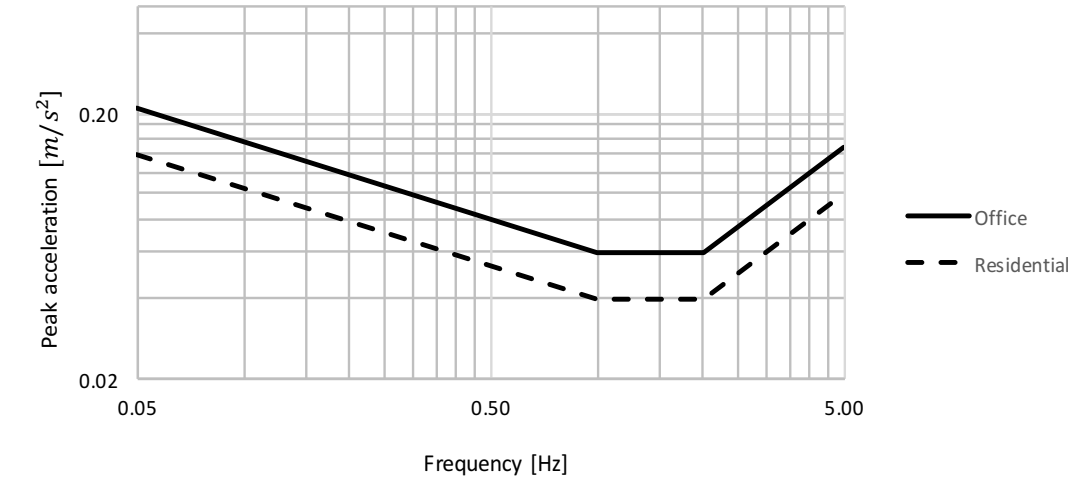

Figure 5-2 Evaluation curves for peak acceleration with one-year return interval in relation to corresponding eigenfrequency, from Figure D.1 in ISO 10137 (SIS, 2008).

5.3.1.2 Standard deviation

Recommended values for standard deviation of acceleration, $\sigma_{\ddot{u}_x}(z)$, are stated in ISO 6897 (International Organisation for Standardization, 1984). The evaluations curves are shown in Figure 5-3 and are based on five-year return interval which has to be taken into account when defining the wind velocity in Section 3.5.1.

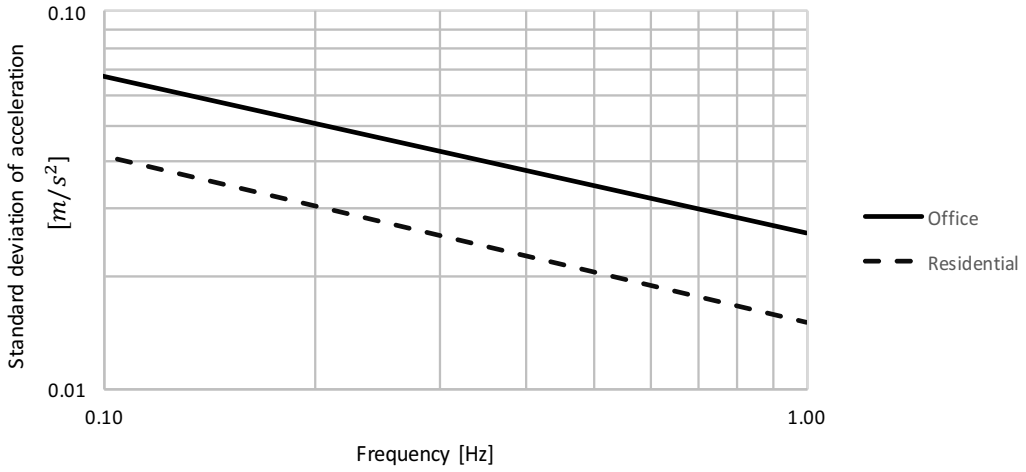

Figure 5-3 Threshold for standards deviation of acceleration, from Figure 1 and Figure 2 in IS0 6897 (International Organisation for Standardization, 1984).

6 Development of Analytical Model with Varying Support Stiffness

The main objective of this Thesis is to investigate how the acceleration in a building is affected by support conditions. An analytical model is therefore developed as a tool to calculate the fundamental frequency and corresponding mode shape, for adjustable stiffness of the foundation. This is done by modal analysis according to the theory presented in Chapter 2, and calculations are performed by MATLAB-program in Appendix C.

This chapter aims to describe a proposed idealization of a tall building with deep foundation, how the model for modal analysis and corresponding MATLAB-program is being built and a verification of the analytical model.

6.1 Idealization

For office buildings, where regularly an open working environment is desirable, loads are commonly carried by a rigid core to the foundation. The structural stiffness of the building is therefore highly dependent on the stiffness of the core, and particularly the bending stiffness for horizontal actions on the building.

6.1.1 Foundation

Buildings founded close to the bedrock have good ability to anchor the reaction forces in solid rock, and for such a situation, it is reasonable to idealize it as a fixed support. However, with foundation on piles, horizontal loads will result in a moment around the centroid axis in the base of the building. This moment can be expected to be carried by the piles in the foundation. If loads are of such magnitude that the piles deform axially with $\pm\Delta L$, the building will be exposed to a certain rotation, θ_{rot}, around the gravity centre in the base. The principle is shown in Figure 6-1 *(a)*.

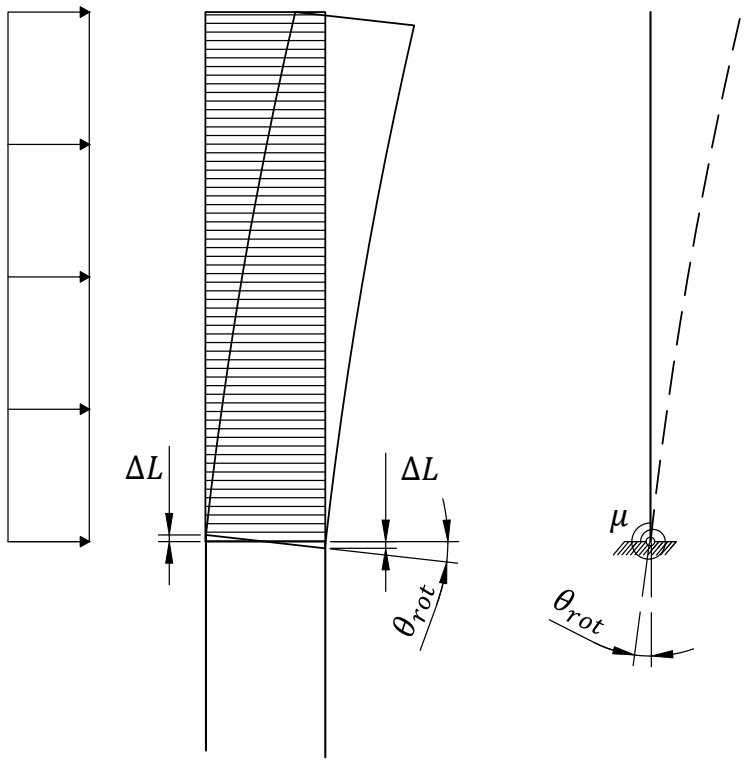

Figure 6-1 Example on behaviour of tall building subjected to horizontal loading.

With this expected behaviour, the foundation can be seen as rather flexible and the idealization of a fixed support does not hold. Since the resulting moment may cause a rotation of the building support, the idealization of the support needs to be partially fixed. The piles will counteract the rotation and thus result in a rotational stiffness, μ. An idealization corresponding to the situation is shown in Figure 6-1 *(b)*.

Where the resulting moment and the corresponding rotation are related according to:

$$M = \mu\theta_{rot} \tag{6-1}$$

How the rotational stiffness may be estimated, are further discussed in Section 6.4.2.

6.1.2 Building

As mentioned in Section 6.1, the bending stiffness of the core is important when designing for horizontal loads since the main purpose of the core is to transfer loads to the foundation.

Shear deformations are neglected according to Euler-Bernoulli beam theory and the structural system can therefore be idealized as a cantilever beam with sectional properties, EI, A and L representing the core of the building. This is reasonable since the height of the core is large compared to its depth. The idealization is shown in Figure 6-2, divided into an arbitrary number of elements, n with $3(n+1)$ degrees of freedom, preferably one element per storey.

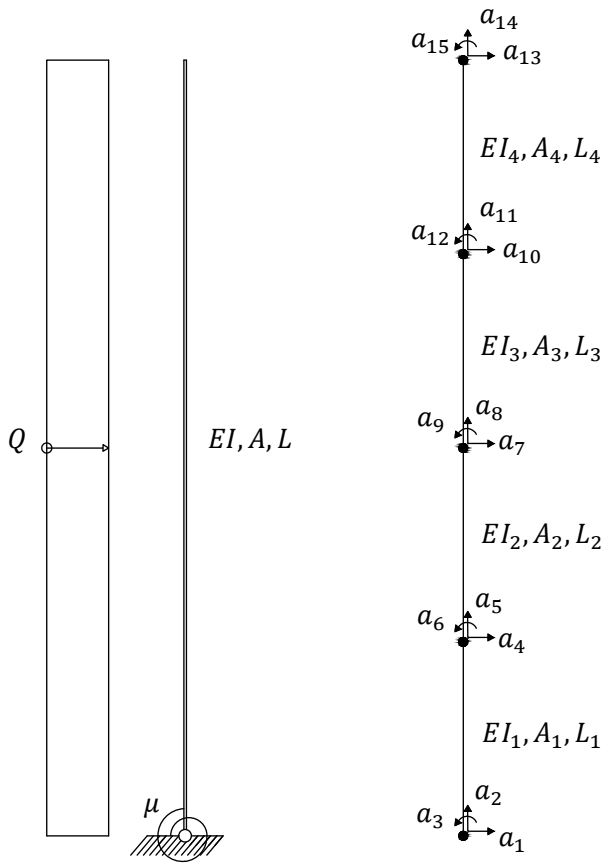

Figure 6-2 Idealization as beam elements.

Axial deformations of the core are here neglected and thus, the vertical degrees of freedom, will be disregarded from the analysis.

6.2 Modal analysis

6.2.1 Mass and stiffness matrix

The core is divided into an arbitrary number of elements, n, with $n + 1$ nodes and $2(n + 1)$ degrees of freedom. For simplicity, the modal analysis is based on lumped mass method, which means that the mass along each element is replaced by point masses at its two adjacent nodes. Since the building contains significant amount of mass which is not included in the core (floors, walls, installations), also these masses are estimated and lumped to the corresponding node.

According to (Chopra, 2012), it is reasonable to neglect the rotational inertia forces and thus set $m_{jj} = 0$ for all cells that corresponds to rotational degrees of freedom, j, in the mass-matrix. An example of discretization is shown in Figure 6-3.

With the idealization of a cantilever, divided into beam elements, a stiffness matrix can be formulated. The replacement of a rotational spring instead of fixed support will only affect the rotational DOF in the bottom of the cantilever, as illustrated by the example in Figure 6-3.

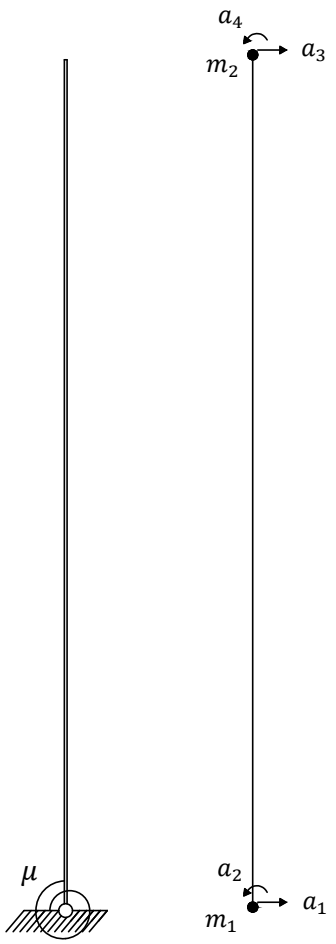

$$\boldsymbol{k} = \begin{bmatrix} k_{11} & k_{12} & k_{13} & k_{14} \\ k_{21} & k_{22}+\mu & k_{23} & k_{24} \\ k_{31} & k_{32} & k_{33} & k_{34} \\ k_{41} & k_{42} & k_{43} & k_{44} \end{bmatrix}$$

$$\boldsymbol{m} = \begin{bmatrix} m_1 & 0 & 0 & 0 \\ 0 & 0 & 0 & 0 \\ 0 & 0 & m_2 & 0 \\ 0 & 0 & 0 & 0 \end{bmatrix}$$

Figure 6-3 Example of discretization of a beam element.

6.2.2 Fundamental frequency and mode shape

As mentioned in Section 2.2.1.2, the effect of damping on the fundamental frequency can be neglected for structure in civil engineering. The fundamental frequencies and corresponding mode shapes is determined by solving the eigenvalue problem stated by Equation (2-55) in Section 2.3.2. A building with n storeys, and $N = 2(n+1)$ degrees of freedom, will generate matrices with the size of $N \times N$, which induces that the matrices will be large for a tall building. Solution methods are iterative in nature, since it is equivalent of finding roots to a N-degree polynomial. Since there are no explicit formulas for finding polynomial degree larger than 4, the eigenvalue problem has to be solved numerically. In this Thesis, it is done by the MATLAB-code, see Appendix C.

The solution to the eigenvalue problem will result in a matrix, $\boldsymbol{\Phi}$, with columns describing each mode and a vector, $\boldsymbol{\omega}$, with eigenfrequencies corresponding to N numbers of modes describing the dynamic response of the structure with rotational and horizontal degrees of freedom, as visualized in Figure 6-4 *(b)*.

However, when calculating the acceleration for the first mode, only the horizontal translation is of interest and thus the mode shape is reduced to include only horizontal degrees of freedom, which then are numbered $(1, 2, \dots, m)$, where $m = n + 1$. The eigenfrequency corresponding

to the first mode is reffered to as the fundamental frequency, ω_n. The resulting mode vector and frequency is shown in Figure 6-4 *(c)*.

It is further, convenient to normalize the mode shapes such that the maximum value is equal to 1. Figure 6-4 *(a)* shows an example of a normalized first mode with respect to horizontal displacements.

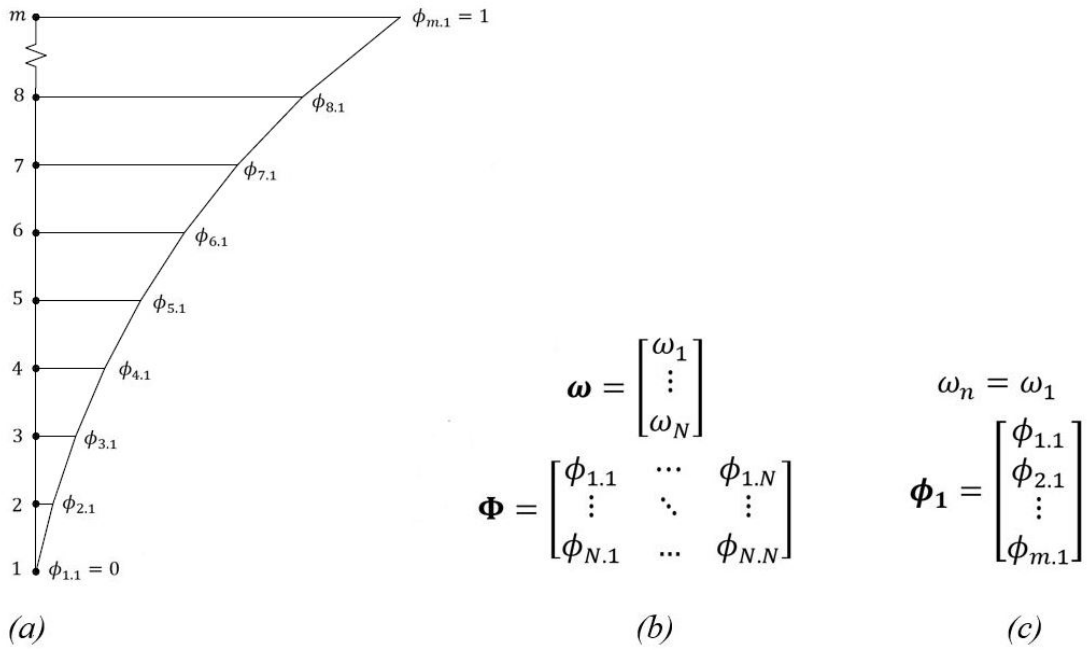

Figure 6-4 Mode shape corresponding to the first mode.

6.3 Determination of acceleration

With fundamental frequency and mode shape, the acceleration can be determined. The MATLAB-program is designed to run all four approaches described in Chapter 4 and 5 in vector form. The mode shape corresponding to the first mode is extracted from the first column of matrix, $\boldsymbol{\phi}$, in Figure 6-4 *(c)* to a vector.

The calculations of acceleration contain several integrals, both with respect to geometry and frequency domain. To perform these integrals numerically by MATLAB, rectangular rule is used as integration method.

To increase accuracy of the integration, each storey in the model is divided into 20 integration points, which results in a mode shape vector of length $(20n + 1)$. The vector representing the frequency domain will be set to the same length.

6.4 Verification of analytical model

To verify that the analytical model is well developed, a homogeneous core of a tall building is modelled in FEM-Design 16 (StruSoft, 2016) and compared to the analytical model in MATLAB of a cantilever with the same sectional properties. The chosen core is 40 storeys, with total height, $H = 152\ m$, width, $L_1 = 18\ m$, and depth, $L_2 = 15\ m$.

To verify that the idealization of a rotational spring is equivalent of a flexible foundation and that the stiffness matrix is correctly assembled, different support conditions are tested in both models and corresponding fundamental frequencies are compared.

6.4.1 FEM Design model

The core walls are modelled with 2D shell elements and the slabs as 2D plate elements. Shell elements are connected to each other with rigid connection, and the connection between shell element and plate elements are modelled as pinned supports without moment transmission.

The bottom of the core is modelled with fixed supports in x- and y-direction and the flexible foundation is represented as a line support with changeable stiffness, $K_{z\prime}$, in z-direction.

Since the analytical model is based on masses lumped to the nodes, the core walls in FEM-Design is modelled without density. Instead, the corresponding weight (from core walls and storeys) are represented by an increased density of slabs located in each storey level in the core, resulting in the same distribution of masses as for the analytical model. Mass calculations and estimation of equivalent densities are presented in Appendix A.

An analysis for calculations of eigenfrequencies, considers masses in x- and y-direction. Mesh size is chosen as 0,95 m.

6.4.2 MATLAB model

6.4.2.1 Estimation of equivalent spring stiffness

As mentioned in Section 6.2.1 are the support conditions taken into account by changed stiffness in the rotational degree of freedom in the bottom of the cantilever. The line supports are therefore represented by equivalent springs which are re-calculated to a rotational stiffness by moment equilibrium. Figure 6-5 *(a)* illustrates how the line supports are idealized as springs, and the corresponding rotational spring with displacement is shown in Figure 6-5 *(b)*.

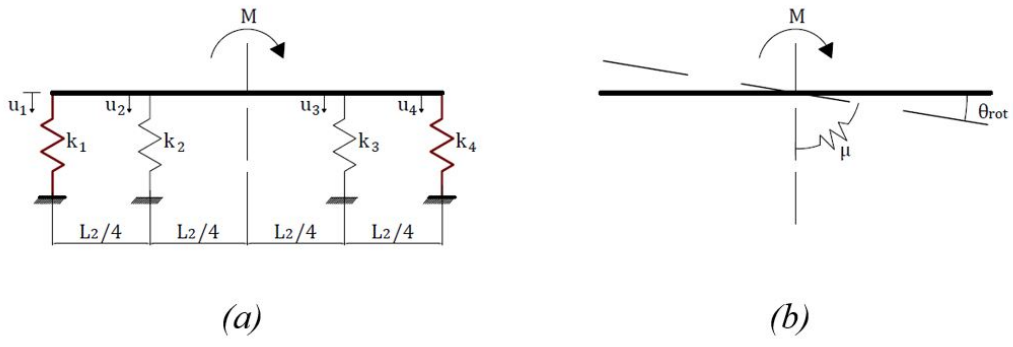

Figure 6-5 Idealization of line support stiffness.

Since the vibrations according to the first mode is of interest, rotational stiffness around y-axis is sought. The width, L_1, will contribute with stiffness from line supports acting along the sides, represented by springs with stiffness, k_1 and k_4, determined as:

$$k_1 = k_4 = K_{z'} L_1 \tag{6-2}$$

The depth, L_2, is divided by a symmetry line and represented by two springs with stiffness, k_2 and k_3, which are determined as:

$$k_2 = k_3 = K_{z'} \frac{L_2}{2} \tag{6-3}$$

An illustration of a core with the line support stiffness idealized as equivalent springs, is shown in Figure 6-6.

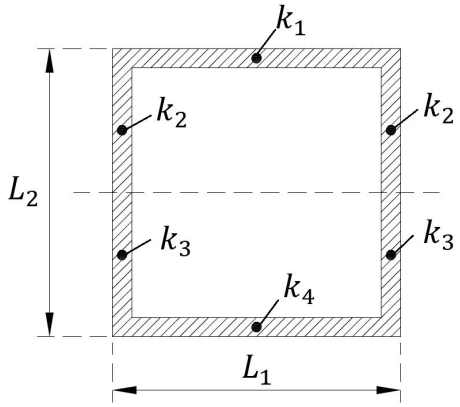

Figure 6-6 Illustration of core with line support stiffness idealized as equivalent springs.

By using constitutive relations for springs, and moment equilibrium around the symmetry line, the following can be obtained:

$$M = \mu\theta_{rot} = k_4 u_4 \frac{L_2}{2} + 2k_3 u_3 \frac{L_2}{4} - 2k_2 u_2 \frac{L_2}{4} - k_1 u_1 \frac{L_2}{2} \tag{6-4}$$

Note that also the opposite side with width, L_2, will contribute with the same amount of stiffness, and thus are these spring forces multiplied with 2 in expression (6-4).

By assuming small angles, the compatibility conditions can be written as:

$$u_1 = -\theta_{rot} \frac{L_2}{2} \tag{6-5}$$

$$u_2 = -\theta_{rot} \frac{L_2}{4} \tag{6-6}$$

$$u_3 = \theta_{rot} \frac{L_2}{4} \tag{6-7}$$

$$u_4 = \theta_{rot} \frac{L_2}{2} \tag{6-8}$$

With these, expression (6-4) can be simplified to:

$$\mu = k_4 \frac{L_2^2}{4} + 2k_3 \frac{L_2^2}{16} + 2k_2 \frac{L_2^2}{16} + k_1 \frac{L_2^2}{4} \tag{6-9}$$

And by using (6-2) and (6-3), the rotational stiffness is finally expressed as:

$$\mu = K_{z'}L_1\frac{L_2^2}{4} + 2K_{z'}\frac{L_2}{2}\frac{L_2^2}{16} + 2K_{z'}\frac{L_2}{2}\frac{L_2^2}{16} + K_{z'}L_1\frac{L_2^2}{4}$$
$$\Rightarrow \mu = \frac{K_{z'}L_2^2}{4}\left(2L_1 + \frac{L_2}{2}\right) \quad (6\text{-}10)$$

The rotational stiffness determined by the line supports are then used in the stiffness matrix as described in Section 6.2.1. The lumped masses will result in a mass matrix as described in Section 6.2.1.

With mass matrix and stiffness matrix, the fundamental frequency is solved from the eigenvalue problem.

6.4.3 Results of verification

The two models are compared for four different support conditions, and the results are presented in Table 6-1.

Table 6-1 Comparison of fundamental frequencies for different line support stiffness.

Fundamental frequency [Hz]			
$K_{z'}$ [MN/m/m]	FEM DESIGN	MATLAB	Difference
Fixed	0.33	0.347	5%
3000	0.311	0.317	2%
500	0.229	0.229	0%
100	0.128	0.126	-2%

As can be seen in the table, the analytical model seems to be representable for a homogenous core. However, one must be aware of that 2D elements in FEM-Design take account for both bending and shear deformations, while the analytical model only represents bending deformations. As mentioned in Section 6.1.2, shear deformations are neglectable, but will however induce some difference between the two models.

Since the main purpose of the analytical model is to develop a tool for calculating a more representable mode shape for a case of flexible foundation, the results are sufficient.

7 Parameter Study

To investigate what effect the support conditions has on the horizontal acceleration, the four methods described in Chapter 4 and 5 are considered in a parameter study. This is done by using MATLAB-program in Appendix C for the analytical model described in Chapter 6.

The relationship between horizontal acceleration and support conditions is complex, and various parameters affects the acceleration both positively and negatively in a non-linear way. To increase the knowledge of how the horizontal acceleration is affected by the support conditions, important parameters for of all four methods are studied. Further, the accelerations for all methods are plotted and compared.

Finally, influence of important parameters are changed to investigate their potential effects on the results.

7.1 Input parameters

7.1.1 Studied building

A tall building with reasonable dimensions have been chosen to generate input for the MATLAB-program. The building is forty storeys tall with core, columns and slabs in concrete. It is assumed that the core is the only member that is load bearing for horizontal actions, and thus is the flexural rigidity, EI, is determined by the dimensions of the core. Dimensions of the chosen plan are shown in Figure 7-1 and other relevant input parameters are presented in Table 7-1.

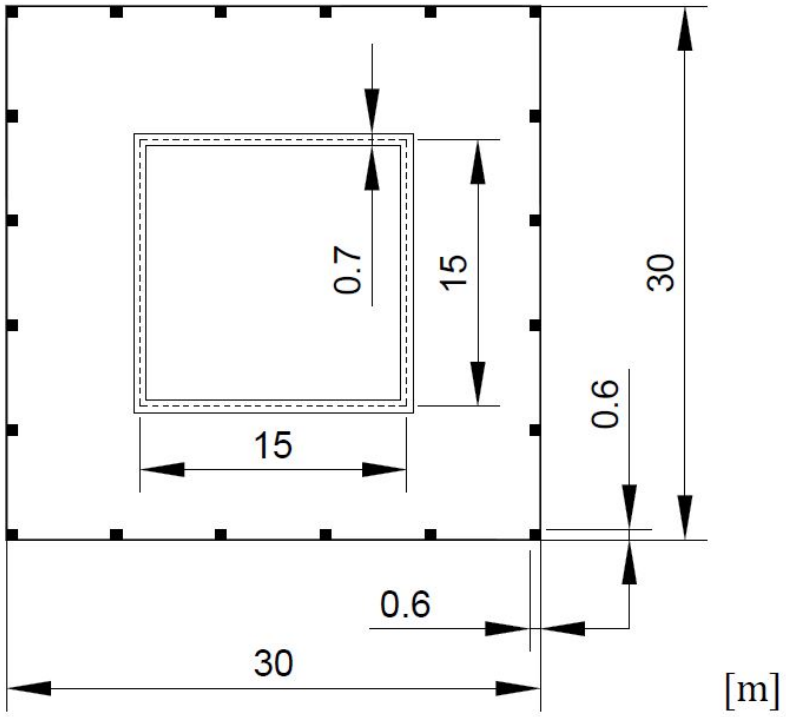

Figure 7-1 Illustrations of the studied building.

Table 7-1 Relevant input parameters for studied building

Category	Value	Unit
Storeys	40	
Storey height	3,8	m
Total height	152	m
Thickness of slab	0.25	m
Modulus of elasticity, E_{cm}	34	GPa
Mass per storey 0-39	1 052 000	kg
Mass for top slab	818 700	kg
Total mass of building	42 910 000	kg
Re-occurrence interval for wind	5	years
Terrain category	III	
Structural damping, δ_s	0.1	
Force coefficient, c_f	1.55	
Power law exponent, α	0.21	

Masses are lumped to corresponding node, and the mass matrix is constructed as described in Section 6.2.1. Mass per storey for level 0-39 and for the top slab, are calculated in Appendix B. The top node will attract less mass than the other nodes, since it attracts only half the mass from the core and columns than other nodes.

The equivalent rotational spring stiffness, μ, used in the stiffness matrix is determined according to the method described in Section 6.4.2. In this parameter study, the stiffness of the line support will be varying linearly with 30 different values between 100 MN/m/m to 3 000 MN/m/m.

For the analyses, the analytical mode shape determined from the eigenvalue problem is used. The analytical mode shape is based on the actual support conditions, and will vary when stiffness of the support, K_z, changes. The process for determining the analytical mode shape is described in Section 6.2.2.

7.1.2 Comment on results of parameter study

Note that the results from the parameter study is highly dependent on the dimensions and input parameters chosen in the parameter study. Estimated acceleration corresponding to a certain line support stiffness can not be seen as a representable value for a general case. The actual stiffness of the support is relative and dependent on several parameters, e.g. geometry and the relationship between the stiffness of the structure and the stiffness of the foundation.

7.1.3 Choices regarding wind turbulence

To increase comparability for the results between the four methods, consistent choices and modifications regarding wind turbulence have been made.

7.1.3.1 Wind-spectral density

As described in Section 4.1.3.2, there are several empirical expressions for wind-spectral densities. In this report two of them have been mentioned, von Kármán's and Kaimal's. Both of them describe the same phenomenon, and the choice is up to the designer of the code. To be able to compare the results of this parameter study, von Kármán's expressions is adapted for all four methods, since this is the one used in Swedish norms EKS 10.

Von Kármán's wind-spectral density is defined as:

$$R_N(\omega, z) = \frac{\omega S_u(\omega)}{\sigma_u^2(z)} = \frac{4f_L}{(1 + 70{,}8f_L^2)^{5/6}} \tag{7-1}$$

7.1.3.2 Integral length scale

In line with the recommendation in Section 4.1.3.2, the integral length scale is assumed to be, $L_u^x = 150$ m, for all four methods in the parameter study when determining the wind-spectral density. This is a good approximation according to K. Handa (Personal communication, April 26, 2017).

7.1.3.3 Decay constant

When determining the normalized Co-spectrums, $\hat{C}o_{ui}$, one has to assume decay constants, C_{uz} and C_{uy}, as input. K. Handa (Personal communication, April 26, 2017), suggests that $C_{uz} = C_{uy} = 8$ is a representable assumption, and this is also what EKS 10 is based on. Since the choice of decay constants is already done when developing the method in Eurocode 1 Part 1-4 and EKS 10, it is not possible to change this input for these methods. The decay constants are therefore assumed to be in accordance with Handa's recommendation and the influence of chosen decay constants is studied in Section 7.9.4.

7.2 Effects on mode shape

As mentioned in Section 6.1.1, a pile foundation has been idealized as a hinged support with a rotational spring. As can be seen from Equation (6-1), the lower the rotational stiffness, the less moment can be restrained by the foundation. In other words, the rotational stiffness of the structure decreases and the less it resembles a foxed joint.

The mode shape, $\phi(z)$ describes how the building translates in the corresponding mode, and thus highly dependent on horizontal stiffness. Figure 7-2 shows how the analytical mode shape, $\phi_x(z)$, determined from the eigenvalue problem as described in Section 6.2.2, is affected by three different rotational stiffness of the support. As a comparison, also the simplified mode shape according to Equation (5-1) proposed in Eurocode 1 Part 1-4 is plotted.

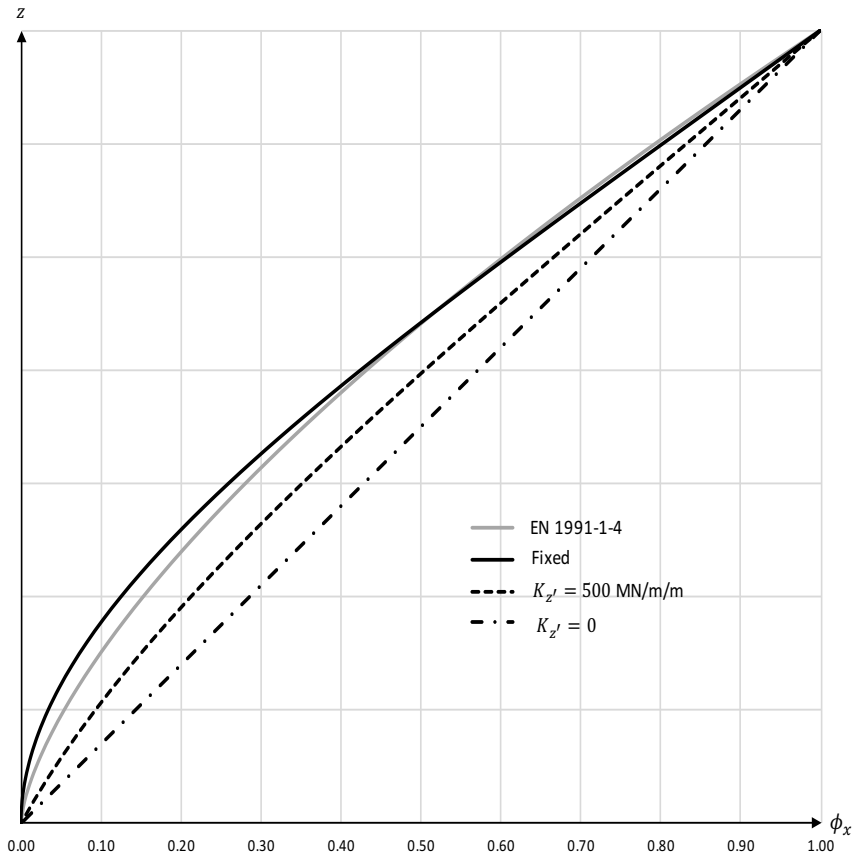

Figure 7-2 Variation of mode shape, $\phi_x(z)$, due to change in support conditions, compared to the one proposed in EN 1991-1-4 (CEN, 2005).

As can be seen from the figure, the simplified mode shape stated in Eurocode 1 Part 1-4 is a good representation for a stiff foundation. Further, it can be observed that the analytical mode shape, $\phi_x(z)$, deviates further from the simplified mode shape, as the stiffness of the support decreases.

7.3 Effects fundamental frequency

The fundamental frequency is highly dependent on stiffness of the structure and thus also on the support conditions. The relationship can be noticed by examining the following expressions from Section 2.2.4:

$$\widetilde{M} = \int_0^H m(z)\phi(z)^2 dz \tag{7-2}$$

$$\widetilde{K} = \int_0^H EI(z)\{\phi''(z)\}^2 dz \tag{7-3}$$

$$\omega_n = 2\pi f_n = \sqrt{\frac{\widetilde{K}}{\widetilde{M}}} \tag{7-4}$$

As can be observed in Figure 7-2, the integral of the mode shape, $\phi_x(z)$, increases with decreasing stiffness of the support. A consequence, the generalized mass, $\widetilde{M}$ in Equation (6-2), increases which will lower the fundamental frequency.

The opposite can be said about the generalized stiffness, $\widetilde{K}$, that the integral of the curvature, $\phi_x''(z)$ decreases with decreasing stiffness of the support. Decreasing generalized stiffness of the structure lead to lower fundamental frequency.

With previous conclusions and by observing Equation (6-4), it is clear that the fundamental frequency will decrease with decreasing stiffness of the support. The fundamental frequency is plotted for various line support stiffness, $K_{z'}$ and the behaviour can be seen in Figure 7-3. For convenience, fundamental frequency is presented as, f_n, measured in [Hz] instead of circular frequency, ω_n.

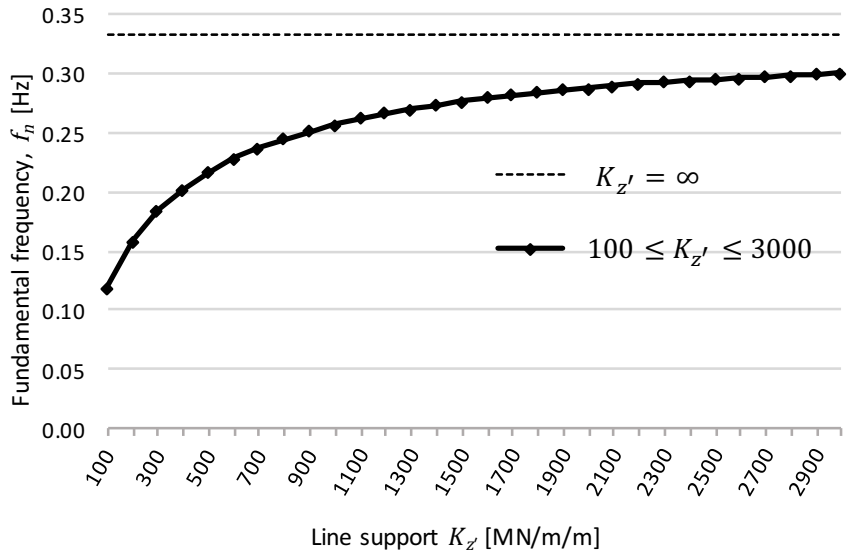

Figure 7-3 Relationship between fundamental frequency, f_n, and stiffness of the support.

To put the stiffness of the support into relation with a fixed support, the fundamental frequencies are compared in Table 7.2.

Table 7.2 Comparison between fundamental frequency for fixed support and maximum studied support stiffness.

$K_{z'}$ [MN/m/m]	Frequency [Hz]	Difference [%]
∞	0.333	90%
3000	0.301	

7.4 Strømmen

The standard deviation of acceleration, $\sigma_{\ddot{u}_x}$, according to the theory based on (Strømmen, 2010) is derived in Chapter 4, and a final expression for the resonant part is stated in Section 4.2.2.1, as:

$$\sigma_{\ddot{u}_x}(z) = \sqrt{\omega_n^4 \sigma_{Rx}^2(z)} = \sqrt{\omega_n^4 \left[\frac{\phi_x(z)}{{\omega_n}^2 \widetilde{M}_x}\right]^2 \left[\frac{\pi \omega_n S_{\tilde{Q}_x}(\omega_n)}{4(\zeta_i - \zeta_{aei})}\right]} \tag{7-5}$$

The horizontal acceleration in the top of the building, where $\phi_x(z_{top}) = 1$, is of interest, and thus can the expression in this parameter study be simplified to:

$$\sigma_{\ddot{u}_x}(z) = \frac{1}{\widetilde{M}_x} \sqrt{\left[\frac{\pi \omega_n S_{\tilde{Q}_x}(\omega_n)}{4(\zeta_i - \zeta_{aei})}\right]} \tag{7-6}$$

As can be observed in the expression, the acceleration is dependent on the generalised mass, $\widetilde{M}_x$, fundamental frequency, ω_n, spectral density of loading, $S_{\tilde{Q}_x}(\omega_n)$, and total damping ratio, ζ_{tot}. These parameters will be studied separately.

7.4.1 Generalised mass

Generalised mass for first mode in along-wind direction is defined in Section 4.1.1, as:

$$\widetilde{M}_x = \int_0^H \phi_x(z)^2 m_x(z) dz \tag{7-7}$$

As concluded in Section 7.3 and from Figure 7-2, the integral of the mode shape, $\phi_x(z)$, and consequently the generalised mass, $\widetilde{M}_x$, will increase with decreasing stiffness of the support. The relationship between generalised mass and support condition is shown in Figure 7-4. The generalised mass can be compared with the total mass of the building that is 42 910 000 kg, see Table 7-1.

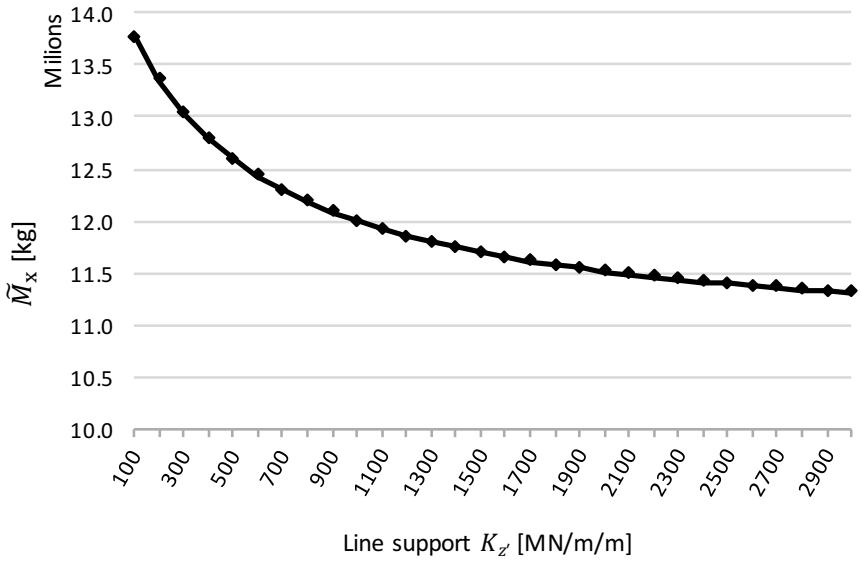

Figure 7-4 Relationship between generalised mass and stiffness of the support.

As can be observed in Equation (7-6), an increased generalised mass, $\widetilde{M}_x$, will decrease the horizontal acceleration. The effect of a flexible support on the mass, will results in lower horizontal acceleration.

7.4.2 Spectral density of loading

The spectral density of loading, $S_{\tilde{Q}_x}$, is dependent on several parameters which are affected by the support condition in a non-linear way. The spectral density of loading is defined according to Equation (4-27) as:

$$S_{\tilde{Q}_x}(\omega_n) = \left[(\rho L_1 c_f) J_x(\omega_n)\right]^2 \tag{7-8}$$

The width of the building perpendicular to wind flow, L_1, drag coefficient, c_f, and density of air, ρ, are constant parameters independent of stiffness of foundation. However, the joint acceptance function, $J_x(\omega_n)$, defined in Equation (4-34) is highly dependent on stiffness of the support and is defined as:

$$\begin{aligned} J_x^2(\omega_n) = &\iint_0^H (\phi_x(z_1)\phi_x(z_2)V(z_1)^2V(z_2)^2)\cdot \\ &\cdot\left(I_u(z_1)I_u(z_2)\frac{S_u(\omega_n)}{\sigma_u^2}e^{-|z_1-z_2|\frac{C_{uz}\omega_n}{2\pi V(z_{top})}}\right)dz_1dz_2\cdot \\ &\cdot\iint_{-\frac{L_1}{2}}^{\frac{L_1}{2}} e^{-|y_1-y_2|\frac{C_{uy}\omega_n}{2\pi V(z_{top})}}dy_1dy_2 \end{aligned} \tag{7-9}$$

In the joint acceptance function, several terms are dependent on either fundamental frequency, ω_n, or the mode shape, $\phi_x(z_i)$. Wind velocity, $V(z_i)$, and turbulence intensity, $I_u(z_i)$, are however not dependent on these, and thus neither the support conditions.

As concluded in Section 7.3, the integral of the mode shape, $\phi_x(z_i)$, will increase with decreasing stiffness of the support, and thus increase the joint acceptance function.

As can be seen in Equation (7-9), both integrals over respectively Co-spectrum, are dependent to the fundamental frequency, ω_n, and the terms will increase for decreasing fundamental frequency of the building. Consequently, these terms will have a positive contribution to the joint acceptance function for decreasing stiffness of the support.

The wind-spectral density, $\frac{S_u(\omega_n)}{\sigma_u^2}$, is also dependent on the fundamental frequency and consequently indirectly on the support conditions. As described in Section 0, von Kármán's wind-spectral density is used for all four methods, and its frequency-dependence is presented in Figure 7-5.

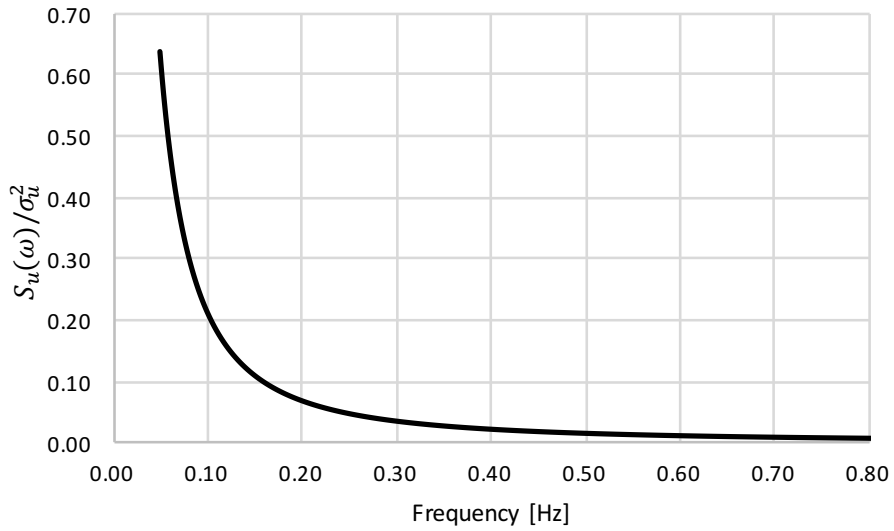

Figure 7-5 von Kármán's wind-spectral density for frequencies in the range of tall buildings.

What can be observed in Figure 7-5, is that wind load fluctuates more frequently at lower frequencies. This means that, structures with low fundamental frequency is more likely to reach resonance with the fluctuating wind, which will thus result in greater response.

As concluded in Section 7.3, the fundamental frequency will decrease for decreasing stiffness of the support. Consequently, the wind-spectral density will have increase the joint acceptance function, $J_x(\omega_n)$, for decreasing stiffness of the support. The relationship of wind-spectral density for various stiffness of the support, is plotted in Figure 7-6.

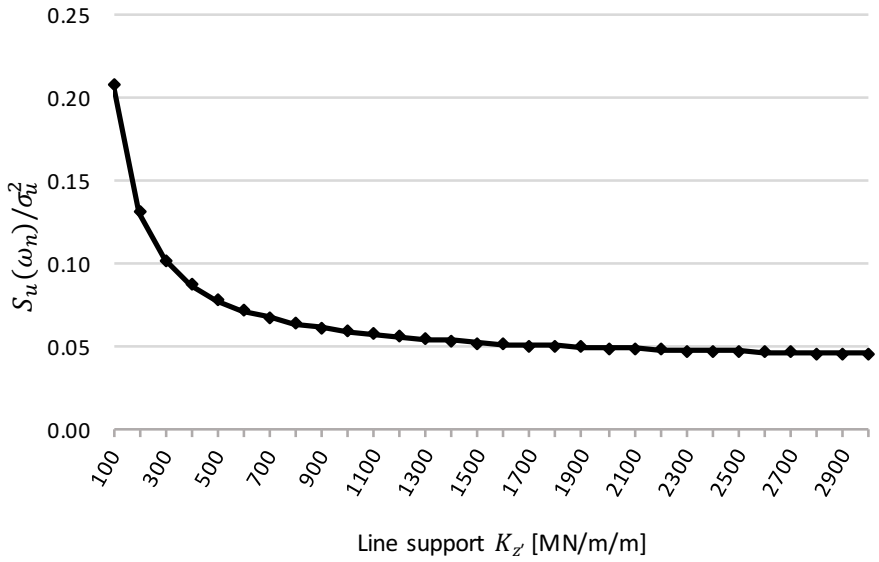

Figure 7-6 Graph of how wind spectral density changes with the line support stiffness.

With the conclusions made above, it is clear that the joint acceptance function, $J_x(\omega_n)$, increases with decreasing stiffness of the support. As can be seen in Equation (7-7), the spectral density of loading, $S_{\tilde{Q}_x}$, is directly proportional to $J_x^2(\omega_n)$. By observing Equation (7-6), it can be noted that its impact on the horizontal acceleration is in square root. For convenience, it is plotted in this form, and the behaviour can be seen in Figure 7-7.

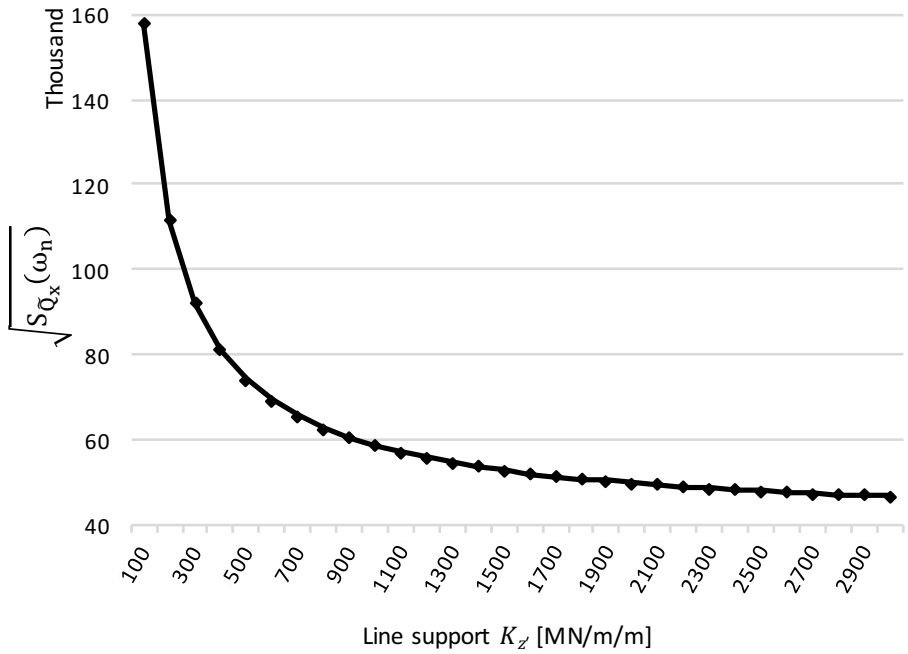

Figure 7-7 Shows the square root of spectral density, $\sqrt{S_{\tilde{Q}_x}(\omega_n)}$, versus stiffness of line support.

As can be observed in Equation (7-6), will an increasing spectral density of loading, $S_{\tilde{Q}_x}$, will increase the horizontal acceleration. The effect of a flexible support on the spectral density of loading, will results in larger horizontal acceleration.

7.4.3 Damping ratio

The last term to investigate in Equation (7-6), is the total damping ratio, $(\zeta_i - \zeta_{aei})$. The mechanical damping ζ_i is the same throughout this thesis, while the aerodynamic changes according to EKS 10 (Boverket, 2015) for all four methods as:

$$\zeta_{aei} = \frac{c_f \rho L_1 V(z_s)}{4\pi f_n m_e} \tag{7-10}$$

The numerator contains constants independent on the stiffness of the support, but the denominator will be dependent on the support conditions. The fundamental frequency, f_n, measured in [Hz] is handled in Section 7.3, and decreases with decreasing stiffness of the support as can be seen in Figure 7-3. This relationship results in a positive effect on the aerodynamic damping ratio for decreasing stiffness of the support.

The denominator also contains m_e, which is the equivalent mass per meter with regard to the mode shape and is defined as:

$$m_e = \frac{\widetilde{M}_x}{\int_0^H {\phi_x}^2(z)dz} \tag{7-11}$$

As concluded in Section 7.4.1, the generalised mass is dependent on the support conditions and will increase with decreasing stiffness of the support according to Figure 7-4. However, the equivalent mass will get a negative impact from the increasing denominator, when the stiffness of the support decreases. The behaviour of the equivalent mass for the studied building are shown in Figure 7-8.

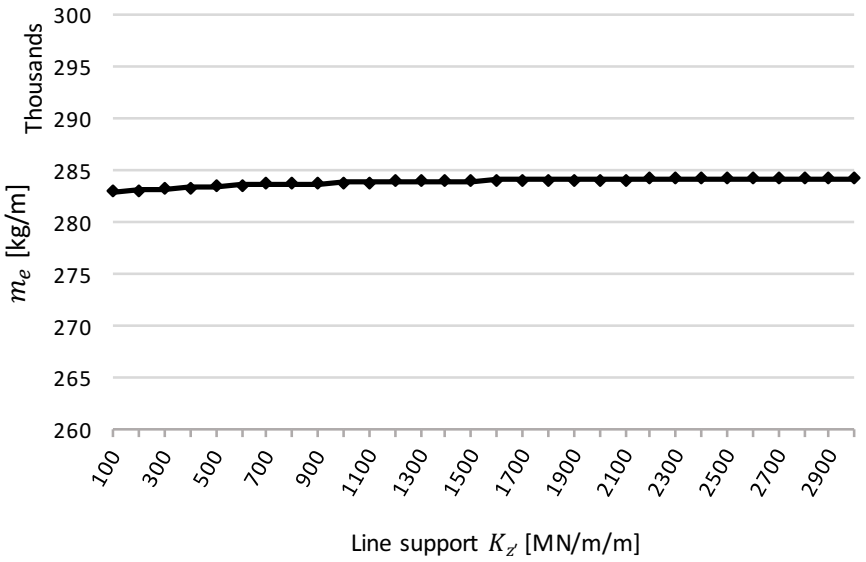

Figure 7-8 Equivalent mass for the specified house for different values of line support stiffness.

As can be observed in the figure, for this reference building when the mass is nearly evenly distributed, the equivalent mass can almost be regarded as independent on the stiffness of line support.

The effects described above, will result in an increased aerodynamic damping ratio, ζ_{aei}, which contribute to an increased total damping ratio, for decreasing stiffness of the support. The square root of total damping ratio is plotted for various stiffness of the support in Figure 7-9 below.

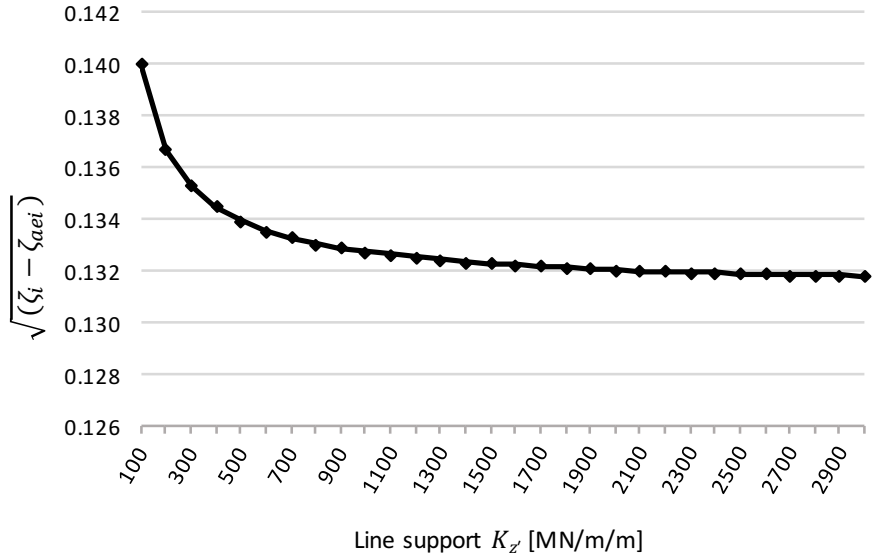

Figure 7-9 Relationship between square root of total damping ratio and stiffness of the support.

As can be observed in Equation (7-6), increased total damping ratio, will decrease the horizontal acceleration. The effect of a weak support on the total damping ratio, will results in lower horizontal acceleration.

7.4.4 Final acceleration according to Strømmen

Each parameter affecting the final horizontal acceleration in Equation (7-6), have been investigated with respect to decreased stiffness of the support. The effects this has on generalised mass, total damping ratio and fundamental frequency decreases the acceleration, while effects on spectral density of loading increases the acceleration. The behaviour of standard deviation of acceleration, $\sigma_{\ddot{u}_x}$, with respect to stiffness of the support are shown in Figure 7-9.

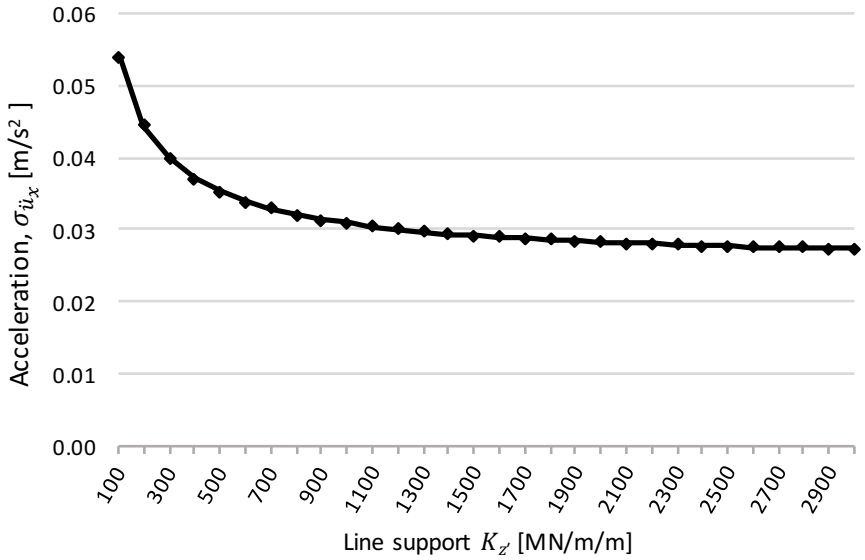

Figure 7-10 Relationship between standard deviation of acceleration, $\sigma_{\ddot{u}_x}$, according to Strømmen and stiffness of the support.

What can be observed in Figure 7-10, is that horizontal acceleration in the top of the building increases when the stiffness of the support decreases.

7.5 Handa

Standard deviation of acceleration, $\sigma_{\ddot{u}_x}$, according to the theory based on (Handa, 1982) is derived in Chapter 4, and final expression for the resonant part is stated in Section 4.2.2.2, as:

$$\sigma_{\ddot{u}_x}(z) = \sqrt{\omega_n^4 4 \left[W \frac{\phi_x(z)}{{\omega_n}^2 \widetilde{M}_x} \right]^2 I_{\bar{u}}^2(z) \frac{H_c V_c}{(\zeta_i - \zeta_{aei})} \frac{\omega_n S_u(\omega_n)}{\sigma_u^2}} \qquad (7\text{-}12)$$

In this parameter study, the horizontal acceleration in the top of the building, $z = z_{top}$, is of interest, and thus can the expression be simplified to:

$$\sigma_{\ddot{u}_x}(z) = 2\frac{W}{\widetilde{M}_x} I_u(z_{top}) \sqrt{\frac{H_c V_c}{(\zeta_i - \zeta_{aei})} \frac{\omega_n S_u(\omega_n)}{\sigma_u^2}} \tag{7-13}$$

Some of the terms in Equation (7-13) have already been investigated with respect to support conditions already. The effect on fundamental frequency, ω_n, is studied in Section 7.3, generalised mass, $\widetilde{M}_x$, in Section 7.4.1, wind-spectral density, $\frac{S_u(\omega_n)}{\sigma_u^2}$, in Section 7.4.2 and total damping ratio, $(\zeta_i - \zeta_{aei})$, in Section 7.4.3.

The effect of support conditions on generalised wind load, W, correlation factors, H_c and V_c, are investigated in Section 7.5.2. Finally, the effects on standard deviation of acceleration is studied.

7.5.1 Generalised wind load

The generalised wind load is defined in Section 4.2.2.2 as:

$$W = HL_1 \frac{1}{2} \rho c_f V\left(z_{top}\right)^2 \int_0^1 \phi_x(\tau)(\tau)^{2\alpha} d\tau \tag{7-14}$$

From Equation (7-14), it can be observed that only the mode shape, ϕ_x, is affected by the support conditions and, as stated in Section 7.2, the integral of the mode shape will increase with decreasing stiffness of the support.

The relationship between stiffness of the support and generalised wind load is shown in Figure 7-11.

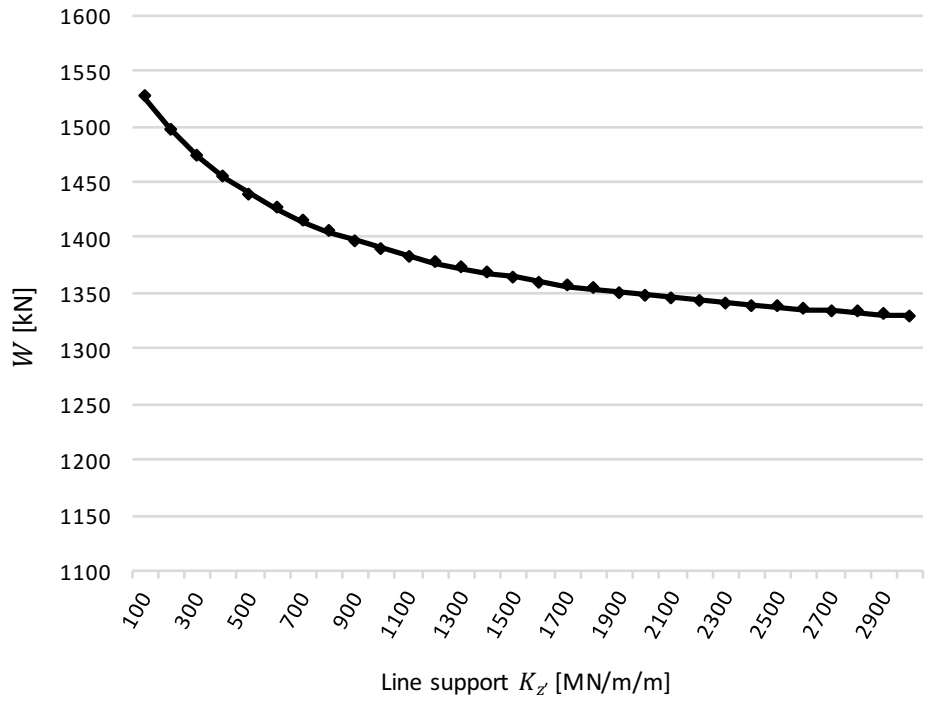

Figure 7-11 Relationship between generalised wind load, W, and stiffness of the support.

As can be observed in Equation (7-13), an increased generalised wind load, W, will increase the horizontal acceleration. The effect of a weak support on the generalized wind load, will result in larger horizontal acceleration.

7.5.2 Correlation factors

The correlation factors, V_c and H_c, defined in Section 4.2.2.2, are dependent on the support conditions and the effect will be studied below. The vertical correlation factor, V_c, is expressed as:

$$V_c = \frac{\iint_0^1 \phi_x(\tau_1)\phi_x(\tau_2)(\tau_1\tau_2)^{\alpha} e^{-|\tau_1-\tau_2|\frac{C_{uz}H\omega_n}{2\pi V(z_{top})}} d\tau_1 d\tau_2}{\left[\int_0^1 \phi_x(\tau)(\tau)^{2\alpha} d\tau\right]^2} \tag{7-15}$$

From Equation (7-15), it can be observed that the vertical correlation factor is affected by the support condition, both by the effect on mode shape, ϕ_x, and the fundamental frequency, ω_n. As described in Section 7.2 the integral of the mode shape is increased with decreasing stiffness of the support. It is mentioned in Section 7.3 that fundamental frequency decreases for decreasing stiffness of the support.

The vertical correlation factor, V_c, affects the standard deviation of acceleration in Equation (7-13) with its square root ($\sqrt{V_c}$), and for convenience it is plotted in this form in Figure 7-12.

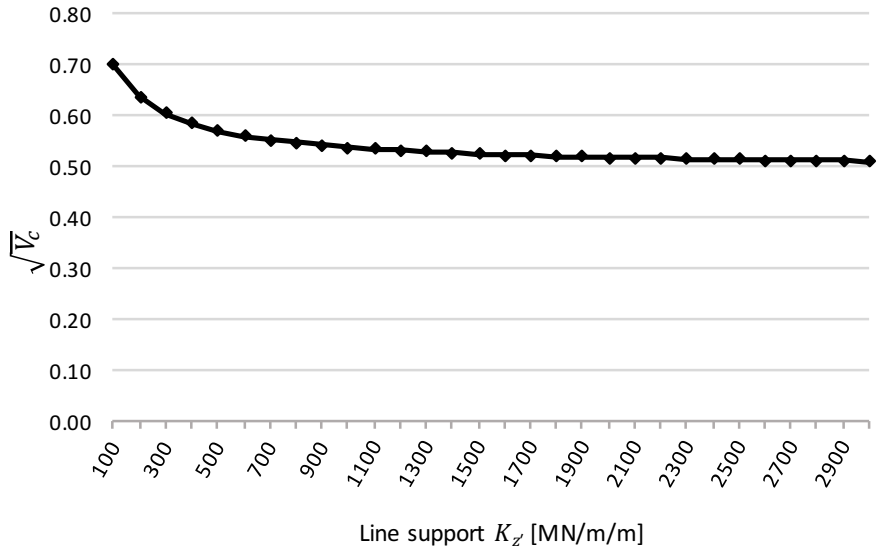

Figure 7-12 Relationship between vertical correlation factor and stiffness of the support.

The horizontal correlation factor, H_c, is defined by:

$$H_c = \iint_0^1 e^{-|\theta_1-\theta_2|\frac{C_{uy}L_1\omega_n}{2\pi V(z_{top})}} d\theta_1 d\theta_2 \tag{7-16}$$

From Equation (7-16), it can be observed that the horizontal correlation factor is dependent on the fundamental frequency which decreases for decreasing stiffness of the support. The

behaviour of horizontal correlation factor, with respect to stiffness of the support, is shown in Figure 7-13. With the same way of reasoning as for the vertical correlation factor, it is presented as $\sqrt{H_c}$.

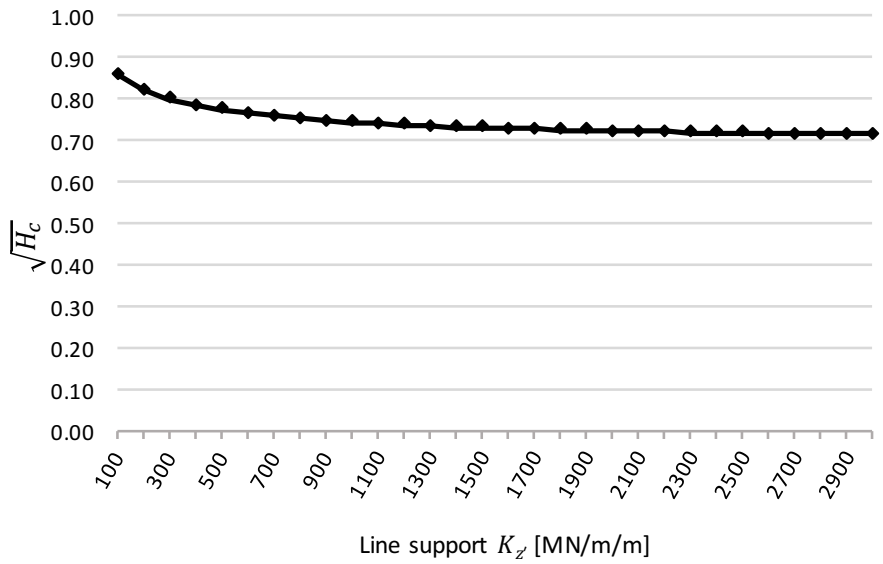

Figure 7-13 The figure shows the relationship between the square root of horizontal correlation factor and stiffness of the support.

As can be seen in Figure 7-12 and Figure 7-13, both the vertical and horizontal correlation factor increases for decreasing stiffness of the support. From Equation (7-13), it is clear that the correlation factors will increase the horizontal acceleration. Consequently, the effect of a weak support on the correlation factors, V_c and H_c, will result in larger horizontal acceleration.

7.5.3 Final acceleration according to Handa

Each parameter affecting the final horizontal acceleration in Equation (7-13), have been investigated with respect to decreased stiffness of the support. The effects on generalised mass, total damping ratio and fundamental frequency results in negative impact on the acceleration, while effects on generalised wind load, wind-spectral density and correlation factors contribute to increased acceleration. The behaviour of standard deviation of acceleration, $\sigma_{\ddot{u}_x}$, with respect to stiffness of the support are shown in Figure 7-14.

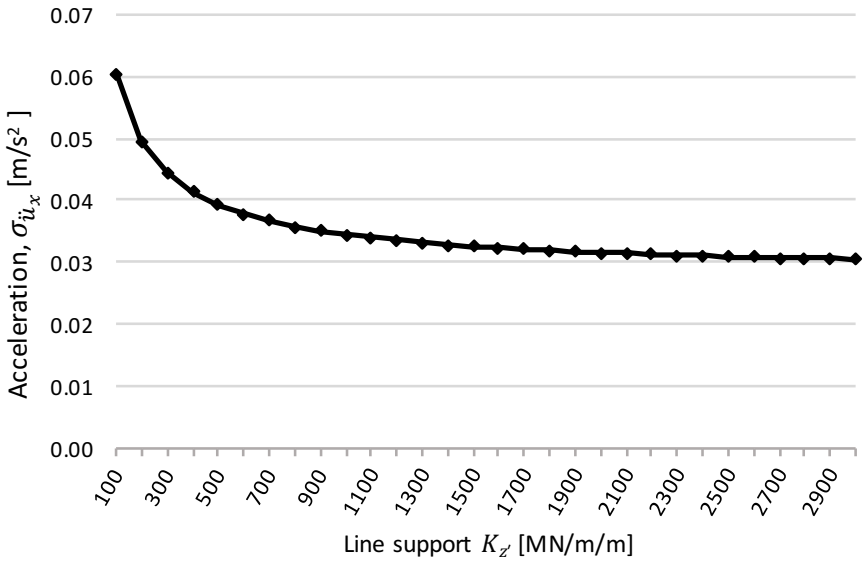

Figure 7-14 Relationship between standard deviation of acceleration, $\sigma_{\ddot{u}_x}$, according to Handa and stiffness of the support.

7.6 EKS 10

EKS 10 have a simplified expression to determine the acceleration for a building due to fluctuating wind load and it takes the form of:

$$\sigma_{\ddot{u}_x}(z) = \frac{3I_u(z_{top})R_{EKS}q_m(z_{top})L_1 c_f \phi_x(z)}{m_e} \tag{7-17}$$

Most of the terms in Equation (7-17) is either constants or independent of changing stiffness of line support. For estimation of acceleration at top of the building is $\phi_x(z_{top}) = 1$, which means that the only terms that will change with the stiffness of foundation is R_{EKS} and m_e.

The equivalent mass, m_e, have been treated in Section 7.4.3, where the behaviour of the equivalent mass can be observed in Figure 7-8. It can be concluded that the equivalent mass can be treated as a constant for the reference building in the parameter study. Therefore, the only parameter that will change with line support stiffness is the resonance response coefficient, R_{EKS}.

This means that the acceleration according to EKS 10 in this parameter study, is only dependent on the support conditions through changes in R_{EKS}.

7.6.1 Resonance response coefficient

The resonance response coefficient contains many variables.

$$R_{EKS} = \sqrt{\frac{2\pi \frac{f_x S_u(f_x)}{\sigma_u^2} \phi_b \phi_h}{\delta_s + \delta_a}} \tag{7-18}$$

It is the same wind-spectral density, which behaviour can be observed in Figure 7-7. The figure shows that for less line support stiffness, the wind-spectral density increases, therefore increasing R_{EKS}. Total damping of the building, is treated in Figure 7-9. There it was clear that the damping increases when stiffness of lines support decreases, which in turn decreases R_{EKS}. Left to investigate is the influence of size coefficient, ϕ_b and ϕ_h, which are related to the width and height of the structure respectively.

The size coefficient is simplified expression of the correlation factor presented in Section 4.2.2.2. It is therefore expected that ϕ_b and ϕ_h have similar values as H_c and V_c.

The vertical size coefficient is defined as

$$\phi_h = \frac{1}{1 + \frac{2f_x H}{V(z_{top})}} \tag{7-19}$$

In Figure 7-15, the square root of the vertical size coefficient, $\sqrt{\phi_h}$, have been plotted, to easier see what effect it will have on R_{EKS}. For less line support stiffness, the vertical size coefficient increases, therefore have a positive effect on R_{EKS}.

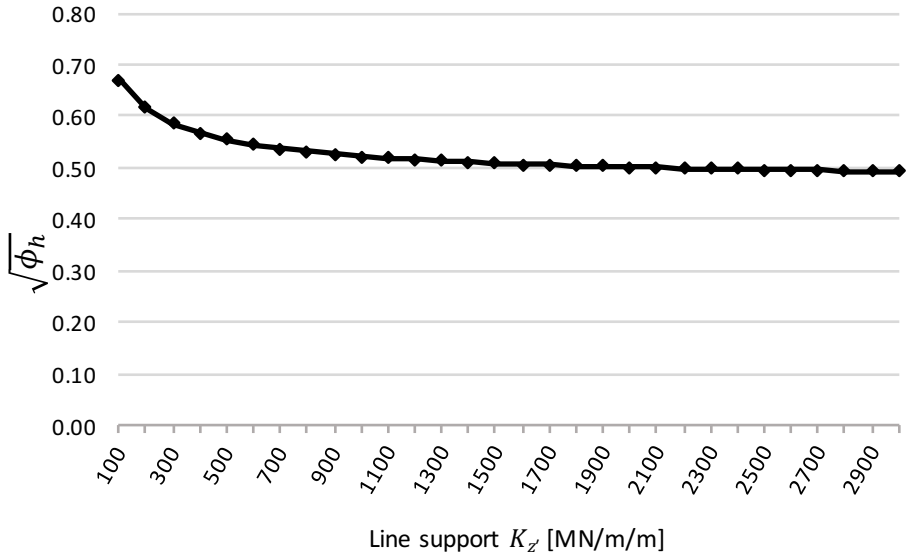

Figure 7-15 Square root of vertical size coefficient according to EKS 10.

The horizontal size coefficient is very similar to the vertical size coefficient, but is dependent on the width of the building instead.

$$\phi_b = \frac{1}{1 + \frac{3{,}2f_x L_1}{V(z_{top})}} \tag{7-20}$$

In Figure 7-16 the square root of the horizontal coefficient is plotted. This one is also increasing with decreasing line support stiffness, but not in the same magnitude as the vertical size coefficient.

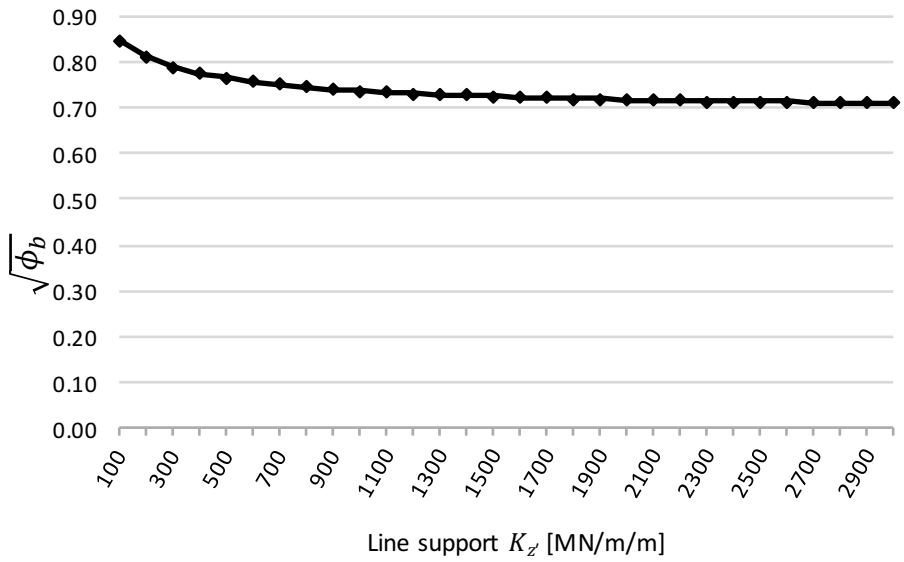

Figure 7-16 Horizontal size coefficient according to EKS 10.

All the terms in the resonant response coefficient, except the damping, increases the resonant response coefficient, R_{EKS}, when the line support decreases. In Figure 7-17 the results have been plotted. It is clear that when the line support decreases the resonant response coefficient increases. For a weak foundation, the resonant response coefficient will increase the horizontal acceleration.

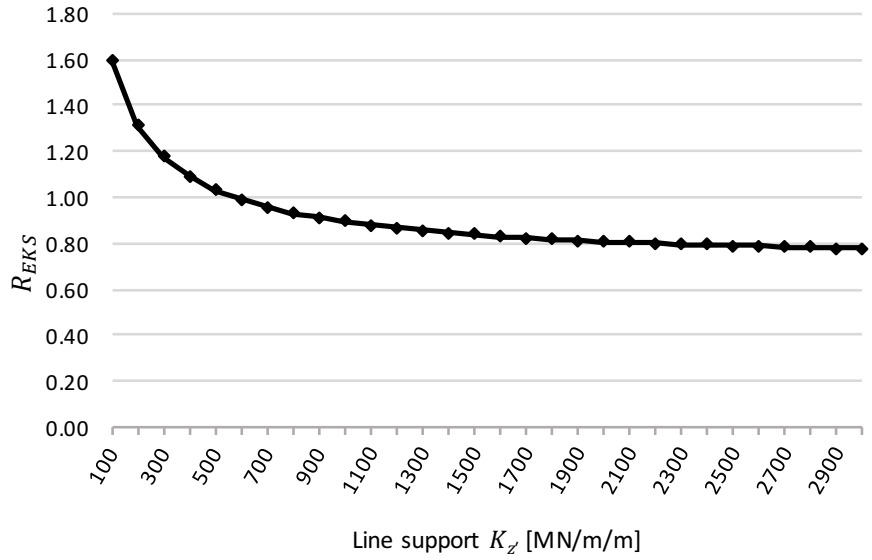

Figure 7-17 Resonant response coefficient.

7.6.2 Final acceleration according to EKS 10

Since the equivalent mass is independent on stiffness of support, it is safe to say that the acceleration is only dependent on the resonance response coefficient, R_{EKS}. Since R_{EKS} increased for smaller values of line support stiffness, the behaviour of the acceleration should

be the same. Comparing Figure 7-17 and Figure 7-18 it is clear that's the case, the form is almost identical.

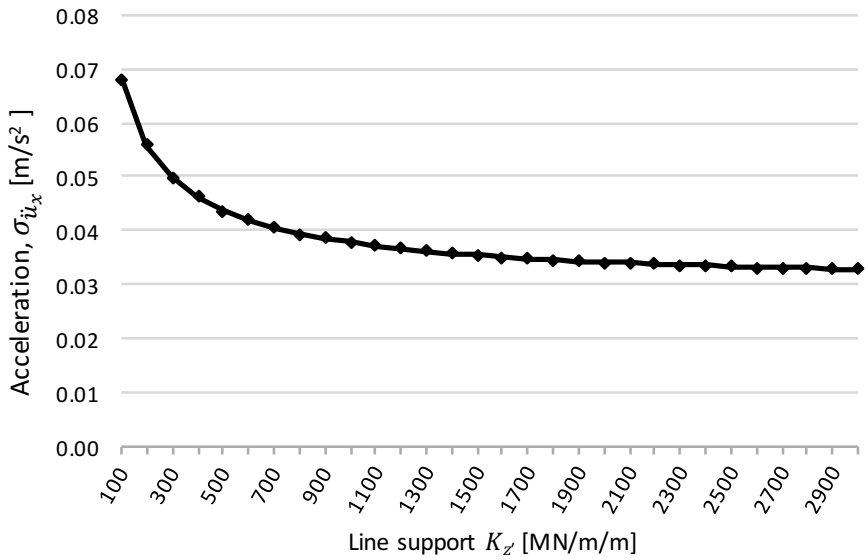

Figure 7-18 Relationship between standard deviation of acceleration, $\sigma_{\ddot{u}_x}$, according to EKS 10 and stiffness of the support.

7.7 Eurocode 1 Part 1-4 Annex B

Standard deviation of acceleration, $\sigma_{\ddot{u}_x}$, according to Eurocode 1 Part 1-4 (CEN, 2005) is explained in Section 5.2.2 , and the final expression for the resonant part is:

$$\sigma_{\ddot{u}_x}(z) = \frac{c_f \rho L_1 I_u(z_s) V^2(z_s)}{m_e} R_{EC} K_x \phi_x(z) \tag{7-21}$$

Firstly, it can be concluded that $\phi_x(z_{top}) = 1$. From Equation (7-21), it can further be observed that the standard deviation of acceleration is dependent on the support condition through the equivalent mass, m_e, resonant coefficient, R_{EC} and dimensionless coefficient, K_x. However, as described in Section 7.4.3, the equivalent mass, m_e, will decrease marginally with decreasing stiffness of the support and can be considered as independent on support conditions in this parameter study.

7.7.1 Resonant coefficient

The resonant coefficient is in Eurocode 1 Part 1-4 is defined in Section 5.2.2, as

$$R_{EC} = \sqrt{\frac{\pi^2}{2(\delta_s + \delta_a)} \frac{f_x S_u(z_s, f_x)}{\sigma_u^2} R_h(\eta_h) R_b(\eta_b)} \tag{7-22}$$

Where the influence of support conditions on wind-spectral density, $S_u(z_s, f_x)/\sigma_u^2$, and total damping, $(\delta_s + \delta_a)$, have been studied previously in Section 7.4.2 and 7.4.3, respectively.

$R_h(\eta_h)$ and $R_b(\eta_b)$ is referred to as the aerodynamic admittance functions, and those functions are dependent on the geometry and the fundamental frequency.

The aerodynamic admittance functions are complicated, and are affected by the decrement of fundamental frequency when stiffness of the support decreases. The vertical admittance function, R_h, is defined as:

$$R_h = \frac{1}{\eta_h} - \frac{1}{2\eta_h^2}(1 - e^{-2\eta_h}) \tag{7-23}$$

Where, η_h, is dependent on the fundamental frequency and defined as:

$$\eta_h = \frac{4.6H}{L_u^z(z_{top})} f_L(z_s, f_x) \tag{7-24}$$

The behaviour of vertical aerodynamic admittance function for various stiffness of the support is plotted in Figure 7-19. For convenience, it is plotted in the form, $\sqrt{R_h}$, since it affects the standard deviation of acceleration in Equation (7-21) in this form.

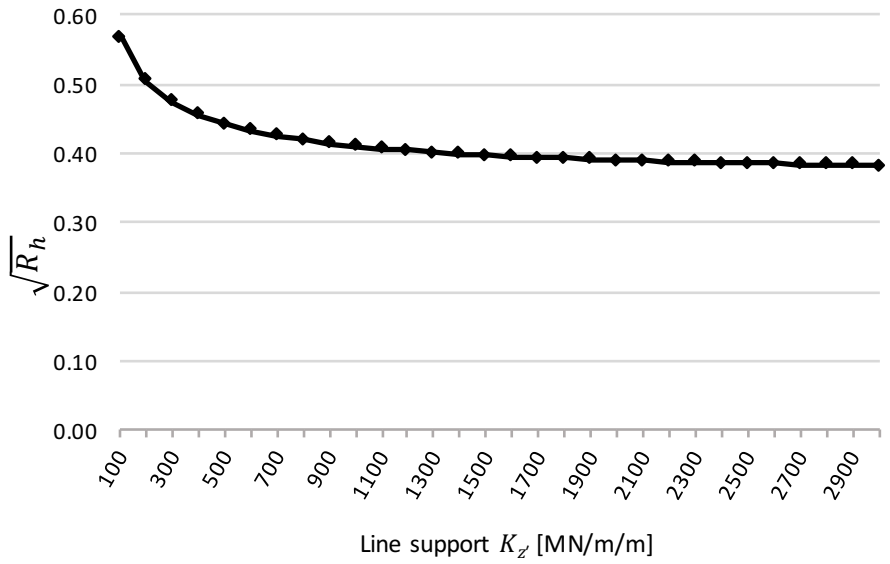

Figure 7-19 Relationship between square root of vertical aerodynamic admittance function and stiffness of the support.

The horizontal aerodynamic admittance function, R_b, is nearly identical to the vertical, except it is dependent on the width of the building instead of the height.

$$R_b = \frac{1}{\eta_b} - \frac{1}{2\eta_b^2}(1 - e^{-2\eta_b}) \tag{7-25}$$

Where, η_b, is dependent on the fundamental frequency and defined as:

$$\eta_b = \frac{4.6L_1}{L_u^z(z_{top})} f_L(z_s, f_x) \tag{7-26}$$

The behaviour of horizontal aerodynamic admittance function for various stiffness of the support is plotted in Figure 7-20 below. It is plotted in the form, $\sqrt{R_b}$, for the same reason as described previously for R_h.

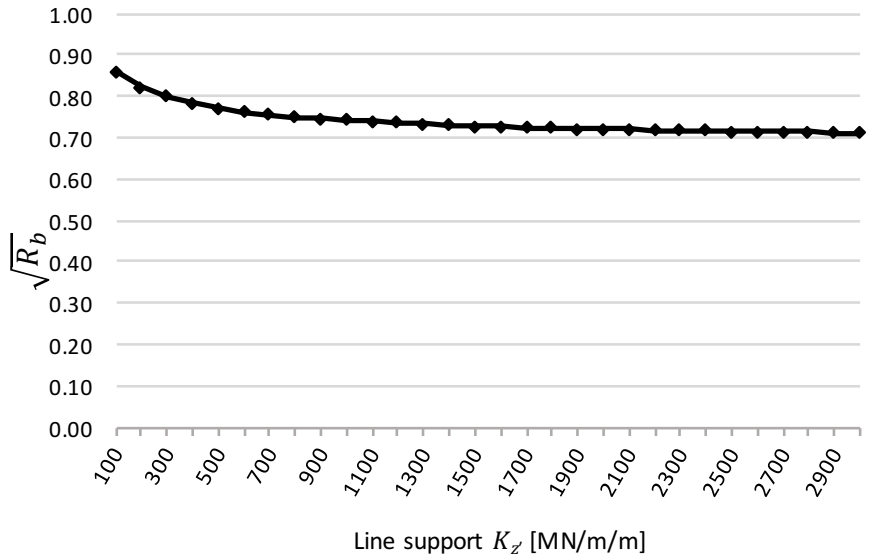

Figure 7-20 Relationship between horizontal aerodynamic admittance function and stiffness of the support.

As shown in Figure 7-19 and Figure 7-20, the aerodynamic admittance function, R_h and R_b, increases for decreasing stiffness of the support. From Equation (7-22), it can be seen that this results in an increased resonant coefficient, R_{EC}. The total behaviour on resonant coefficient, including effects on wind-spectral density and damping are plotted in Figure 7-17.

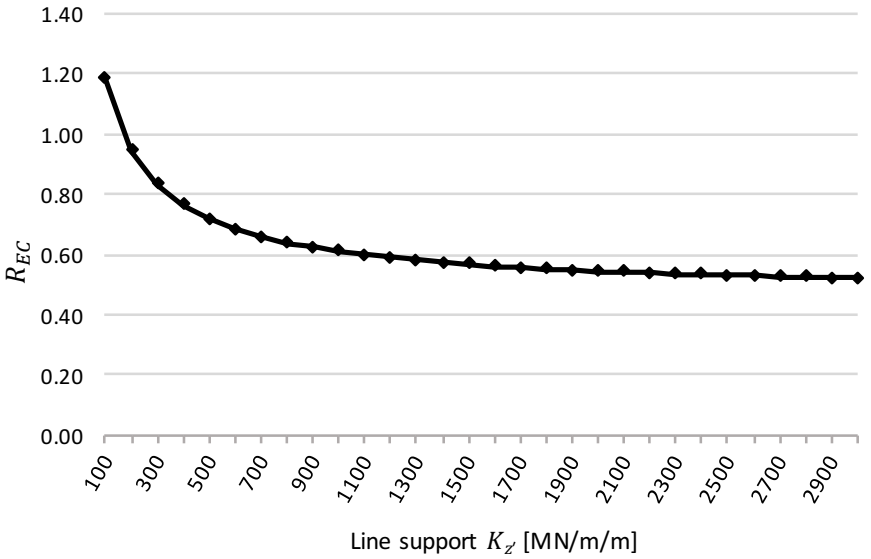

Figure 7-21 Relationship between resonant coefficient and stiffness of the support.

From Equation (7-21), it can be observed that an increased resonant coefficient, R_{EC}, will increase horizontal acceleration. Therefore, the acceleration will increase due to R_{EC} when the stiffness of support is reduced.

7.7.2 Dimensionless coefficient

The dimensionless coefficient, K_x, is dependent on the mode shape, $\phi_x(z)$ and the wind profile.

$$K_x = \frac{\int_0^H V^2(z)\phi_x(z)dz}{V^2(z_s)\int_0^H \phi_x^2(z)dz} \tag{7-27}$$

As concluded in Section 7.2, the integral of mode shape increases when stiffness of the support decreases, i.e. both numerator and denominator of Equation (7-27) increases for decreasing stiffness. The denominator will however increase faster, and the behaviour for various support conditions is presented in Figure 7-22.

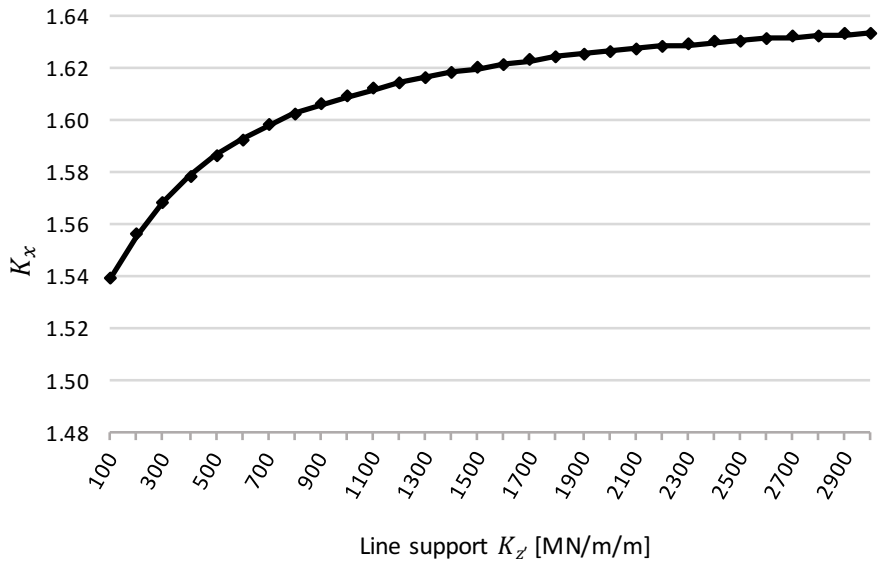

Figure 7-22 Relationship between dimensionless coefficient and stiffness of the support.

From Equation (7-21), it can be observed that if the dimensionless coefficient, K_x, decreases, the horizontal acceleration will also decrease. A weak support will reduce K_x and thus result in lower horizontal acceleration.

7.7.3 Final acceleration according to EN 1991-1-4

Each parameter effecting the final horizontal acceleration in Equation (7-21) have been investigated with respect to decreased stiffness of the support. The resonant coefficient, R_{EC}, increases the acceleration, while the dimensionless coefficient, K_x, will increase the acceleration when the stiffness of support is reduced. The behaviour of standard deviation of acceleration, $\sigma_{\ddot{u}_x}$, with respect to stiffness of the support are shown in Figure 7-23.

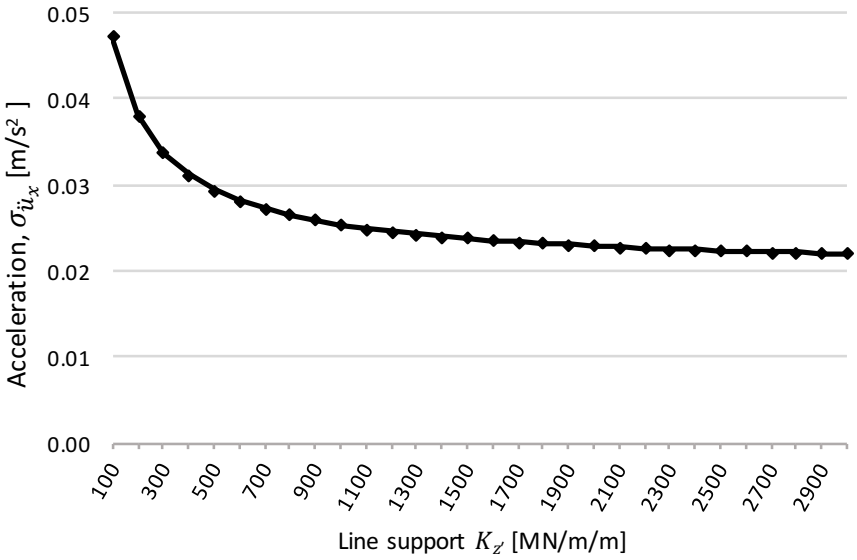

Figure 7-23 Relationship between standard deviation of acceleration, $\sigma_{\ddot{u}_x}$, according to EN 1991-1-4 and stiffness of the support.

7.8 Compared acceleration between the methods

In Section 7.4 - 7.7 the different methods are investigated separately with respect to change of support conditions. In this Section the four methods are compared with each other. The resulting standard deviation of acceleration, $\sigma_{\ddot{u}_x}$, for all four methods are presented in Figure 7-24, for varying stiffness of the support. The corresponding fundamental frequency of the building is plotted as a function of support stiffness in the figure to study the correlation between fundamental frequency and standard deviation of acceleration.

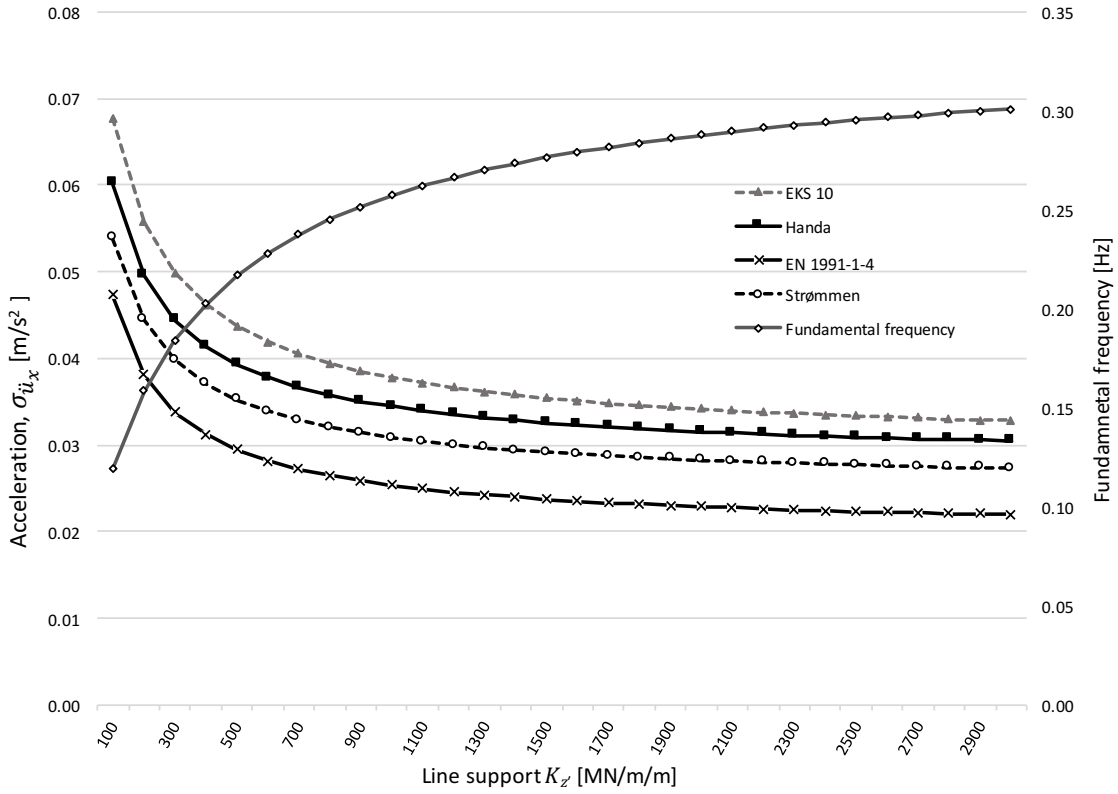

Figure 7-24 Relationship between standard deviation of acceleration for all four method and fundamental frequency versus stiffness of the support.

What can be observed, is that all four methods show the same kind of behaviour. Acceleration increases exponentially, for decreasing stiffness of the support. It is also clear that the EKS 10 is conservative for all support conditions, and that EN 1991-1-4 yields the lowest values of acceleration.

Since EKS 10 is based on the theory presented in Handa's method, these two are compared in Table 7-3 to investigate the difference between them for different support conditions.

Table 7-3 Comparison between EKS 10 and Handa's approach for various support conditions.

$K_{z'}$ [MN/m/m]	**EKS 10** [m/s^2]	**Handa** [m/s^2]	**Difference** [%]
3000	0.0328	0.0305	-7.0%
500	0.0437	0.0393	-10.1%
100	0.0677	0.0602	-11.1%

The results are more similar for rigid support conditions, and this implies that EKS 10 is a simplified version of Handa's method and is applicable for rigid supports. However, the results diverge for decreasing stiffness of the support and this indicates that EKS 10 is less representable for flexible support conditions.

The standard deviation of acceleration for all four methods can be related to the recommended limits presented in Section 5.3.1.2. This is illustrated in Figure 7-25, where the acceleration is plotted together with recommended limits according to ISO 6897.

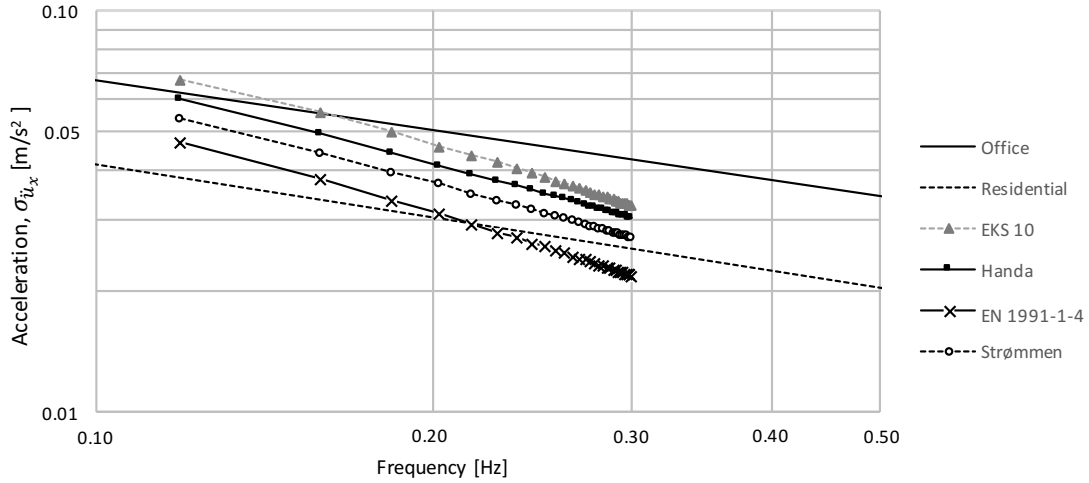

Figure 7-25 Standard deviation of acceleration plotted in ISO 6897 graph.

Something that is clearly visible in Figure 7-25 is that the acceleration according to EN 1991-1-4 is much less that the other methods, especially EKS 10. In Table 7-4, the acceleration between the two design norms EKS 10 and EN 1991-1-4 is compared.

Table 7-4 Comparison between EKS 10 and EN 1991-1-4 approach for various support conditions.

$K_{z'}$ [MN/m/m]	**EKS 10** [m/s²]	**EN 1991-1-4** [m/s²]	**Difference** [%]
3000	0.0328	0.0220	-32.9%
500	0.0437	0.0294	-32.7%
100	0.0677	0.0473	-30.1%

7.9 Influence of important parameters

From the parameter study, it can be concluded that mode shape and fundamental frequency will be affected by the stiffness of the support, and that a flexible foundation will result in increased horizontal acceleration.

What also has been concluded in this study, is that the acceleration is affected by the mode shape, $\phi_x(z)$, flexural rigidity, $EI(z)$ and mass, $m_i(z)$. Thus, the influence of these will be studied separately. As mentioned in Section 7.1.3.3, the assumed decay constants vary between EKS 10 and Eurocode 1 Part 1-4 Annex B. Therefore, the influence of chosen decay constant is also studied.

7.9.1 Influence of mode shape

In previous analyses the analytical mode shape, determined from the eigenvalue problem, was used. As concluded in Section 7.2, the analytical mode shape deviate increasingly from the simplified mode shape proposed in Eurocode 1 Part 1-4 when stiffness of the support decreases.

To investigate what effects the mode shape has on the acceleration, the mode shape is chosen as the one proposed in the norms, see Section 5.1, i.e. a mode shape that is independent on variations of support conditions. The accelerations calculated for the simplified mode shape are compared to the results from the analytical mode shape. The mode shape according to Eurocode 1 Part 1-4, is based on the idealization of a fixed support and is expressed as:

$$\phi_x(z) = \left(\frac{z}{H}\right)^{1,5} \tag{7-28}$$

The results for the simplified mode shape are plotted in Figure 7-26.

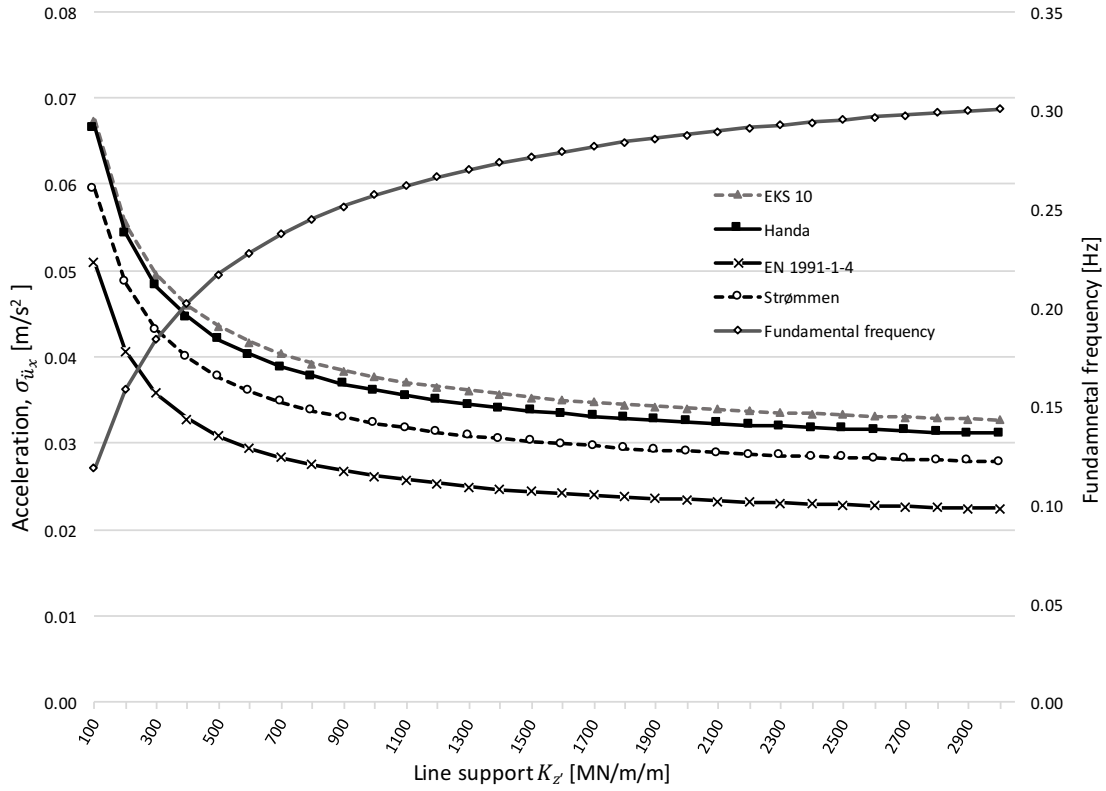

Figure 7-26 Relationship between standard deviation of acceleration for all four methods with simplified mode shape and fundamental frequency versus stiffness of the support.

A noticeable difference between Figure 7-24 and Figure 7-26, is that the acceleration according to the theoretical approach by Handa, tends to the be more similar to the simplified approaches from EKS 10.

Table 7-5 Comparison between EKS 10 and Handa's approach for various support conditions for simplified mode shape.

$K_{z'}$ [MN/m/m]	EKS 10 [m/s^2]	Handa [m/s^2]	Difference [%]
3000	0.0328	0.0311	-5.01%
500	0.0435	0.0421	-3.37%
100	0.0674	0.0665	-1.27%

How each method is affected by the mode shape, is shown in Figure 7-27, where the acceleration is plotted when both the analytical mode shape and the simplified mode shape, according to Equation (7-28), have been used for determining the acceleration.

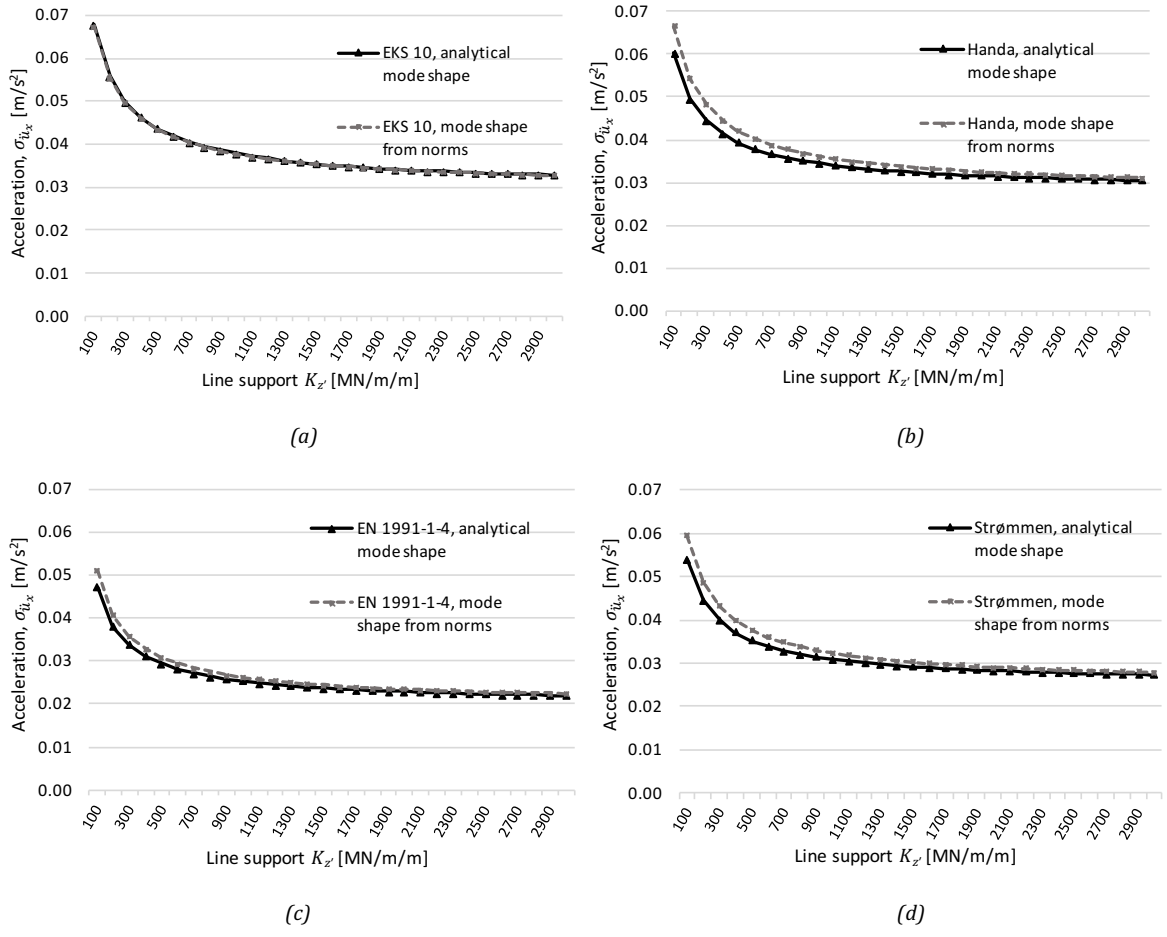

Figure 7-27 Comparison of difference in acceleration when different mode shape is used in calculations.

The results from Figure 7-27, together with the corresponding difference between analytical mode shape and mode shape from norms, are presented in Table 7-6 and Table 7-7.

Table 7-6 Comparison of standard deviation of acceleration for EKS 10 and Handa for different mode shape and stiffness of support.

$K_{z'}$	EKS 10			Handa		
[MN/m/m]	Analytical	Norm	Diff.	Analytical	Norm	Diff.
∞	0.0299	0.0299	0.0%	0.0282	0.0282	0.0%
3000	0.0328	0.0328	-0.1%	0.0305	0.0311	2.0%
500	0.0437	0.0435	-0.4%	0.0393	0.0421	7.1%
100	0.0677	0.0674	-0.5%	0.0602	0.0665	10.5%

Table 7-7 Comparison of standard deviation of acceleration for EN 1991-1-4 and Strømmen for different mode shape and stiffness of support.

$K_{z'}$	EN 1991-1-4			Strømmen		
[MN/m/m]	Analytical	Norm	Diff.	Analytical	Norm	Diff.
∞	0.0200	0.0202	1.0%	0.0253	0.0252	-0.4%
3000	0.0220	0.0224	2.1%	0.0273	0.0279	2.0%
500	0.0294	0.0309	4.9%	0.0352	0.0377	7.0%
100	0.0473	0.0510	7.9%	0.0539	0.0595	10.3%

In Section 7.6, it was concluded that the acceleration according to EKS 10 could neglect any change of mode shape when determining the acceleration in the top of the building. This conclusion is confirmed by the behaviour shown in Figure 7-27 *(a)* and Table 7-6, where the difference in accleration between the two mode shapes is very small for EKS 10. It should be noted, though, that this is only applicable for the case of evenly distributed mass, and that the small difference in acceleration is due to the fact that the mass of the top slab is somewhat smaller than the rest of the slabs. The effect of varying mass distribution is studied further in Section 7.9.3.2.

By observing Figure 7-27 *(b), (c)* and *(d),* it can be seen that Handa, Strømmen and EN 1991-1-4 are affected by the choice of mode shape. Further, the results are conservative for all three cases when using the simplified mode shape instead of the analytical mode shape. For flexible condition, the difference in acceleration for the two theoretical approaches, Handa and Strømmen, is approximately 10 %.

General for all four approaches is that the acceleration converges to the same result when the stiffness of the support increases. This supports the reasoning that the methods in the norms, when using simplified mode shape, are applicable for foundations close to the bedrock where support conditions are rather stiff.

7.9.2 Influence when changing the flexural rigidity of the core

Since the mode shape and fundamental frequency are determined from the eigenvalue problem, they are both dependent on the stiffness of the structure, i.e. flexural rigidity, EI, and the stiffness of the ground. The effect of changing the relationship between EI and stiffness of the ground is studied by scaling up and down the flexural rigidity of the core by a factor of 4. In

these studies, the analytical mode shape is used, to fully account for changes in the support conditions.

7.9.2.1 Increased stiffness

To simulate increased flexural rigidity of the core, the modulus of elasticity, E_{cm}, for the concrete is increased by a factor of 4. Figure 7-28 shows the resulting acceleration and corresponding fundamental frequency.

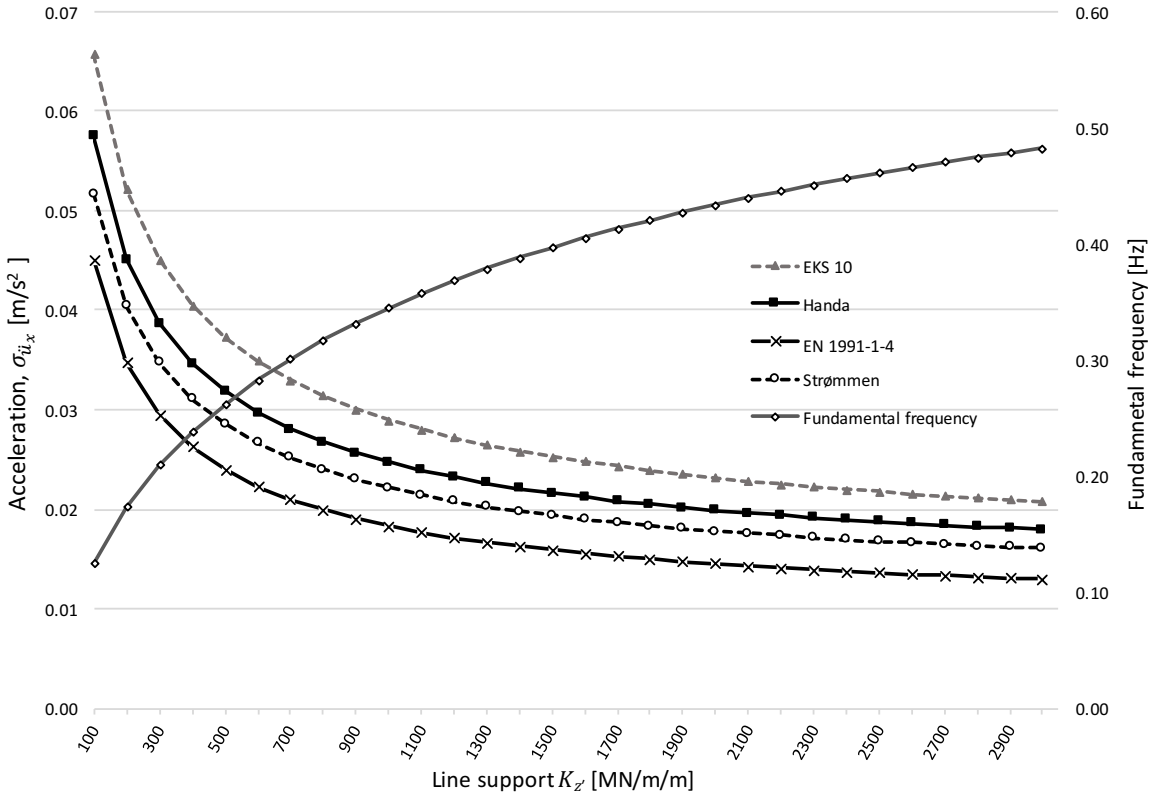

Figure 7-28 Acceleration and fundamental frequency when flexural rigidity is increased by a factor of 4.

What can be noticed from Figure 7-28 , is that maximum acceleration does not differ that much from the result for normal stiffness presented in Figure 7-24, but the difference in minimum acceleration is larger. The slopes of the curves are steeper for the case of increased stiffness compared to normal stiffness in Figure 7-24. This indicates that the effect of support conditions is more significant for structures with large flexural rigidity in relation to stiffness of the foundation, and that it is more difficult to achieve fixed support conditions.

It can also be observed that the difference between EKS 10 and Handa is larger than for normal stiffness, and this is because the analytical mode shape deviate more from the one assumed in the norms. The analytical mode shape tends to the form of a straight line because the relationship between structural stiffness and line support stiffness have increased.

Table 7-8 Comparison between EKS 10 and Handa's approach for various support conditions when stiffness of building is increased.

$K_{z'}$ [MN/m/m]	EKS 10 [m/s^2]	Handa [m/s^2]	Difference [%]
3000	0.0208	0.0180	-13.5%
500	0.0373	0.0318	-14.7%
100	0.0657	0.0575	-12.5%

Table 7-8 shows that the difference in acceleration between the theoretical approach by Handa and EKS 10 is large for all measured support stiffness's, $K_{z'}$. This suggests that the analytical mode shape and the simplified mode shape differ for all measured line support stiffness in the parameter study when the flexural rigidity is increased.

7.9.2.2 Reduced stiffness

To simulate reduced flexural rigidity, the modulus of elasticity, E_{cm}, for the concrete is divided by a factor of 4. Figure 7-29 shows the resulting acceleration and corresponding fundamental frequency.

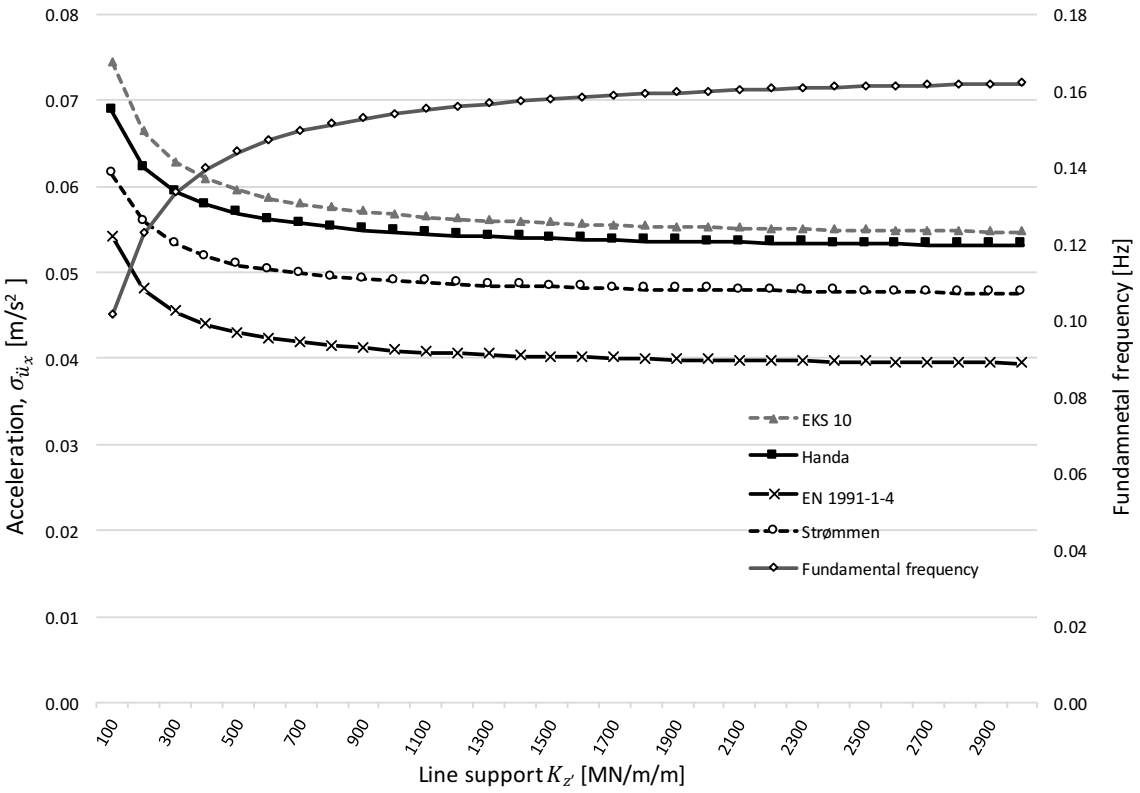

Figure 7-29 Acceleration and fundamental frequency when flexural rigidity is reduced by a factor of 4.

As can be seen in Figure 7-29, the behaviour of fundamental frequency and acceleration is the opposite from what was observed in Figure 7-28. The difference between maximum and

minimum acceleration is small compared to the results for increased stiffness. Further, it can be noticed that the slopes of the curves are less steep for decreased stiffness, i.e. the effect of support conditions is smaller for structures with less flexural rigidity in relation to stiffness of support.

Table 7-9 Comparison between EKS 10 and Handa's approach for various support conditions when stiffness of building is reduced.

$K_{z'}$ [MN/m/m]	EKS 10 [m/s^2]	Handa [m/s^2]	Difference [%]
3000	0.0547	0.0531	-2.8%
500	0.0595	0.0568	-4.5%
100	0.0755	0.0687	-7.7%

Table 7-9 shows that the difference in acceleration between EKS 10 and Handa is rather small, this indicates that the analytical mode shape is more similar to the mode shape stated in the norms (i.e. close to that obtained for a fixed support) when the flexural rigidity is decreased.

7.9.2.3 Conclusion on influence of stiffness

From studies in Section 7.9.2.1 and 7.9.2.2, it is clear that the relation between flexural rigidity, EI, and stiffness of the support, influences what effect support conditions has on the horizontal acceleration. The differences in acceleration and fundamental frequency according to Handa for the two cases, are presented in Table 7-10.

Table 7-10 Comparison of acceleration and fundamental frequency between the base case and the reduced as well as the increased stiffness for Handa's method.

Handa						
$K_{z'}$ [MN/m/m]	EI [m/s^2]	4 EI [m/s^2]	Difference [%]	EI [Hz]	4 EI [Hz]	Difference [%]
3000	0.0305	0.0180	-41%	0.3007	0.4826	60%
500	0.0393	0.0318	-19%	0.2168	0.2618	21%
100	0.0602	0.0575	-4%	0.1189	0.1249	5%
$K_{z'}$ [MN/m/m]	EI [m/s^2]	0.25 EI [m/s^2]	Difference [%]	EI [Hz]	0.25 EI [Hz]	Difference [%]
3000	0.0305	0.0531	74%	0.3007	0.1618	-44%
500	0.0393	0.0568	45%	0.2168	0.1439	-34%
100	0.0602	0.0687	14%	0.1189	0.1013	-15%

In Table 7-10 it can be seen that the acceleration is highly affected by the flexural rigidity of the core. Increasing the flexural rigidity by a factor of 4, decreases the acceleration with 41 % for $K_{z'} = 3000$ MN/m/m and divding the flexural rigidty by factor of 4 increases the acceleration with 74 % for $K_{z'} = 3000$ MN/m/m. Another relationship that can be observed

in Table 7-10 is that the difference in acceleration is almost in the same magnitude as the difference in fundamental frequency.

The behaviour of the acceleration for different EI can be explained by examining the variation of the mode shape. In Figure 7-30 the analytical mode shape is plotted for the two cases of flexural rigidity, when the foundation is regarded as stiff ($K_{z\prime} = 3000\ \mathrm{MN/m/m}$). For comparison, the simplified mode shape according to Eurocode 1 Part 1-4 is shown in Figure 7-30.

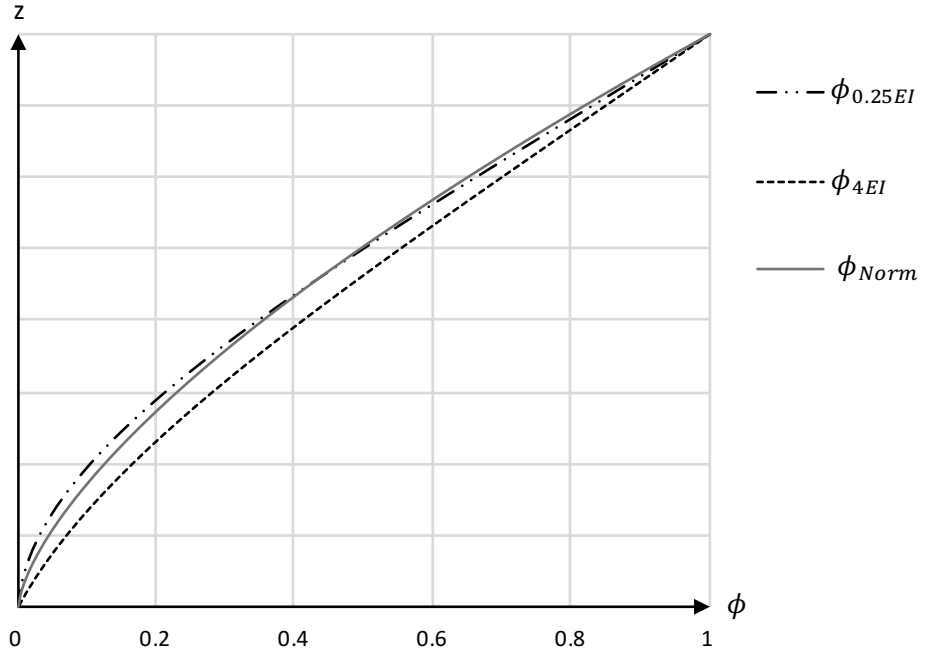

Figure 7-30 Variation of mode shape due to change in flexural rigidity, in case of $K_{z\prime} = 3000\ MN/m/m$, compared to simplified mode shape according to Eurocode 1 Part 1-4.

With increasing flexural rigidity in relation to the stiffness of the support, deformations will start to occur in the foundation, i.e. the rotational DOF in the bottom of the cantilever. The mode shape, ϕ_{4EI}, will consequently tend to illustrate a structure with a less fixed support, as can be seen in Figure 7-30. With deformations occurring in the foundation instead of in the structure itself, the change of stiffness in the support affects the acceleration more than for a building with normal stiffness. This is an explanation to why the curves are steeper in Figure 7-28.

Consequently, the opposite behaviour is shown for the case of low flexural rigidity in relation to stiffness of the support. For this scenario, displacements occur in the structure and the change of stiffness in the support has less effect on the acceleration.

Additionally, what can be concluded from Figure 7-28, Figure 7-29 and Figure 7-30 is that EKS 10 does not take this effect into account, due to the fact that it is independent of mode shape for cases with evenly distributed mass. This means that EKS 10 is a better representation for structures with less the flexural rigidity of the core in relation to support stiffness, and not that representable for the opposite case.

An observation that can be made when looking at Figure 7-24, Figure 7-28 and Figure 7-29, is that the slope for the acceleration and the fundamental frequency is very similar but with opposite signs. This indicates that the acceleration is highly dependent on the fundamental frequency.

The effect of change in support conditions on fundamental frequency for the cases with different flexural rigidity is shown in Figure 7-31.

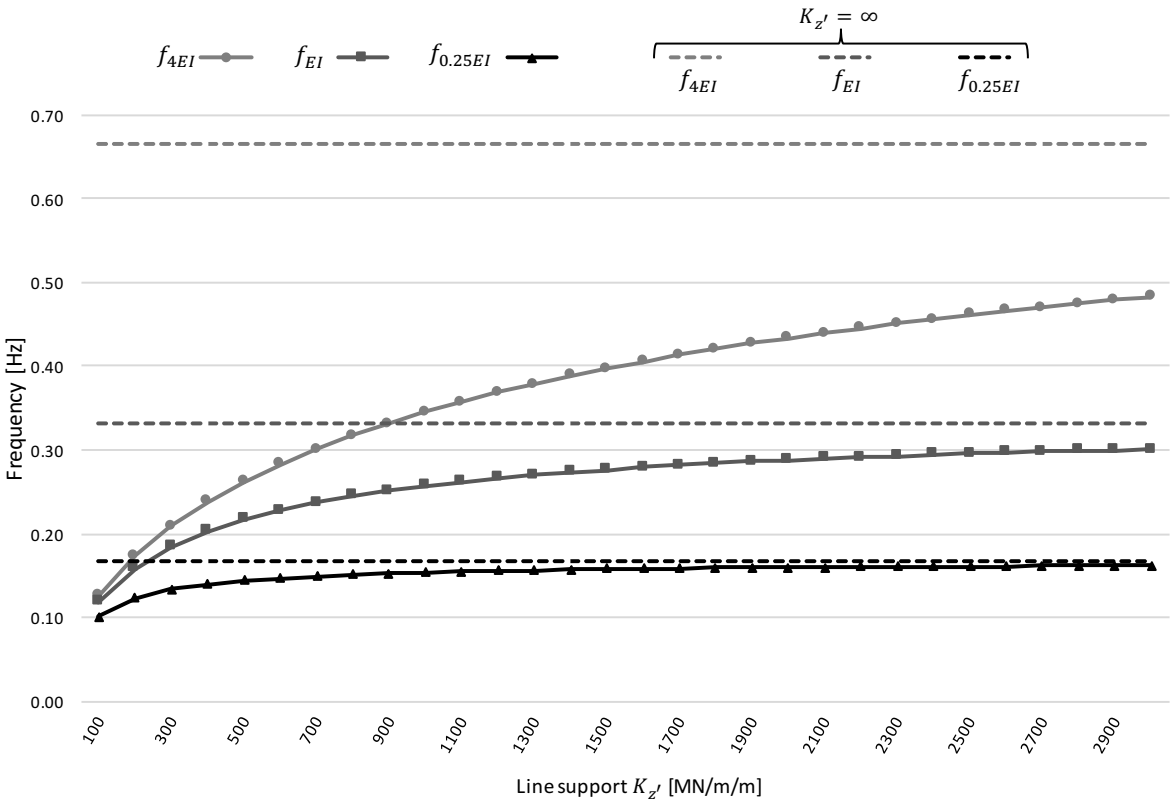

Figure 7-31 Influence of flexural rigidity on the relationship between fundamental frequency and stiffness of the support.

From this it can be seen that the magnitude of the fundamental frequency is very different when stiffness of line support is large, while the results converge for weak conditions. This indicates that the fundamental frequency is more influenced of the flexural rigidity of the building when support conditions are more rigid, and nearly independent of the structural stiffness for very flexible supports.

Table 7-11 compares the fundamental frequency when using the maximum line support stiffness used in this parameter study to a fully fixed foundation. It is clear that when decreasing the stiffness of the core by a factor of four, it can be regarded as fully fixed when using $K_{z'} = 3000$ MN/m/m, something that cannot be said when the stiffness of the core is increased by a factor of four.

Table 7-11 Comparison of fundamental frequency between a fully fixed support and maximum studied stiffness for difference stiffness

$K_{z'}$ [MN/m/m]	Frequency [Hz]	Difference [%]
Normal stiffness		
∞	0.333	90 %
3000	0.301	
Increased stiffness		
∞	0.665	73 %
3000	0.483	
Decreased stiffness		
∞	0.166	97 %
3000	0.162	

7.9.3 Influence of mass

Horizontal acceleration is highly correlated to the mass, both by fundamental frequency and mode shape. It is therefore investigated what effect the change of mass and mass distribution has on the acceleration for various support conditions.

7.9.3.1 Scaling mass

An increase in mass reduces the fundamental frequency, which increases the acceleration. However, an increase in mass also increases the inertia of the building, which reduces the acceleration. To see what effect the mass has on the acceleration, a mass scaling factor is introduced, which is multiplied with the density of the concrete for the studied building described in Section 7.1.1. Masses are calculated and presented in Appendix B.

Standard deviation of acceleration is calculated for the case of flexible support conditions, $K_{z'} = 500\ MN/m/m$, and presented in Figure 7-32.

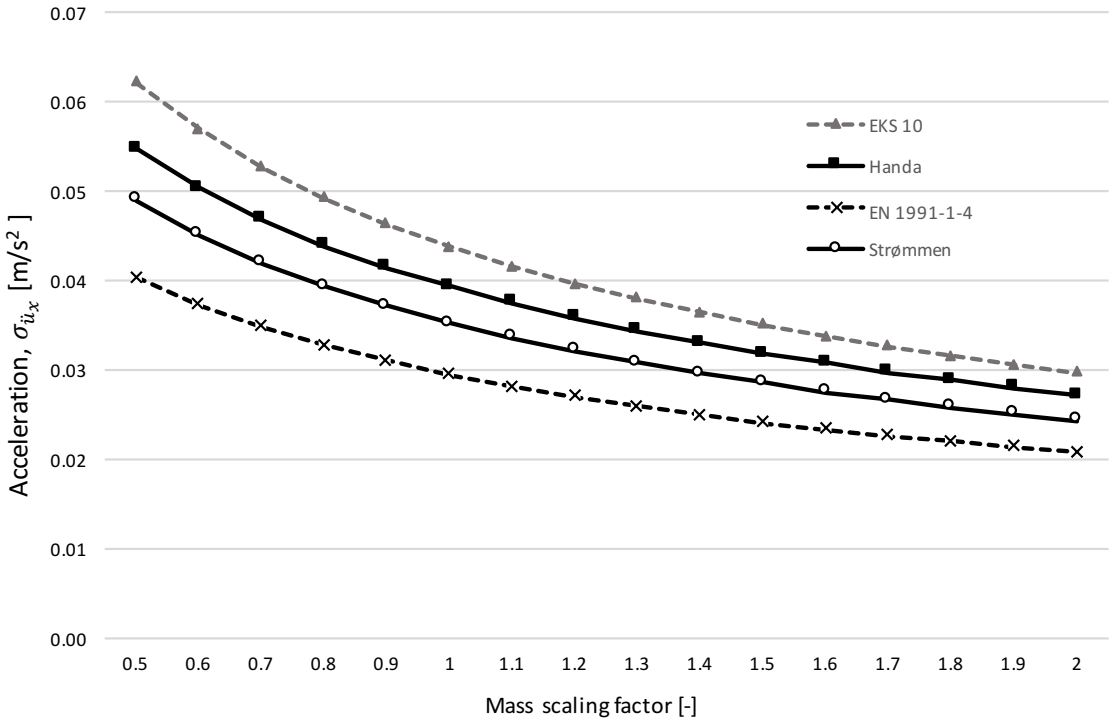

Figure 7-32 Relationship between standard deviation of acceleration for all four methods, and amount of mass, when $K_{z\prime} = 500\ MN/m/m$.

As can be seen in Figure 7-32, an increase of mass reduces the horizontal acceleration in the top of the building. The behaviour is shown for $K_{z\prime} = 500$ MN/m/m, but the conclusion holds for all support conditions.

7.9.3.2 Varying distribution

As shown in Section 7.4.3, the effect support condition on the equivalent mass, m_e, is neglectable for the studied example. Further, it is shown that when calculating standard deviation of acceleration in the top of the building, EKS 10 only accounts for change of mode shape through the estimation of equivalent mass. This lead to the conclusion that EKS 10 is independent of changes on the mode shape. The reasoning is however, only valid if the mass is evenly distributed over the height. This can be seen by examining expression (7-11) for equivalent mass, combined with the expression for generalized mass in Equation (7-7):

$$m_e = \frac{\widetilde{M}}{\int_0^H {\phi_i}^2(z)dz} = \frac{\int_0^H {\phi_i}^2(z)m_i(z)dz}{\int_0^H {\phi_i}^2(z)dz} \tag{7-29}$$

For the case of evenly distributed mass, i.e. when mass per meter, $m_i(z)$, is constant over the height, it can be placed outside the integral, enabling the following simplification:

$$m_e = m_i \tag{7-30}$$

For these situations, the equivalent mass is completely independent of the mode shape, and thus on the support conditions. However, this is not always the case for typical structures in civil engineering. Hence a structure with the same total mass as for the base case described in Section

7.1.1 but with varying mass distribution along the height is studied, to see what impact support conditions has on the acceleration according to EKS 10. The studied structure with mass distribution is shown in Figure 7-33.

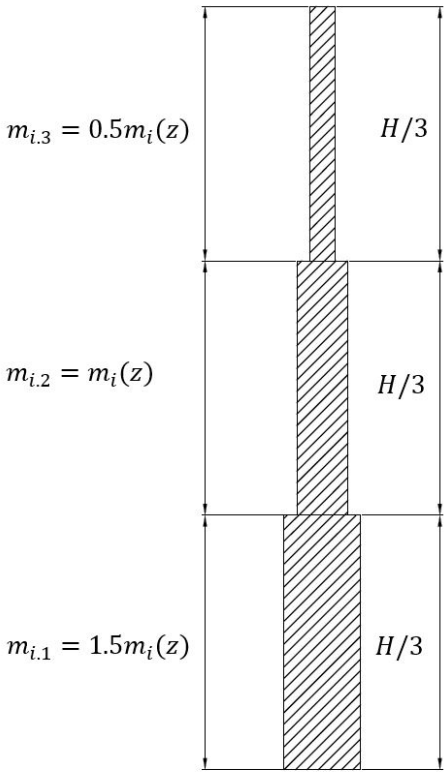

Figure 7-33 Illustration of mass distribution for studied building.

The behaviour of equivalent mass, m_e, for varying stiffness of the support is shown in Figure 7-34.

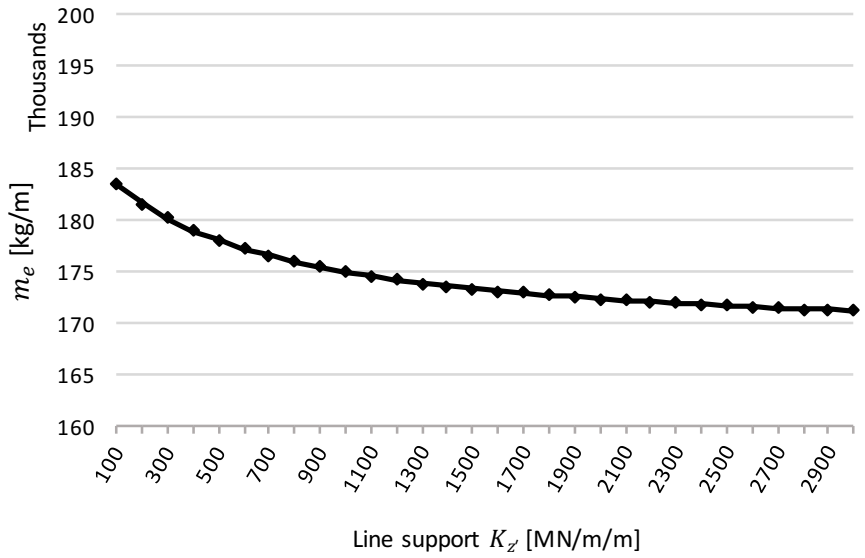

Figure 7-34 Relationship between equivalent mass for a structure with varying mass distribution, and stiffness of the support.

As expected, the equivalent mass per meter is now dependent on the support conditions. Unlike the case of evenly distributed mass, there should now be a difference between EKS 10 when comparing the analytical mode shape to the mode shape from norms.

To study the effect, the results for EKS 10 are plotted with analytical mode shape, taking support conditions into account, and the simplified mode shape which is independent on support conditions. The results are shown in Figure 7-35.

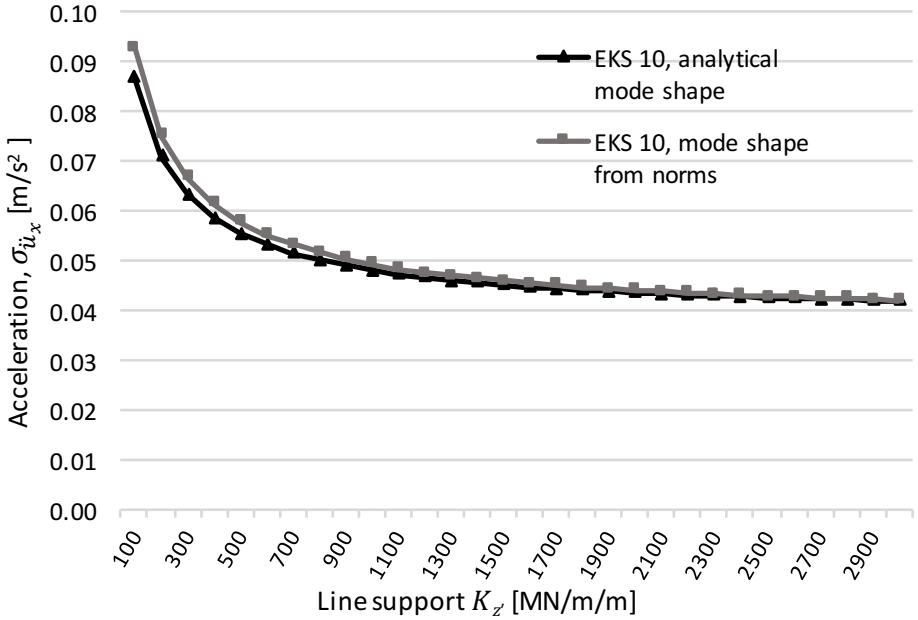

Figure 7-35 Comparison between the analytical mode shape and mode shape from norms for EKS 10 with varying mass distribution.

The two curves in Figure 7-35 are not equal, which means the choice of mode shape when determining acceleration according to EKS 10 is affected when the mass is varying over the height of the building. The acceleration is presented for three support conditions in Table 7-12.

Table 7-12 Comparison of standard deviation of acceleration for EKS 10 for different mode shape and stiffness of support in case of varying mass.

$K_{z'}$	EKS 10		
[MN/m/m]	Analytical	Norm	Diff.
3000	0,0393	0,0395	0,5%
500	0,0522	0,0544	4,2%
100	0,0819	0,0875	6,8%

For rigid supports ($K_{z'} = 3000\text{MN/m/m}$), the results are very similar. However, the results diverge for decreasing stiffness of the support and even if EKS 10 with simplified mode shape, is conservative, it cannot be seen as a correct representation for the situation when the mass is varying.

Obviously, EKS 10 with analytical mode shape accounts for the support conditions to some extent. Figure 7-36 shows a comparison between the theoretical approach according to Handa and EKS 10 with analytical mode shape when the mass is varying.

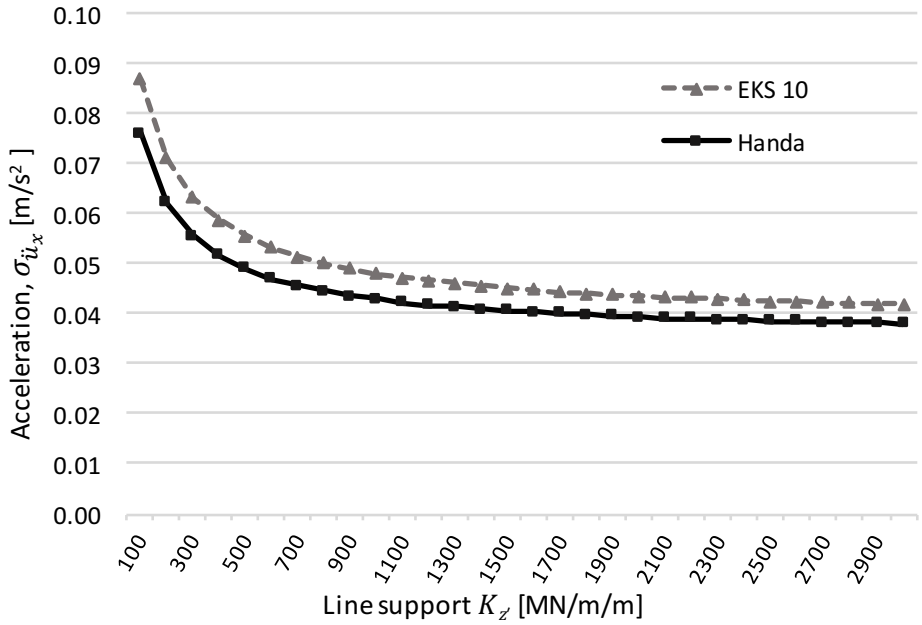

Figure 7-36 Comparison between results from EKS 10 and Handa with analytical mode shape with varying mass.

What can be noticed in the figure is that EKS 10 still is conservative for all support conditions. As mentioned in Section 5.2.1, EKS 10 is derived from Handa's equations with some assumptions. One of these assumptions is that the mode shape stated in Eurocode 1 Part 1-4, is used when simplifying expressions that contains integrals of the mode shape. These assumptions affect the generalised load, W, and correlation factor, V_c, which means that EKS 10 does not consider how these parameters is influenced by the change of mode shape, and this induces some differences.

Further, what can be observed by comparing Figure 7-36 and Figure 7-24, is that the horizontal acceleration increases for the case with varying mass distribution even though the total mass of the structure is the same for both cases. This is because the generalised mass, $\widetilde{M}_x$, is defined as the integral of the product between mass per meter and mode shape in square, see Section 7.4.1. Consequently, an increased mass per meter, $m_i(z)$, has largest effect on generalized mass in the top of the building, where the mode shape is large, and small effect in the bottom of the structure. For the chosen mass distribution in Figure 7-33, where the mass per meter is less in the top of the building compared to the base case, the generalised mass is consequently less. As concluded in Section 7.4.1, a decreased generalised mass increases the horizontal acceleration.

7.9.4 Influence of decay constants

As mentioned in Section 5.2.1 and 5.2.2 the expressions in the norms are based on different assumptions. One of these assumptions is that the normalized Co-spectrums are simplified on the basis of a certain decay constant.

Normalized Co-spectrums are explained in Section 4.1.3.2 and are defined as:

$$\iint \hat{C}o_{ui}(\Delta i, \omega) = \iint e^{-C_{ui}\frac{\Delta i \omega}{2\pi V(z)}} \tag{7-31}$$

According to K. Handa (Personal communication, April 26, 2017), EKS 10 is based on $C_{uz} = C_{uy} = 8$ while (Dyrbye & Hansen, 1997) states that the expressions in Eurocode 1 Part 1-4 are based on $C_{uz} = C_{uy} = 11{,}5$. The normalized Co-spectrums in both directions, z and y, are plotted for these two assumed decay constants in Figure 7-37 and Figure 7-38.

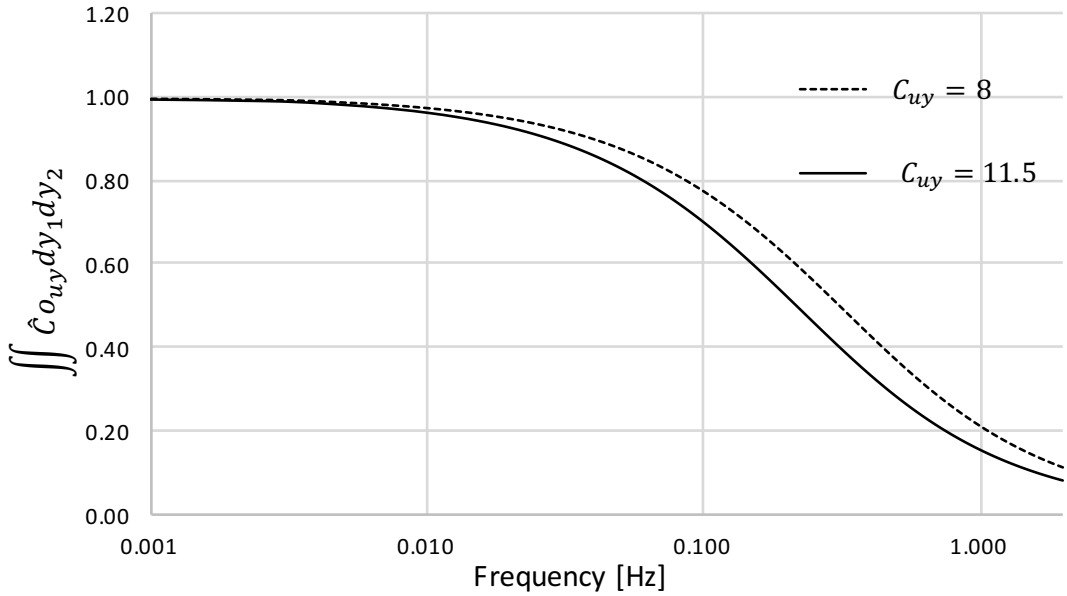

Figure 7-37 Relationship between integral over Co-spectrum in y-direction and frequency, for two choices of decay constants.

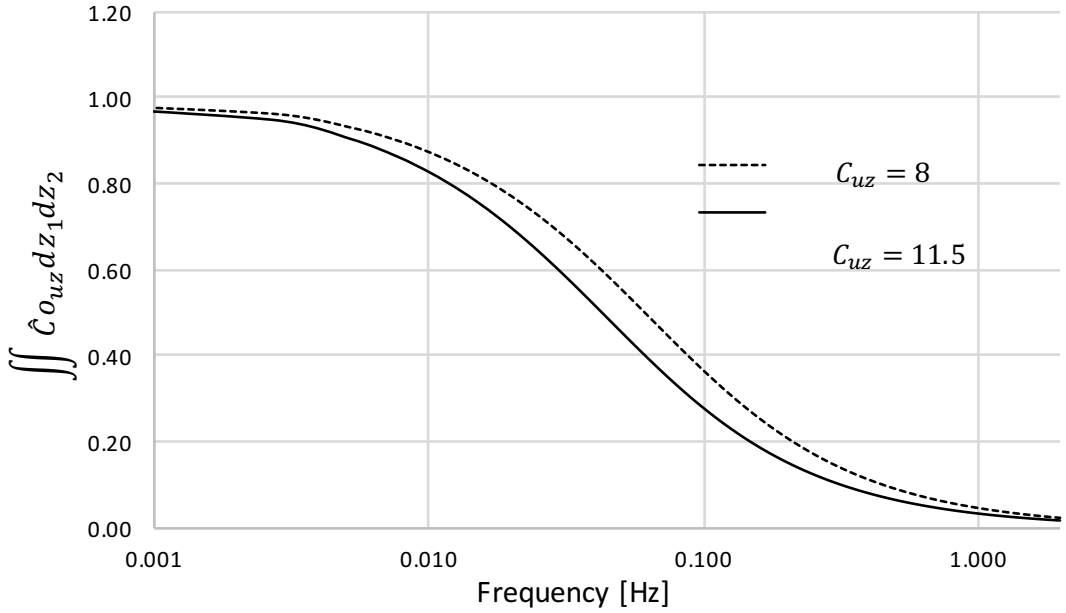

Figure 7-38 Relationship between integral over Co-spectrum in z-direction and frequency, for two choices of decay constants.

What can be noticed from the figures above is that the integrals over the Co-spectrums are larger when assuming decay constants $C_{uz} = C_{uy} = 8$, which is the case for EKS 10, and less when assuming $C_{uz} = C_{uy} = 11.5$, which is the case for Eurocode 1 Part 1-4 Annex B.

As concluded, for Strømmen and Handa, in Section 7.4.2 and 7.5.2, an increase in Co-spectrums will result in greater acceleration. It is therefore studied how the accelerations according to these theoretical approaches are affected when choosing decay constants, $C_{uz} = C_{uy} = 11.5$ instead of $C_{uz} = C_{uy} = 8$, as input. The results are plotted in Figure 7-39.

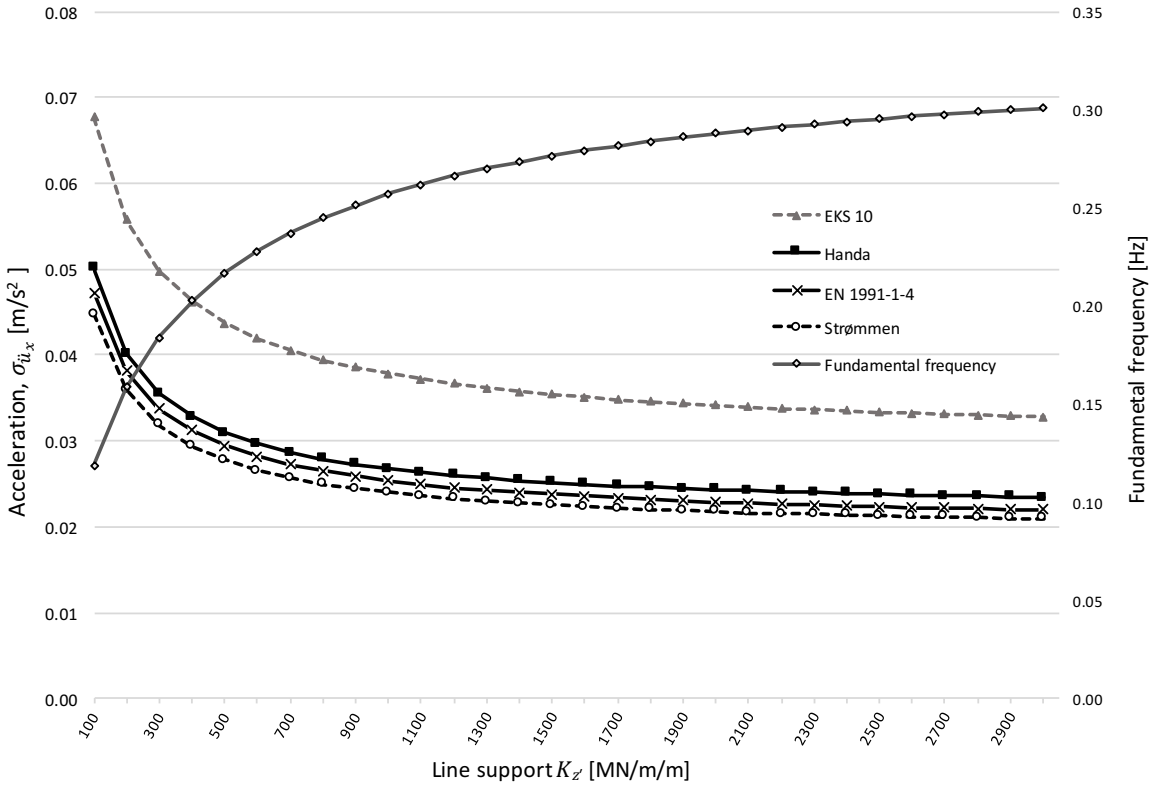

Figure 7-39 Relationship between standard deviation of acceleration, with decays constants $C_{uz} = C_{uy} = 11.5$ *as input for Strømmen and Handa, and stiffness of the support.*

As expected, the acceleration is decreased for Strømmen and Handa and by comparing Figure 7-39 with previous results in Figure 7-26, it can be observed that acceleration deterimined by Strømmen and Handa now tend to be more similar to that of Eurocode 1 Part 1-4 instead of EKS 10.

It can then be concluded that the choice of decay constants is crucial for the magnitude of acceleration.

8 Discussion

8.1 Analytical model

In this Thesis, an analytical model has been developed, see Chapter 6, in order to determine a representable mode shape and fundamental frequency for the structure and current support condition, i.e. a structure with changeable stiffness of the support. With the analytical model, it is then possible to implement the analytical mode shape in the four expressions for horizontal acceleration. However, one should be aware that some assumptions made to create the analytical model could result in deviation from an actual acceleration of a structure exposed to wind.

In this Thesis, the deep foundation was idealised as flexible line support at the base of the core. This assumption results in some characteristic of the foundation that might not fully correspond to the reality of a deep foundation. One consequence is that the structure will rotate around the centre line of the core, which could be questionable. Also, there is no damping included from the foundation, something that should be expected.

The core in the analytical model was modelled with beam elements, with constant flexural rigidity between the floors, i.e. a homogenous core. A core in a real structure usually has openings, since it is often utilized as staircase and for elevator shaft, which require doors. These imperfections could induce shear deformation that beam elements cannot take into consideration, so the mode shape of a real structures could deviate somewhat from the mode shape obtained from the analytical model.

The potential deviation from a real structure mentioned above, could affect the mode shape and fundamental frequency of the building. However, the fundamental behaviour, i.e. that decreased rigidity in the foundation reduces the fundamental frequency and changes the mode shape, would still apply. However, one should be aware that the magnitude of these parameters could be affected.

As described in Section 6.3, the rectangular rule is used for numerical integrations in the MATLAB-program developed. The rectangular rule is a rather simple method and should induce some error compared to the true integral. However, this error is expected to be rather small and since the main purpose of the Thesis was to investigate the relationship between horizontal acceleration and rotational stiffness of the support, the rectangular rule is assumed to be a good simplification. A more advanced integration method could be used for more exact results.

8.2 Results from parameter study

8.2.1 Mode shape

From Section 7.2, it is clear that the mode shape is affected by change of support conditions. It is also shown in Section 7.9.1, that acceleration according to the theoretical approaches decreases when using the analytical mode shape compared to the simplified mode shape stated in the norms. This proves that the horizontal acceleration is affected by changes of mode shape. However, as concluded in Section 7.9.1, EKS 10 is independent of the mode shape unless the mass distribution varies along the height. And even for such a case, there are simplifications made in the development of EKS 10, causing errors in the acceleration for decreasing stiffness of the support. This means that, by using EKS 10 it is not possible to fully account for

decreasing stiffness of the support, since the change of mode shape is not completely accounted for.

However, the effect of mode shape seems to be fully taken into account for the theoretical approaches according to Strømmen and Handa. The results from Section 7.9.1 indicates that also the method presented in Eurocode 1 Part 1-4 Annex B, accounts for change in mode shape. It is however, uncertain if some of the terms in the method are based on simplifications including an assumed mode shape. In Section 7.9.4, when changing decay constant for Strømmen and Handa to what was assumed in Eurocode 1 Part 1-4 Annex B, the results correlates well between the methods for all support conditions. This should indicate that Eurocode 1 Part 1-4 Annex B accounts for change of mode shape due to varying support conditions.

8.2.2 Fundamental frequency

The fundamental frequency decreases with decreasing stiffness of the support, as shown in Section 7.3. Throughout the parameter study, it was proven that the fundamental frequency has a significant impact on the horizontal acceleration. An observation that can be made when looking at a figure that compared the acceleration between the four methods together with the fundamental frequency, for example Figure 7-24, is that the slope of the acceleration and fundamental frequency is similar but with opposite signs.

The reason why the fundamental frequency is an important parameter is mainly due to the fact that the resonant part of the structure moves to lower frequencies, which is the region where the wind turbulence is larger, see von Kármán's wind-spectral density in Figure 7-5. This results in greater response, and thus greater acceleration of the loaded structure.

Further, it was concluded in the parameter study that the effect support condition has on the fundamental frequency is accounted for in all four approaches.

8.2.3 Potential differences between Strømmen and Handa

From the parameter study, it is clear that estimated acceleration according to the theoretical approaches, Strømmen and Handa, differs for all cases. One would expect that the therotical approaches would yield identical acceleration, but some differences have been noticed in the two methods. As stated in Section 4.2.2.2, one obvious difference in the derivations is that Handa expresses the mean wind velocity, $V(z)$, and turbulence intensity, $I_u(z)$, by the power law profile, while Strømmen uses the logarithmic profile. As shown in Figure 3-7, Section 3.5.3.2, there are some differences between the power law profile and logarithmic profile, which should induce differences between the final acceleration for the two approaches.

The transition from the expressions for standard deviation of acceleration for the entire frequency domain, to the final expressions for the resonant part, are not completely clear in the literature. This makes is difficult to completely compare the final expressions. There is, however, no reason to question the validity of the final expressions according to neither Strømmen, nor Handa.

8.2.4 Potential differences between EKS 10 and Eurocode 1 Part 1-4

What was surprising from the parameter study was the large difference in acceleration between the design norms, EKS 10 and Eurocode 1 Part 1-4 Annex B. A possible explanation may be found in the assumptions made when developing the norms.

As can be observed in Section 7.9.1, the acceleration according to Handa and EKS 10 is very similar when input parameters, such as mode shape and decay constants, are the same. This should indicate that EKS 10 is based on Handa's expression when simplified mode shape and decay constants, $C_{uz} = C_{uy} = 8$ are assumed.

In Section 7.9.4, when the decay constants are set to $C_{uz} = C_{uy} = 11.5$, the theoretical methods, Strømmen and Handa, yields acceleration that is close to the acceleration obtained from EN 1991-1-4. This should indicate that EN 1991-1-4 is based on a similar theoretical approach as that of Strømmen and Handa, but with decay constants set to 11.5.

These two conclusions are in accordance to what was stated in Section 5.2.1 and 5.2.2, that the explanation to the large difference in acceleration between the two norms, is that different input parameters were used when developing the expressions, and especially that two different decay constants were implemented.

8.3 Wind-spectral density

Initially in the parameter study, the expressions for calculating horizontal acceleration were modified to increase comparability of the results. One of these modifications was to consistently use von Kármán's wind spectral density for all four methods, as this is the choice in EKS 10. For the approach proposed in (Strømmen, 2010), several wind-spectral densities are mentioned but no one is explicitly chosen. Thus, the modification mainly affects the approach stated in Eurocode 1 Part 1-4, since the wind-spectral density chosen there is according to Kaimal's expression, see Section 5.2.2.

As mentioned in Section 7.1.3.1, the various wind-spectral density are empirical expressions describing the same phenomenon. Further, there is no indication that the choice of wind-spectral density is connected with other simplifications of the approach in Eurocode 1 Part 1-4. Thus, using von Kármán's wind spectral density in Eurocode 1 Part 1-4 should not affect the validity of the method.

One must however be aware of that, by changing the wind-spectral density, the magnitude of horizontal acceleration will be influenced. The choice of wind-spectral density is therefore an important parameter to consider when designing for acceleration.

8.4 Integral length scale

For the parameter study when determining the wind-spectral density, the integral length scale, $L_u^x = 150\,m$, was chosen in accordance with recommendations from K. Handa (Personal communication, April 26, 2017). The modification was made to increase comparability for the results, and was not expected to affect other terms in the expressions.

However, it may be shown that the magnitude of integral length scale has a significant impact on the horizontal acceleration. The choice of integral length scale is therefore an important parameter to consider, when designing for acceleration.

8.5 Decay constant

It was shown in the parameter study that the choice of decay constants, C_{uz} and C_{uy}, for the normalized Co-spectrums are crucial for the magnitude of the horizontal acceleration, see Section 7.9.4. Initially in the parameter study, the decay constants were chosen in accordance with recommendations from K. Handa (Personal communication, April 26, 2017), which resulted in good correspondence between the theoretical approaches and EKS 10.

However, when changing the decay constants in accordance to what was assumed when developing the expressions in Eurocode 1 Part 1-4 Annex B, the estimates from the theoretical approaches tended towards the results from Eurocode instead of EKS 10. This indicates that the magnitude of acceleration is highly dependent on the choice of decay constant, and that one of the main differences between the method in EKS 10 and in Eurocode 1 Part 1-4 Annex B are the originally chosen decay constants.

9 Final Remarks

9.1 Conclusions

The aim of this Thesis was to investigate what influence a deep foundation has on the horizontal acceleration in high-rise buildings. From the parameter study, it was clear that both the fundamental frequency and mode shape of the loaded structure will be affected by decreasing the rotational stiffness of the support, and that the horizontal acceleration will be affected due to those changes.

The parameter study concluded that the horizontal acceleration, for all four methods, increased when the rotational stiffness of the support decreases. It was also shown that the horizontal acceleration is mainly affected by the change of fundamental frequency.

EKS 10 was conservative for all performed studies in the parameter study, this should increase the confidence in using this method regardless of boundary conditions. Since the mode shape is rather demanding to estimate analytically and due to the fact that EKS 10 is nearly independent on the mode shape, it is recommended to use the simplified mode shape proposed in the norms. However, it is necessary to use the correct fundamental frequency that corresponds to the actual support of the building, since the fundamental frequency have large impact on the resulting acceleration.

However, the estimated acceleration could be reduced significantly by using the approach in Eurocode 1 Part 1-4. For the chosen building in the parameter study, acceleration could be reduced up to 33 % compared to EKS 10.

The parameter study showed that it is possible for the designer to decrease the magnitude of horizontal acceleration by making some adjustments of the system. An increase in total mass will result in increasing inertia, which will reduce the horizontal acceleration. It is also beneficial for the horizontal acceleration to increase mass per meter in the top of the structure. Further, the parameter study showed that horizontal acceleration is highly dependent on the rotational stiffness of the entire structure. One method for decreasing the acceleration is therefore to increase the stiffness of the structure. If the flexural rigidity of the core is large compared to the stiffness of the support, the horizontal acceleration is most efficiently reduced by increasing rotational stiffness of the support. If the flexural rigidity of the core is low in relation to the foundation, it is more efficient to focus on increasing the structural stiffness of the structure to reduce horizontal acceleration.

9.2 Further studies

The choice of decay constant turned out to be crucial for the magnitude of horizontal acceleration. Since there are several recommended values in the literature, but no homogeneous opinion about which to assume, the decay constants is a parameter that needs further investigation.

In the study, only the fundamental mode of the structure was investigated. To obtain a more correct acceleration, more modes should be considered in the analysis. Especially if the location of the core is not symmetrical within the building, since that might cause torsion of the building, resulting in excitation in both the horizontal mode and in torsional mode simultaneously.

Vibrations due to vortex shedding may be governing for slender structures, such as high-rise buildings. The behaviour of fundamental frequency and mode shape for decreasing rotational stiffness of the support, as concluded in this Thesis, will be applicable also for this phenomenon. However, the horizontal accelerations due to vortex shedding may have a different relationship with decreasing rotational stiffness of the support, and this needs further investigation.

If even taller buildings are to be constructed in the future, resulting in more vibrations, it could be of interest to install a damper of some sort in the building. The mechanical damping ratio is a tabulated value in the norms, which may not completely reflect the correct situation. Therefore, it would be interesting to investigate the damping further, and add such a possibility in the calculations.

10 References

Boverket. (1997). *Snö och vindlast.* Karlskrona: Boverket.

Boverket. (2015). *Boverkets föreskrifter och allmänna råd om tillämpning av europeiska konstruktionsstandarder (eurokoder).* Boverket.

CEN. (2005). *Eurocode 1: Actions on structures - Part 1-4: General actons - Wind actions.* Brussels: European Committee for Standardization.

Chopra, A. K. (2012). *Dynamics of Structures* (Fourth Edition ed.). Berkley, California, USA: PEARSON.

Davenport, A. (1962). *The response of Slender, Line-Like Structures to a Gusty Wind.* Proceedings of the Institution of Civil Engineerings.

Dyrbye, C., & Hansen, S. O. (1997). *Wind Loads on Structures.* Chichester: John Wiley & Sons Ltd.

Geological Survey of Sweden. (2017, 02 15). *SGUs Kartvisare, Jordlagerföljder*. Retrieved from SGU, Sveriges Geologiska Undersökningar: https://apps.sgu.se/kartvisare/kartvisare-lagerobservationer.html

Handa, K. (1982). *Kompendium i Byggnadsaerodynamik.* Gothenburg: Chalmers University of Technology.

International Organisation for Standardization. (1984). *International Standard ISO 6897.* International Organisation for Standardization.

Irwin, P., Denoon, R., & Scott, D. (2013). *Wind Tunnel Testing of High-Rise Buildings: An output of the CTBUH Wind Engineering Working Group.* New York: Taylor & Francis Group. Retrieved from https://store.ctbuh.org/PDF_Previews/Books/2013_WindTunnelGuide_Preview.pdf

Kwok, K. C., Burton, M. D., & Abdelrazaq, A. K. (2015). *Wind-Induced Motion of Tall Buildings: Designing for habitability.* Virginia: American Society of Civil Engineers.

SIS. (2008). *SS-ISO 10137:2008.* Stockholm: SIS, Swedish Standards Institute.

Skidmore, Owings & Merrill, LLP. (2013). *Timber tower research project, Final report.* Chicago: Skidmore, Owings & Merrill, LLP.

Strømmen, E. N. (2010). *Theory of Bridge Aerodynamics.* Trondheim: Springer-Verlag Berlin Heidelberg.

The University of Texas, M. M. (2017). *Chapter 10: Vestibular System: Structure and function*. Retrieved from http://neuroscience.uth.tmc.edu/s2/chapter10.html

Västra Götalandsregionen. (2016). *Rapport 2016:7 Befolkningsprognos Västra Götaland 2016-2030.* Gothenburg: Västra Götalandsregionen.

von Kármán, T. (1948). *Progress in the statistical theory of turbulence.*

Appendix A Mass calculations for verifications

Mass calculations per storey, used for verification

Densities

$\rho_{concrete} := 2500 \frac{kg}{m^3}$ Density of concrete

$\rho_{slab} := 650 \frac{kg}{m^2}$ Mass per area for slab

Geometry

$h := 3.8\ m$ Height of storey

$t_1 := 0.7\ m$ Thickness of core walls

$t_2 := 0.25\ m$ Thickness of slab in core

$A_{columns} := 20 \cdot 0.6\ m \cdot 0.6\ m = 7.2\ m^2$ Area of columns per storey

$A_{core.walls} := 15\ m \cdot 2 \cdot t_1 + 18\ m \cdot 2 \cdot t_1 = 46.2\ m^2$ Area of core walls

$A_{core.slab} := 15\ m \cdot 18 = 270\ m$ Area of slab inside core

$A_{slab} := 30\ m \cdot 30\ m = 900\ m^2$ Area of slab outside core

$V_{columns} := A_{columns} \cdot h = 27.36\ m^3$ Volume of columns per storey

$V_{walls} := A_{core.walls} \cdot h = 175.56\ m^3$ Volume of core walls

Masses

$m_{slab} := A_{slab} \cdot \rho_{slab} = \left(5.85 \cdot 10^5\right)\ kg$ Mass of slab per storey

$m_{walls} := V_{walls} \cdot \rho_{concrete} = \left(4.389 \cdot 10^5\right)\ kg$ Mass of core walls per storey

$m_{columns} := V_{columns} \cdot \rho_{concrete} = \left(6.84 \cdot 10^4\right)\ kg$ Mass of columns per storey

$m_{tot} := m_{slab} + m_{walls} + m_{columns} = \left(1.092 \cdot 10^6\right)\ kg$ Mass per storey, 0-39

$m_{tot.top} := m_{slab} + \frac{m_{walls}}{2} + \frac{m_{columns}}{2} = \left(8.387 \cdot 10^5\right)\ kg$ Mass in top slab

FEM-design

$\rho_{eq.slab} := \frac{m_{tot}}{A_{core.slab} \cdot t_2} = \left(1.618 \cdot 10^4\right) \frac{kg}{m^2}$ Equivalent density, 0-39

$\rho_{eq.slab.top} := \frac{m_{tot.top}}{A_{core.slab} \cdot t_2} = \left(1.242 \cdot 10^4\right) \frac{kg}{m^2}$ Equivalent density, top slab

Appendix B Mass calculations for parameter study

Mass calculations per storey for parameter study

Densities

$\rho_{concrete} := 2500 \frac{kg}{m^3}$ Density of concrete

$\rho_{slab} := 650 \frac{kg}{m^2}$ Mass per area for slab

Geometry

$h := 3.8\ m$ Height of storey

$t_1 := 0.7\ m$ Thickness of core walls

$t_2 := 0.25\ m$ Thickness of slab in core

$A_{columns} := 20 \cdot 0.6\ m \cdot 0.6\ m = 7.2\ m^2$ Area of columns per storey

$A_{core.walls} := 15\ m \cdot 2 \cdot t_1 + 15\ m \cdot 2 \cdot t_1 = 42\ m^2$ Area of core walls

$A_{core.slab} := 15\ m \cdot 15 = 225\ m$ Area of slab inside core

$A_{slab} := 30\ m \cdot 30\ m = 900\ m^2$ Area of slab outside core

$V_{columns} := A_{columns} \cdot h = 27.36\ m^3$ Volume of columns per storey

$V_{walls} := A_{core.walls} \cdot h = 159.6\ m^3$ Volume of core walls

Masses

$m_{slab} := A_{slab} \cdot \rho_{slab} = \left(5.85 \cdot 10^5\right)\ kg$ Mass of slab per storey

$m_{walls} := V_{walls} \cdot \rho_{concrete} = \left(3.99 \cdot 10^5\right)\ kg$ Mass of core walls per storey

$m_{columns} := V_{columns} \cdot \rho_{concrete} = \left(6.84 \cdot 10^4\right)\ kg$ Mass of columns per storey

$m_{tot} := m_{slab} + m_{walls} + m_{columns} = \left(1.052 \cdot 10^6\right)\ kg$ Mass per storey, 0-39

$m_{tot.top} := m_{slab} + \frac{m_{walls}}{2} + \frac{m_{columns}}{2} = \left(8.187 \cdot 10^5\right)\ kg$ Mass in top slab, top slab

$m_{total} := m_{tot} \cdot 40 + m_{tot.top} = \left(4.291 \cdot 10^7\right)\ kg$ Total mass of the building

Influence of mass
Mass calculations when scaling density.

$$X := \begin{bmatrix} 2 \\ 1.8 \\ 1.6 \\ 1.4 \\ 1.2 \\ 1 \\ 0.8 \\ 0.6 \end{bmatrix}$$ Vector with scaling factor

$\rho_{concrete.X} := X \cdot \rho_{concrete}$ Scaling density of concrete

$\rho_{slab.X} := X \cdot \rho_{slab}$ Scaling mass per area for slab

New masses

$m_{slab.X} := A_{slab} \cdot \rho_{slab.X}$ Mass of slab per storey

$m_{walls.X} := V_{walls} \cdot \rho_{concrete.X}$ Mass of core walls per storey

$m_{columns.X} := V_{columns} \cdot \rho_{concrete.X}$ Mass of columns per storey

$$m_{tot.X} := m_{slab.X} + m_{walls.X} + m_{columns.X} = \begin{bmatrix} 2.105 \cdot 10^6 \\ 1.894 \cdot 10^6 \\ 1.684 \cdot 10^6 \\ 1.473 \cdot 10^6 \\ 1.263 \cdot 10^6 \\ 1.052 \cdot 10^6 \\ 8.419 \cdot 10^5 \\ 6.314 \cdot 10^5 \end{bmatrix} kg$$ Mass per storey, 0-39

$$m_{tot.top.X} := m_{slab.X} + \frac{m_{walls.X}}{2} + \frac{m_{columns.X}}{2} = \begin{bmatrix} 1.637 \cdot 10^6 \\ 1.474 \cdot 10^6 \\ 1.31 \cdot 10^6 \\ 1.146 \cdot 10^6 \\ 9.824 \cdot 10^5 \\ 8.187 \cdot 10^5 \\ 6.55 \cdot 10^5 \\ 4.912 \cdot 10^5 \end{bmatrix} kg$$ Mass in top slab, top slab

Appendix C MATLAB code

C.1 Main code

----------Master thesis----------

```
  %Wind-Induced Accelleartion in High-Rise Buildings

clc ; close all; clear all
```

PART 1 - Input and structural properties

Input

```
Input; %Calls for the matlab file with all the input
```

Determine the coordinates of the cantilever

```
%-----------------------------------------------------------------
[Coord]=coordinates(n_storeys,height_n,add_1); %Function that calls
% for the coordinates of the cantilever, where each coordinate
%represent a floor level

Ey=Coord(:,2);  %Coordinates of in y Dofi
Ex=Coord(:,1);  %Coordinates of in x Dofi

Eyp=[Ey(1:n_storeys) Ey(2:n_storeys+1)];
%Creates y-coordinates for an element
Exp=[Ex(1:n_storeys) Ex(2:n_storeys+1)];
%Creates x-coordinates for an element

%-----------------------------------------------------------------
```

Determine the stiffness matrix and mass matrix

```
%-------------------------------------------------------------------------
[K,Edof,M,C] = stiffnesmatrix(Eyp,Exp,ep1,ep2,ep3,n_storeys,krs,khs,n1,n2);
%Provides the global stiffness matrix,mass matrix, damping matrix
% and the topologi matrix of each element in core

%-------------------------------------------------------------------------
[M] = massmatrix(m1,m2,m3,n1,n2,K,M,mtop); % Function file that adds the
%lumped mass from each floor
```

Calculates the natural frequencies and mode shapes

```
%-----------------------------------
b=2:3:size(K,1);        %Degrees of freedom that are  zero

[La,Modeshapes]=eigen(K,M,b'); %Calculates the eigenvalue problem

Freq=sqrt(La)/(2*pi);  %Determines the frequencies of the building

%Extraxts the horzontal values of the modeshape vector
```

```
Modeshapef=Modeshapes(:,1);Modeshapef=Modeshapef(1:3:end);

Modeshapef=abs(Modeshapef/norm(Modeshapef,inf));
%Extracts the horizontal dofs and then normalizes the vector with a value
%equal to 1 in the top of the vector

fundamental_frequency=Freq(1); %Extracts the fundamental frequency in HZ
w_fundamental=Freq(1)*2*pi; %Circualar natural frequenzy

%-----------------------------------
```

Plot the result of mode shape 1 and 2

```
%Following is just plotfunctions in CALFEM, when plotting the first
% two mode shape of the core

figure(1),clf
eldraw2(Exp,Eyp,[2 3 0]);
Edb=extract(Edof,Modeshapes(:,1));
FreqText=num2str(Freq(1));
title('First two modeshapes');
eldisp2(Exp,Eyp,Edb,[1 2 0],100000);

Edb2=extract(Edof,Modeshapes(:,2));
eldisp2(Exp,Eyp,Edb2,[1 4 0],10000);
```

Determines generalized mass and equivalent mass

```
[Mg,me,Mode_square] = Generel_Equiv_mass(m1,m2,m3,n1,n2,...
    Modeshapef,height_n,mtop);
```

PART 2 - Acceleration according to EKS 10

```
[Accel_EKS,max_acc,betaair,xf_L_u] = EKS_acc(width,Ey,ksi,vb,c0,...
   fundamental_frequency,cf,me,beta,kl,Ter,rho,href,p1_x);
```

PART 3 - Acceleration according to Strømmen

```
Lx=linspace(0,Ey(1),N_int); %Height vector, to be used when integrating
%over the height of the bulding
```

Expansion of mode shape

```
[MS_int] = Modeshape_expansion(Ey,Modeshapef,n_int_per_storey,Lx);
```

Wind Behaviour, such as mean wind velocity vs height and mean turbulence

```
[Iu,v_mean,vtop,v_mean_zs,Iu_zs] = Wind_Behaviour(Lx,Ter,vb5);
```

Spectral Density

```
[Kaimal,Karman] = WindSpectralDensity(Ey,N_int,vtop,...
                                      w,xf_L_u,v_mean_zs,Ter);
```

Frequency Response Function

```
zetaair=betaair/(2*pi); %Determine the aerodynamic damping
[Hhat_N,Hhat] = FrequencyResponseFunction(zeta,w,w_fundamental,zetaair);
```

Coherence width and height

```
[Co_b,Co_h] = Coh_b(width,N_int,w,vtop,Cuu,Ey);
```

Joint Acceptance function

```
[J_sqr,J_sqr_NORM]=JointAF(Iu,Lx,Cuu,MS_int,v_mean,vtop,w,Mode_square,...
                        Kaimal,Karman,w_fundamental,v_mean_zs,rho,width,cf);
```

Response Spectrums

```
[Response_spectra_Acc,Response_spectra] = reponsespectrums(w,rho,...
Hhat_N,J_sqr_NORM,width,w_fundamental,me,depth,Kaimal,v_mean,inc,cf,Co_b);
```

Acceleration for the resonance response

```
[Accel_Strommen] = resonance(Mg,w_fundamental,J_sqr,rho,width,cf,Hhat_N,...
                   w,zeta,zetaair,Co_b)
```

PART 4 - Acceleration according to Eurocode Appendix B

```
[Accel_EC] = EC(cf,rho,Iu_zs,me,width,zeta,zetaair,Ey,...
             fundamental_frequency,Ter,v_mean_zs,v_mean,MS_int,Iu)
```

PART 5 - Acceleration according to Kamal Handa theoretical method

Mean deflection

```
[y_m] = y_m1(cf,rho,width,vtop,MS_int,powerlaw,w_fundamental,Mg,Ey);
```

HC-reduction factor for width

```
[H_C] = H_C1(width,fundamental_frequency,vtop,N_int,Cuu);
```

VC-reduction factor

```
[V_C] = V_C1(powerlaw,Ey,MS_int,vtop,Cuu,fundamental_frequency);
```

Wind Spectral density

```
[F] = Wind_Spec(vtop,fundamental_frequency,xf_L_u);
```

Acceleration according to Handa

```
[Dev_dis,Accel_Handa] = Handa(Iu,y_m,F,V_C,H_C,zetaair,zeta,w_fundamental);
```

C.2 Input file

Input file for all calculation

Input to determine the behavior of the core

```
%------------------INPUT---------------------
n_storeys=40;     %Number of storeys
height_n=3.8;     %Typical storey height
add_1=0;          %Extra height of first floor
A=0;              %Needed for input, but not relevant for modeshapes
%-------------------------------------------
n1=75;            %Number of  from the top including n1 (roof = 1)
                  %with a specific E1,I1,m1

E1=34e9;          %E-modulus for lateral bearing system for n1
I1=1578.4;        %Moment of inertia for core for n1
mtop=818700;      %Weight of roof
m1=1052400;       %Weight of each floor in levels n1
ep1=[E1 A I1 0];

%-------------------------------------------
n2=80;            %Number st  from from n1-n2 with a specific
                  %with a specific E2,I2,m2

E2=34e9;          %E-modulus for lateral bearing system
I2=1578.4;        %Moment of inertia for core
m2=750000;        %Weight of each floor
ep2=[E2 A I2 0];
%-------------------------------------------
%If n2<n_storeys, then the rest of the core is assumed to have the
%following properties

E3=34e9;          %E-modulus for lateral bearing system
I3=580;           %Moment of inertia for core
m3=750000;        %Weight of each floor
ep3=[E3 A I3 0];
%-------------------------------------------

khs=1e16;           %Stiffness for horizontal spring
a=15;               %width of core, short side (central line)
b=15;               %Width of core, long side  (central line)
kl=500e6;           %Stiffness line support along core
```

```
[krs] = rotaionalstiffness(kl,a,b); %Function file that determines
%rotational stiffness of foundation with regard to geomertry
%and flexibility of a line support

%krs=10e15;         %Use this as input if fixed support
```

Input for determine the acceleration in Part 4 according to EC

```
ksi=0.855 ;     %Omräkningsfaktor for 5 years
vb=25;          %Reference wind velocit
vb5=ksi*vb;     %Reference wind velocity return period 5 years
rho=1.25;       %Densisty of air

width=30;       %Widht of the building
depth=30;       %Depth of building


cf=1.55;        %Formfactor
c0=1;           %Topoligy factor
href=10;        %According to BSV 97
p1_x=1;         %Fundamental mode in wind direction
beta=0.1;       %Mechanical logarthimic damping of the structure
kl=1;           %Turbolense factor

TerrainCat=3;   %Choose terrain cattegory

if TerrainCat==1
    Ter=[0.00 1 0.16];
elseif TerrainCat==2
             Ter=[0.05 2 0.19];
elseif TerrainCat==3
                 Ter=[0.3 5 0.22];
elseif TerrainCat==4
                     Ter=[1 10 0.24];
end
```

Input for full dynamic analysis

```
zeta=beta/(2*pi);       %Damping
Cuu=8;                  %Decay constant
n_int_per_storey=20;    %Number of intergration per floor


N_int=n_storeys*n_int_per_storey+1;
% Number of integration points, 20 per floor + top

w=linspace(0.001,4*pi,N_int); %Which frequency we will look at, can
% increase/decrease what frequency domain we will include, now times 4 pi

inc=20;         %How many points to increse integration over resonance part
                %in acceleration response spectra

powerlaw=0.21;  %Power exponant to express wind and turbulance
```

C.3 Function file rotational stiffness

```
function [krs] = rotaionalstiffness(kls,a,b)
%Determines the rotaional stiffness of the core due to flexibel line
%support in vertical diraction in form of a rotational spring
krs=(kls*a^2/4)*(2*b+a/2);
end
```

C.4 Function file coordinates

```
function [Coord]=coordinates(n_storeys,height_n,add_1)
%Function that determines the coordinates of the cantilever

h_storey=n_storeys*height_n+add_1;
Ey=zeros(n_storeys+1,1);
Ex=zeros(n_storeys+1,1);

%Adds the height coordinates in vector form
for i=1:n_storeys;
    h=h_storey-(i-1)*height_n;
    Ey(i) = h;
end;
Coord=[Ex Ey];
```

C.5 Function file stiffness matrix

```
function [K,Edof,M,C] = stiffnesmatrix(Eyp,Exp,ep1,ep2,ep3,n_storeys,...
                                       krs,khs,n1,n2)
%Stiffnesmatrix determines the total stiffness of the cantilever

Edof=zeros(n_storeys,7);    %Topology for all Dofs

K=zeros((n_storeys+1)*3);
M=zeros((n_storeys+1)*3);
C=zeros((n_storeys+1)*3);

for i=1:n_storeys
   if i <= n1       %Creates K matriced for the top floors
[k,m,c]=beam2d(Exp(i,:),Eyp(i,:),ep1);
edof=...
[i i+(i-1)*2 i+1+(i-1)*2 i+2+(i-1)*2 i+3+(i-1)*2 i+4+(i-1)*2 i+5+(i-1)*2];
Edof(i,:)=edof;

   elseif i <= n2   %Creates K matrice for the middle floors
[k,m,c]=beam2d(Exp(i,:),Eyp(i,:),ep2);
edof=...
[i i+(i-1)*2 i+1+(i-1)*2 i+2+(i-1)*2 i+3+(i-1)*2 i+4+(i-1)*2 i+5+(i-1)*2];
Edof(i,:)=edof;
```

```
   else             %Creates K matriced for the bottom floors
[k,m,c]=beam2d(Exp(i,:),Eyp(i,:),ep3);

edof=...
[i i+(i-1)*2 i+1+(i-1)*2 i+2+(i-1)*2 i+3+(i-1)*2 i+4+(i-1)*2 i+5+(i-1)*2];
Edof(i,:)=edof;
   end
K=assem(edof,K,k);  %Assembles in global stiffnessm matrix
M=assem(edof,M,m);
C=assem(edof,C,c);
end

%Adds stiffness of rotational spring
K(size(K,1),size(K,1))=K(size(K,1),size(K,1))+krs;

%Adds stiffness of horizontal spring
K(size(K,1)-2,size(K,1)-2)=K((size(K,1)-2),(size(K,1)-2))+khs;
```

C.6 Function file mass matrix

```
function [M] = massmatrix(m1,m2,m3,n1,n2,K,M,mtop)
%Determines the lumped mass matrix for the total building

for j=1:3:size(K,1)
    %Adds the weight of top floors
    if j <= n1*3
    M(j,j)=M(j,j)+m1;

    %Adds the weight of middel floors
    elseif j<=n2*3
    M(j,j)=M(j,j)+m2;

    %Adds the weight of bottom floors
    else
     M(j,j)=M(j,j)+m3;
    end

    %Define the weight of the roof
    M(1,1)=mtop;
end
```

C.7 Function file generalised and equivalent mass

```
function [Mg,me,Mode_square] = Generel_Equiv_mass(m1,m2,m3,n1,n2,...
                                Modeshapef,height_n,mtop)

%Determines the general and equivalent mass for acceleration calculations
%according to design codes and theorertical methods

Mg=0;            %Creates starting values of variables
```

```
me=0;
Mode_square=0;

for i=1:length(Modeshapef)

if i==1
    M1=mtop*Modeshapef(i)^2; %Creates generalized mass for roof

elseif i<=n1  %If different mass per floor
    M1=m1*Modeshapef(i)^2; %Creates generelized mass per node

elseif i<=n2 %If different mass per floor
     M1=m2*Modeshapef(i)^2; %Creates generelized mass per node

else
     M1=m3*Modeshapef(i)^2; %Creates generelized mass per node
end

  Mg=M1+Mg; %Sums generlized mass per node
end

for i=1:(length(Modeshapef)-1) %This loop determines area of the
% fundamental modeshape in square
Mode_square1=((Modeshapef(i+1)^2 ...
    +(1/2)*(Modeshapef(i)^2-Modeshapef(i+1)^2))*height_n);

Mode_square=Mode_square1+Mode_square; %Sums this area up
end
me=Mg/Mode_square; %Determines the equivalent mass by dividing
%genrelised mass by the fundamental modeshape in square

end
```

C.8 Function file acceleration EKS 10

```
function [Accel_EKS,max_acc,betaair,xf_L_u] = EKS_acc(width,Ey,...
    ksi,vb,c0,fundamental_frequency,cf,me,beta,kl,Ter,rho,href,p1_x)

kr=0.22;                    %Terrainfactor
cr=kr*log(Ey(1)/Ter(1));    %Rawness factor
vb5=ksi*vb;                 %Reference wind velocity return period 5 years
vmh=cr*c0*vb5;              %Mean wind velocity at higth h

pb=1/(1+((3.2*fundamental_frequency*width)/vmh));
%Size factor with regard to the width of the building
ph=1/(1+((2*fundamental_frequency*Ey(1))/vmh));
%Size factor with regard to the height of the building

%Length of intergration, according to Handas recommendations
xf_L_u=150;

yc=xf_L_u*fundamental_frequency/vmh;

F=4*yc/((1+70.8*yc^2)^(5/6)); %Karmans wind energy spectrum
```

```
zs=0.6*Ey(1);                  %Standard height
cr1=Ter(3)*log(zs/Ter(1));     %Rawness factor at height zs
vmzs=cr1*c0*vb5  ;             %Mean wind wind velocity at height zs

betaair=(cf*rho*width*vmzs)/(2*fundamental_frequency*me);
%Aerodynamic damping expressed as logharitmic decrement

R=sqrt((2*pi*F*pb*ph/(beta+betaair)));
%factor for resonance response

Bsquare=exp(-0.05*(Ey(1)/href)+(1-(width/Ey(1)))*(0.04+0.01*(Ey(1)/href)));
%Factor for background response
v=fundamental_frequency*(R/(sqrt(Bsquare+R^2)));
%Mean value for cross frequency

kp=sqrt(2*log(v*600))+0.6/sqrt(2*log(v*600));  %Peak factor
Iv=kl/(c0*log(Ey(1)/Ter(1)));       %Turbulence factor at height Ey(x)
qmh=(rho*vmh^2)/2;                  %Velocity pressure at heihgt Ey(x)

Accel_EKS=(3*Iv*R*qmh*width*cf*p1_x)/me;
%Calculates the standard deviation acceleration according to EC
max_acc=kp*Accel_EKS;
%Max acceleration according to EC
end
```

C.9 Function file expansion of mode shape

```
function [MS_int] = Modeshape_expansion(Ey,Modeshapef,n_int_per_storey,Lx)

%Expands mode shape for better precision in integration

MS_int1=[1];

%Linearly expresses  the mode shape between the horizontal dofs
for i=1:length(Ey)-1;
diff=(Modeshapef(i)-Modeshapef(i+1))/(n_int_per_storey+1);
Modeshapef_expanded=...
    linspace(Modeshapef(i)-diff,Modeshapef(i+1),n_int_per_storey);
MS_int1=[MS_int1 Modeshapef_expanded];
end

MS_int=fliplr(MS_int1);
end
```

C.10 Function file wind properties

```
function [Iu,v_mean,vtop,v_mean_zs,Iu_zs] = Wind_Behaviour(Lx,Ter,vb5)


%Follwing equation comes from eurocode
for i = 1:length(Lx);
```

```
    if Lx(i) <= Ter(2)
       v_mean(i)=Ter(3)*vb5*log(Ter(2)/Ter(1));
    else
       v_mean(i)=Ter(3)*vb5*log(Lx(i)/Ter(1));
    end
end

%Wind velocity at reference height
v_mean_zs=Ter(3)*vb5*log((max(Lx)*0.6)/Ter(1));

%Wind velocity at top of building
vtop=max(v_mean);


%Plots the mean wind velocity
figure(3)
hold on
plot(v_mean,Lx), axis([0 vtop*1.3 0 max(Lx)]), grid
hold off


%Turbular intensity, According to Eq 3.14 in Strömmen
sigma_u=vb5*Ter(3);
for i = 1:length(Lx);
    Iu(i)=sigma_u/v_mean(i);
end

%Turbulance at reference height
Iu_zs=sigma_u/v_mean_zs;


%Plots the turbulance
figure(4)
plot(Iu,Lx),grid

end
```

C.11 Function file wind spectral density

```
function [Kaimal,Karman] = WindSpectralDensity(Ey,N_int,vtop,...
                           w,xf_L_u,v_mean_zs,Ter)

%Function file that determines the wind spectral density for
%Karman and Kaimal



%For EuroCode Appendix B
alpha=0.67+0.05*log(Ter(1));
Lzs=300*((0.6*Ey(1))/200)^alpha;


%--------Kaimal-----------
```

```
%Determine the autospectral density for frequencies within the vector w

Kaimal=zeros(1,length(w));
for j = 1:length(w)
fL=(w(j)/(2*pi))*xf_L_u/vtop;
Kaimal(j)=(fL/(1+10.2*fL)^(5/3));
end

%-------KARMAN------
%Determine the autospectral density for frequencies within the vector w

Karman=zeros(1,length(w));
for i =1:length(w)
fL=(w(i)/(2*pi))*xf_L_u/vtop;
    Karman(i)=(4*fL/(w(i)))/(1+70.8*fL^2)^(5/6);
end
Karman=Karman';


%Plots Kaimal
figure(5)
loglog(w,Kaimal),grid, title('Kaimals Spectral Density')
xlabel('\omega')


%Plots Karman
figure(6)
loglog(w,Karman),grid, title('Karmans Spectral Density')
xlabel('\omega')
```

C.12 Function file frequency response function

```
function [Hhat_N,Hhat] = FrequencyResponseFunction(zeta,w,...
    w_fundamental,zetaair);

%Function file that determines the frequency response function

zetatot=zeta+zetaair; %Damping values according to eks 10

%Creates the frequency response function
Hhat=zeros(1,length(w));
for j=1:length(w)
    Hhat(j)=(1-(w(j)/w_fundamental)^2+(2*1i*zetatot)*...
        ((w(j)/w_fundamental)))^-1;
end
Hhat_N=abs(Hhat);

%Plots the frequency response function
figure(7)
hold on
plot(w,Hhat_N),title('Frequency Response Function'),grid
xlabel('\omega')
```

```
ylabel('Hhat')
hold off
```

C.13 Function file coherence

```
function [Co_b,Co_h] = Coh_b(width,N_int,w,vtop,Cuu,Ey);

%Creates the horizontal coherence for the witdh of the building and
%the vertical coeherence for the heihgt of building

b_x=linspace(0.001,width,N_int);
N=length(w);
Co_b=zeros(1,N)';

%Loop that reates the horizontal coeherence
for k=1:N
    Co_b_step=0;
    for i=1:N
        for j=1:N
            diff_b=abs(b_x(i)-b_x(j));
            co_b=exp((-diff_b*Cuu*w(k))/(2*pi*vtop));
     Co_b_step=Co_b_step+co_b;

        end
    end
 Co_b(k)=Co_b_step*(1/N)^2;
end


%Loop creats vertical coherence (used only for plot)
L_x=linspace(0.001,Ey(1),N_int);
Co_h=zeros(1,N)';
for k=1:N
    Co_l_step=0;
    for i=1:N
        for j=1:N
            diff_l=abs(L_x(i)-L_x(j));
            co_l=exp((-diff_l*Cuu*w(k))/(2*pi*vtop));
     Co_l_step=Co_l_step+co_l;

        end
    end
 Co_h(k)=Co_l_step*(1/N)^2;
end

%Plots horizontal coherence
figure(12)
semilogx(width*(w/(2*pi))/vtop,Co_b),grid

%Plots vertical coherence
figure(13)
semilogx(Ey(1)*(w/(2*pi))/vtop,Co_h),grid
end
```

C.14 Function file joint acceptance function

```
function [J_sqr,J_sqr_NORM] = JointAF (Iu,Lx,Cuu,MS_int,v_mean,vtop,w,...
          Mode_square,Kaimal,Karman,w_fundamental,v_mean_zs,rho,width,cf)

%Function file that determines the joint accaptence function for the
%the building according to prof Strömmen methods


Jd=zeros(1,length(Lx));

%Numerical integration over two variables using the Rectangular Rule
for k = 1:length(w)
    Jstep = 0;
    for i = 1:length(Lx)
        for j = 1:length(Lx)
            dx = abs(Lx(i)-Lx(j));
            Co_hat = exp((-Cuu*dx*w(k))/(2*pi*vtop));
            Jstep = Jstep + ...
((v_mean(i)^2)*(v_mean(j)^2)*MS_int(i)*MS_int(j)*...
((Iu(i)*Iu(j)*Co_hat)*Karman(k)));
        end
    end
    Jd(k) = Jstep;
end
J_sqr = Jd*((max(Lx)/(length(Lx)))^2);
%Multiplying by step size

%Nomralising the joint acceptance function
J_sqr_NORM=J_sqr/Mode_square^2;


%Plots the joint accaptence function
figure(8)
loglog(w,J_sqr),grid,title('Joint acpetence function in square')
xlabel('\omega')
ylabel('J^{2}')

%Creates the load spectrum of the wind
Sq=zeros(1,length(w));
for i=1:length(w)
Sq(i)=(rho*width*cf)^2*J_sqr(i);
end

%Plots the load spectrum of the wind
figure(9)
loglog(w,Sq),grid,title('Load Spectrum')
xlabel('\omega')
ylabel('f*Sq')
end
```

C.15 Function file response spectrums

```
function [Response_spectra_Acc,Response_spectra] = reponsespectrums(w,...
    rho,Hhat_N,J_sqr_NORM,width,w_fundamental,me,depth,Kaimal,...
    v_mean,inc,cf,Co_b);


%Creates Response spectra and acceleration spectra over frequency domain
for j = 1:length(w)
   Response_spectra(j)=((rho*cf*width/(w_fundamental^2*me)...
       *Hhat_N(j))^2*J_sqr_NORM(j)*Co_b(j));
   Response_spectra_Acc(j)=Response_spectra(j)*(w(j)^4);
end

N=length(w); %Number of intergration points


%Plots responce spectra of acceleration in log scale
figure(10)
loglog(w,Response_spectra_Acc),grid,title('Response Spectra for Acc'),...
        axis([0.001 15 10e-17 10e-2])
xlabel('\omega')


%Plots response sepctra of displacment
 figure(11)
 hold on
 plot(w,Response_spectra),grid,title('Response Spectra')
 xlabel('\omega')
 ylabel('S_r(\omega)')
 hold off
end
```

C.16 Function file acceleration in resonance Strømmen

```
function [Accel_Strommen] = resonance(Mg,w_fundamental,J_sqr,rho,width,...
                            cf,Hhat_N,w,zeta,zetaair,Co_b)

%Determines the accelartion just for the resonance according to Strömmen

N=length(w);

%Integrating the response function over the frequency domain
Int_H_hat=0;
for i = 1:N
    Int_H_hat=Int_H_hat+(Hhat_N(i))^2;
end
Int_H_hat=Int_H_hat*(max(w)/N);


%Position of the natural frequency and corresponding acceptence
```

```
%function value
Position=floor(w_fundamental/(max(w)/N)); %Floor to be conservative
J_sqr_pos=J_sqr(Position);
Co_b_pos=Co_b(Position);

%Standard deviation of response in resoncance part
Stand_dev_dis_resp=(1/(w_fundamental^2*Mg))^2*((rho*width*cf)^2*...
                    J_sqr_pos*Co_b_pos*Int_H_hat);

%Standard deviation of acceleration in resoncance part
Accel=w_fundamental^2*sqrt(Stand_dev_dis_resp);

%Standards deviation of acceleartion in resonance part
Accel_Strommen=w_fundamental^2*sqrt((1/(w_fundamental^2*Mg))^2*...
((pi*w_fundamental*(rho*width*cf)^2*J_sqr_pos*Co_b_pos)/...
(4*(zetaair+zeta))));
end
```

C.17 Function file acceleration according to EN 1991-1-4

```
function [Accel_EC] = EC(cf,rho,Iu_zs,me,width,zeta,zetaair,...
        Ey,fundamental_frequency,Ter,v_mean_zs,v_mean,MS_int,Iu);

%To determine the According to EN 1991-1-4 Appendix B

%%%---Determines the resonance response------

%Power Spectral
alpha=0.67+0.05*log(Ter(1));

%Integral length scale
Lzs=300*((0.6*Ey(1))/200)^alpha; %According to EC
Lz=150;                          %According to Kamal Handa

%Wind spectral density
fL=fundamental_frequency*Lz/v_mean_zs;
SL=(4*fL)/(1+70.8*fL^2)^(5/6);

%Correlation factors
nah=((4.6*Ey(1))/Lzs)*fL;
nab=((4.6*width)/Lzs)*fL;
Rh=(1/nah)-(1/(2*nah^2))*(1-exp(-2*nah));
Rb=(1/nab)-(1/(2*nab^2))*(1-exp(-2*nab));

%Resonant response coeffcient
R_EC=sqrt((pi^2/((zeta+zetaair)*2*pi*2))*SL*Rb*Rh);


%-------Dimensionless koefficient Kx----------


%Rectangular rule for integration
N=length(v_mean);
sum=0;
```

```
for i=1:N
sum=v_mean(i)^2*MS_int(i)+sum;
end
int1=sum*(Ey(1)/N);

%Rectangular rule for integration
sum=0;
for i=1:N
sum=MS_int(i)^2+sum;
end
int2=sum*(Ey(1)/N);

Kx=int1/(v_mean_zs^2*int2);

%-----Accel-----
%Final expression for acceleration according to EC
Accel_EC=(cf*rho*width*Iu_zs*v_mean_zs^2)*(R_EC*Kx)/me;
end
```

C.18 Function file mean deflection

```
function [y_m] = y_m1(cf,rho,width,vtop,MS_int,powerlaw,...
                        w_fundamental,Mg,Ey)

%Function file that determines the mean defelection
y_int=0;
N=length(MS_int);

%Integration with rectangular rule
for i=1:N
y_int=y_int+MS_int(i)*(i/N)^(2*powerlaw);
end
y_int=y_int*(1/N);

%Mean deflection at top of the building
y_m=(1/2)*rho*cf*Ey(1)*width*vtop^2*y_int/(w_fundamental^2*Mg)
end
```

C.19 Function file coherence for width

```
function [H_C] = H_C1(width,fundamental_frequency,vtop,N_int,Cuu)

%Function file that determines the horizontal correletion of wind
%acting on facade of building


%Rectangular rule used as integration method in loop
H_C_int=0;
for i=1:N_int
for j=1:N_int
diff_b=abs((j/N_int)-(i/N_int));
```

```
H_C_int=H_C_int+exp(-(diff_b)*Cuu*width*fundamental_frequency/vtop);
end
end

H_C=H_C_int*(1/N_int)^2;

end
```

C.20 Function file coherence for height

```
function [V_C] = V_C1(powerlaw,Ey,MS_int,vtop,Cuu,fundamental_frequency)

%Correlation factor with regard to height of building


%Rectangular rule used as integration method
N=length(MS_int);
int1=0;
for i=1:N
for j=1:N
diff_h=abs((j/N)-(i/N));
int1=int1+MS_int(j)*MS_int(i)*exp(-Cuu*diff_h*Ey(1)*...
    fundamental_frequency/vtop)*((i/N)*(j/N))^powerlaw;
end
end
int1=int1*(1/N)^2;

%Rectangular rule used as integration method
int2=0;
for i=1:N
int2=int2+(MS_int(i)*(i/N)^(2*powerlaw));
end
int2=int2*(1/N);

%Final expression
V_C=(int1)/int2^2;
end
```

C.21 Function file wind spectral density Handa

```
function [F] = Wind_Spec(vtop,fundamental_frequency,xf_L_u)

%Wind spectral density at the fundamental frequency of the building
%according to Karman

F=(4*fundamental_frequency*xf_L_u/vtop)/...
    (1+70.8*(fundamental_frequency*xf_L_u/vtop)^2)^(5/6);

end
```

C.22 Function file acceleration in resonance Handa

```
function [Dev_dis,Accel_Handa] = Handa(Iu,y_m,F,V_C,H_C,zetaair,...
                                       zeta,w_fundamental)
%Final expression for standard deviation of acceleration according
%to handa

%Standard deviation of displacement for resonant part
Dev_dis=sqrt((4*y_m^2*Iu(length(Iu))^2*(H_C*V_C*F)/(zetaair+zeta)));

%Standard deviation of acceleration for resonant part
Accel_Handa=w_fundamental^2*Dev_dis;
end
```